TRIFLUORO ALKYL OLIGO(ETHYLENE GLYCOL)-TERMINATED ALKANETHIOL SELF-ASSEMBLED MONOLAYERS: SYNTHESIS, CHARACTERISATION, AND PROTEIN ADSORPTION PROPERTIES

Nelly Bonnet

A Thesis Submitted for the Degree of PhD
at the
University of St Andrews

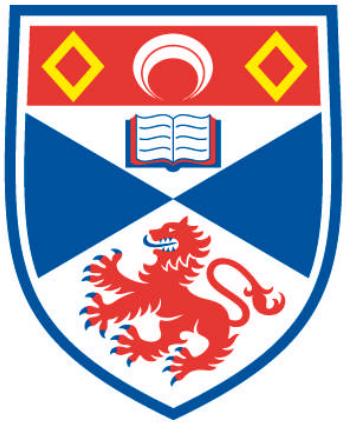

2010

Trifluoro Alkyl Oligo(Ethylene Glycol)-terminated Alkanethiol Self-Assembled Monolayers: Synthesis, Characterisation, and Protein Adsorption Properties

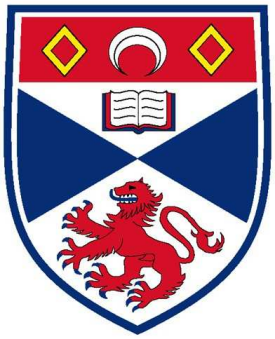

A thesis presented by

Nelly Bonnet

to the

University of St Andrews

in application of

THE DEGREE OF DOCTOR OF PHILOSOPHY

St Andrews

Declaration

I, Nelly Bonnet, hereby certify that this thesis, which is approximately 30000 words in length, has been written by me, that it is the record of my work carried out by me and that it has not been submitted in any previous application for a higher degree.

I was admitted as a research student in September 2005 and as a candidate for the degree of Doctor of Philosophy in August 2006; the higher study for which this is a record was carried out in the University of St Andrews between 2005 and 2008.

Date signature of candidate

I hereby certify that the candidate has fulfilled the conditions of the Resolution and Regulations appropriate for the degree of Doctor of Philosophy in the University of St Andrews and that the candidate is qualified to submit this thesis in application for that degree.

Date signature of supervisor

In submitting this thesis to the University of St Andrews I understand that I am giving permission for it to be made available for use in accordance with the regulations of the University Library for the time being in force, subject to any copyright vested in the work not being affected thereby. We also understand that the title and abstract will be published, and that a copy of the work may be made and supplied to any bona fide library or research worker, my thesis will be electronically accessible for personal or research use unless exempt by award of an embargo as requested below, and that the library has the right to migrate my thesis into new electronic forms as required to ensure continued access to the thesis. We have obtained any third-party copyright permissions that may be required in order to allow such access and migration, or have requested the appropriate embargo below.

The following is an agreed request by candidate and supervisor regarding the electronic publication of this thesis:

Embargo on both all printed copy and electronic copy for the same fixed period of two years on the following ground:

publication would preclude future publication

Date signature of candidate signature of supervisor

Acknowledgements

I wish to express my sincere appreciation to Dr. Georg Hähner, for giving me the opportunity to research under his supervision and for providing informative discussions during this enlightening and dynamic three years.

I am also thankful to Pr. David O'Hagan for his supervision during the months spent in his lab for the synthesis of my surfactants.

I am extremely grateful to all the academicals and technical staff of the chemistry department; Dr. Steve Francis, Dr. Olivier Gaudin, Dr. Manfred Buck, Dr. Tomas Lebl, Melanja Smith and Caroline Horsburgh.

I would like to thank all the GH and DOH members who have made the lab a pleasant environment in which to work. Thank you Brunette, Margit, Nat, Thomas, Matt, Pitak, Guillaume, Luke, Daniel, Deng, Francis, Gennady…

A special thank goes to my family and all my friends for their support: Vivi, Roro, Benji, Kat, Angel, Gary, Jürgen, Paul, Jacorien, Jenny, Caroline, Aga, Marcin, Marzia, Iza…Minette!

Lastly, thanks and MERCI to Titi.

Abstract

Self-assembled monolayers have been proven to be well-ordered and to give stable ultrathin films. They show a remarkably high diversity with respect to their functionalisation giving rise to many possible applications. This thesis is focused on the potential use of these molecular thin films in life sciences. The reproduction of a membrane-like environment with these tightly packed and organized unimolecular layers has led to important breakthroughs in their nanotechnological application as biomaterials. Their straightforward modification allows the chemical and physical properties of biological interfaces to be altered. In particular, Oligo(ethylene glycol) based alkanethiol self-assembled monolayers were intensively studied as biointerfaces for their ability to resist the non specific adsorption of proteins. The electrostatic repulsion which originates from these monolayers was seen as one of the possible factors causing this protein repulsion. On the other hand proteins adsorb on alkanethiol self-assembled monolayers. This can be partially attributed to an attractive hydrophobic interaction between the biomolecules and the surface.

As a result of the understanding of these two driving forces which are relevant for non-specific protein adsorption/repulsion, novel self-assembling molecules were tailored in an attempt to adjust the adsorption of proteins at the SAM-liquid interface. This was conceivable with these newly designed SAMs since they allow a combination of these forces. We have chosen the ionic strength of the liquid environment as the external parameter which could act on the amount of adsorbed proteins because the electrostatic force created by oligo(ethylene glycol) groups depends on it.

In addition to the synthesis of six new molecules, the preparation and characterisation of the novel self-assembled monolayers are reported in this thesis. The density of the monolayers was estimated by X-ray photoelectron spectroscopy and ellipsometry, and the wettability properties were studied by measuring the contact angle. The total force

acting on proteins from the SAMs was studied with an atomic force microscope, equipped with a tip mimicking proteins, by measuring force-distance curves. An *in-situ* technique was investigated in order to study the influence of the variation of this total force on the quantity of adsorbed proteins by varying the ionic strength.

Contents

Chapter 1

Brief Review on Self-Assembled Monolayers and Their Applications

As a consequence of the strong tendency towards miniaturisation, considerable attention is being paid to the development of ultrathin films, of which the most promising candidates are self-assembled monolayers (SAMs). The ease of their preparation, in combination with the great flexibility with respect to functionalisation, has prompted an increasing level of interest in SAMs within various fields. Applications of SAMs are wide-ranging from electronics to biosensors in life sciences.

I) Self-Assembled Monolayers

Self-Assembled Monolayers (Figure I-1) are nanometer thick organic films comprised of a single layer of molecules that adsorb spontaneously by chemisorption on a substrate.[1, 2]

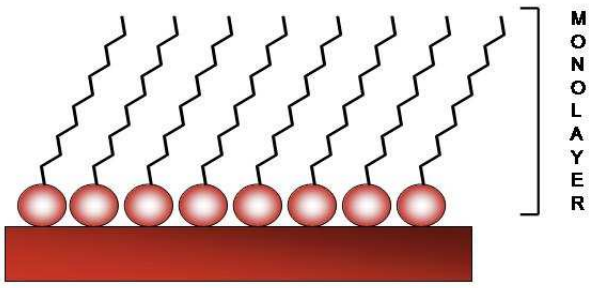

Figure I-1: Scheme of a self-assembled monolayer

The first preparation of a monomolecular layer by self-assembly of a surfactant onto a clean metal surface was published in 1946 by Zisman. [3] However, the level of interest increased exponentially after the pioneering work of Nuzzo and Allara [4] who showed that SAMs can be prepared from dilute solutions of disulfides.

Figure I-2 shows that SAMs can be prepared relatively easily by immersing a substrate into a millimolar solution of a self-assembling molecule.

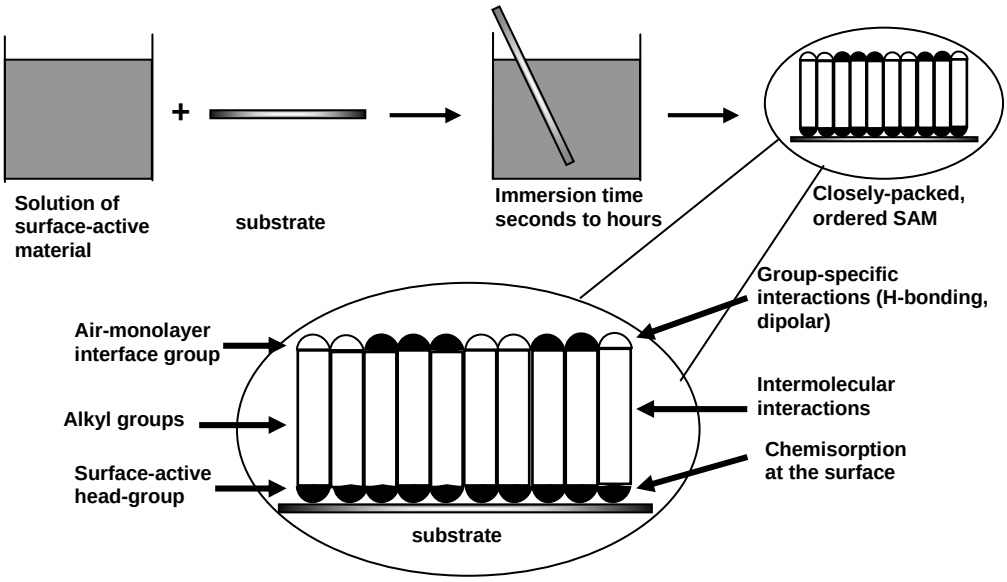

Figure I-2: Self-assembled monolayers are formed by simply immersing a substrate into a solution of the surface-active material. The driving force for the spontaneous formation of the 2D assembly includes chemical bond formation of molecules with the surface and intermolecular interactions. Reproduced from [1]

Each end of the surfactant hydrocarbon chain has its own function. A strong tendency for preferential adsorption onto the substrate is attributed to one group, while the tail group pointing outwards from the surface defines the chemical characteristics of the film (Figure I-3).

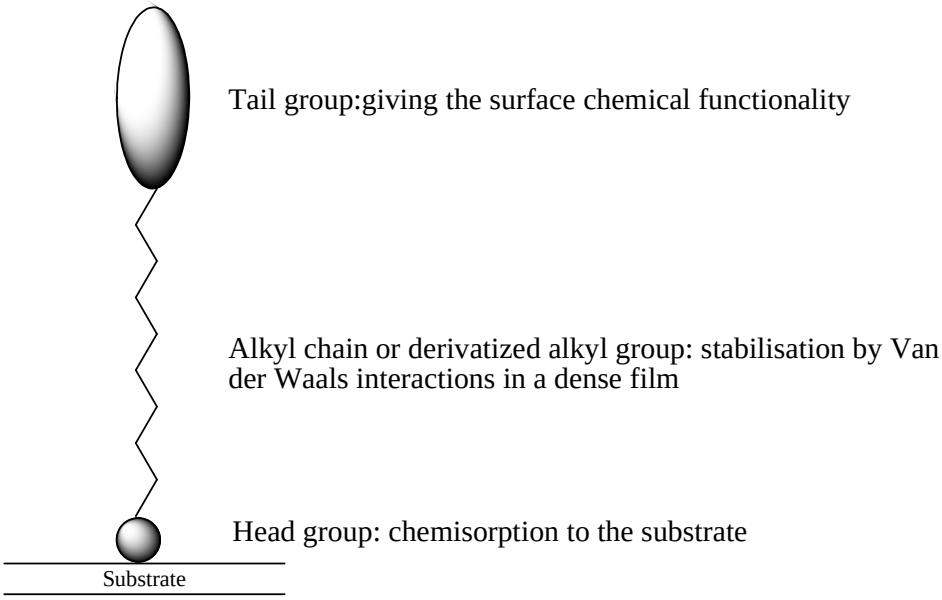

Figure I-3: Function of each part of the self-assembling molecule

The head group of the self-assembling molecule enables coordination to the substrate surface by a strong, exothermic chemisorption process, on the order of 100 $kJ.mol^{-1}$. [22] SAMs are known to be highly ordered as a consequence of interchain Van der Waals interactions between neighbouring alkyl chains when all available binding sites are occupied. SAMs represent ideal systems for the fabrication of well-defined organic coatings as they display high, crystal-like, two dimensional order. [2] The air-monolayer interface group, as called by A. Ulman (Figure I-2), gives SAMs the characteristics of functional organic coatings. Moreover, the chemical properties of a film can be controlled in a relatively straightforward manner by simply changing the terminal group functionality. The surface properties can also be modified by chemical transformation of the terminal group once the SAM film is formed. [5]

The large number of potential substrate/head group combinations gives rise to diverse array of SAM systems. For example, organosilane, [6] alkylsiloxane, [7] and alkyltrichlorosilane head groups [8, 9] are ideal for the formation of SAMs on hydroxylated surfaces such as silica and glass.

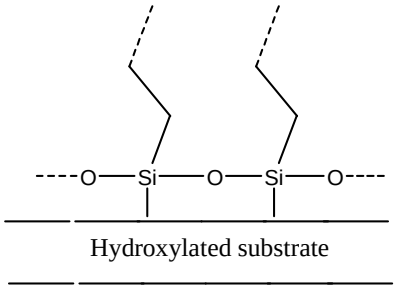

Figure I-4: Schematic of self-assembled monolayer on hydroxylated substrate

Other viable head group/substrate pairs include alcohols and amines on platinium, [10] siloxane on titanium, [11] carboxylic acids on aluminium oxide [12] and thiols bonding on copper, [13-15] silver, [15-17] and palladium. [18, 19]

Of all the SAM systems described to date, the best characterised and most studied is that of alkanethiols on gold and this will be discussed further in the following sections.

II) Alkanethiol based Self-Assembled Monolayers on Gold

Subsequent to the discovery of Nuzzo and Allara that monolayers of dialkyldisulfide can be formed on gold, organosulfur molecules were found to bond to a range of other metals. However, gold remains the most commonly employed substrate for monolayer creation because its deposition by thermal evaporation, giving a Au(111) surface (Figure I-5), is easy and importantly Au does not have a stable surface oxide

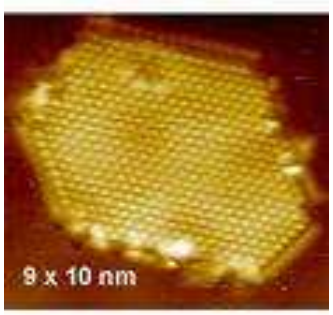

Figure I-5: Surface of gold (111). Reproduced from [20]

The removal of the physically and chemically bound contaminants from gold is a facile process as a consequence of its inert nature, a characteristic that also permits manipulations under aerobic conditions. [21]

The best described SAM system derived from the spontaneous adsorption of alkanethiols onto a Au(111) surface is shown in Figure I-6.

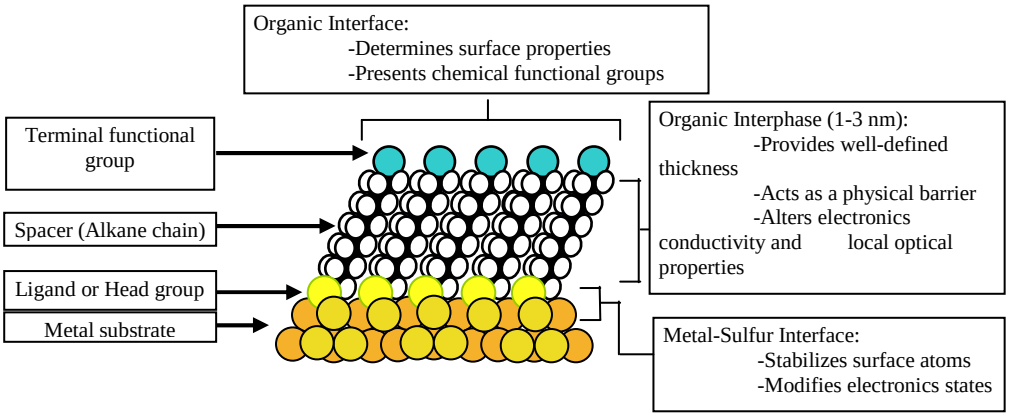

Figure I-6: Alkanethiol-based SAM on gold. Reproduced from [21]

The thiol (SH) head group and gold substrates have been shown to work excellently for SAM formation because of their strong affinity for one another. [2] Chemisorption of the surfactant molecules on the Au substrate gives rise to thermodynamically stable monolayers [2, 4] that can be inert towards contact with air, water, or ethanol for periods of several months depending on the nature of the SAM. [22]

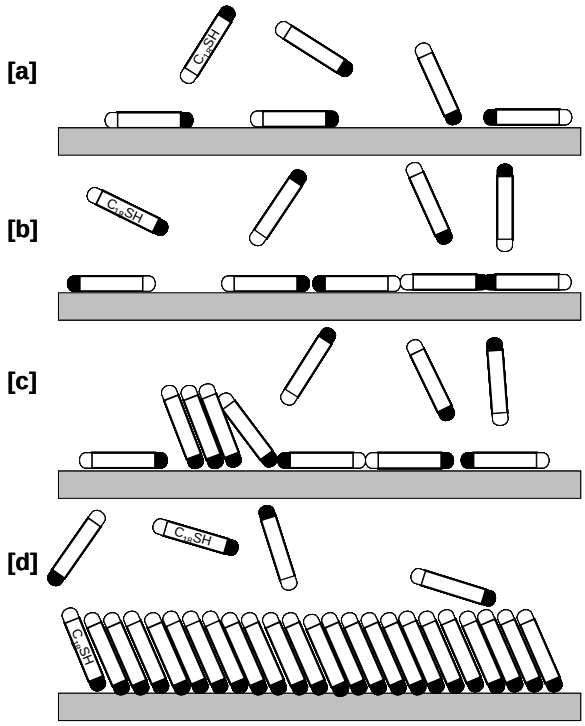

Figure I-7: Schematic mechanism diagram for the self-assembly of alkanethiol on Au(111). (a) Initial adsorption, (b) lying-down phase. (c) Two-dimensional phase transition from a lying-down to a standing-up configuration. (d) Formation of a complete SAM. Reproduced from [23]

It is generally accepted that alkanethiol SAMs form in two main steps comprising a rapid adsorption of an imperfect monolayer following by a slow ordering process (Figure I-7). Bain *et al.* studied the kinetics of these steps by dipping a gold substrate in an ethanolic solution of octadecanethiol and measuring the contact angle on the substrate and the thickness of the organic layer over time. [24] The two phases of SAM formation were observed by an increasing contact angle that is relatively rapid in the early stages of immersion but reaches a plateau only after longer periods. The influence of the surfactant concentration was also studied (Figure I-8) and revealed that the time taken for the SAM to be fully ordered, as determined by the onset of the plateau, is inversely proportional to surfactant concentration. However, a concentration of 1 mM is sufficient to obtain an ordered film in a reasonable time (for instance, by letting the substrate immersed in the solution overnight).

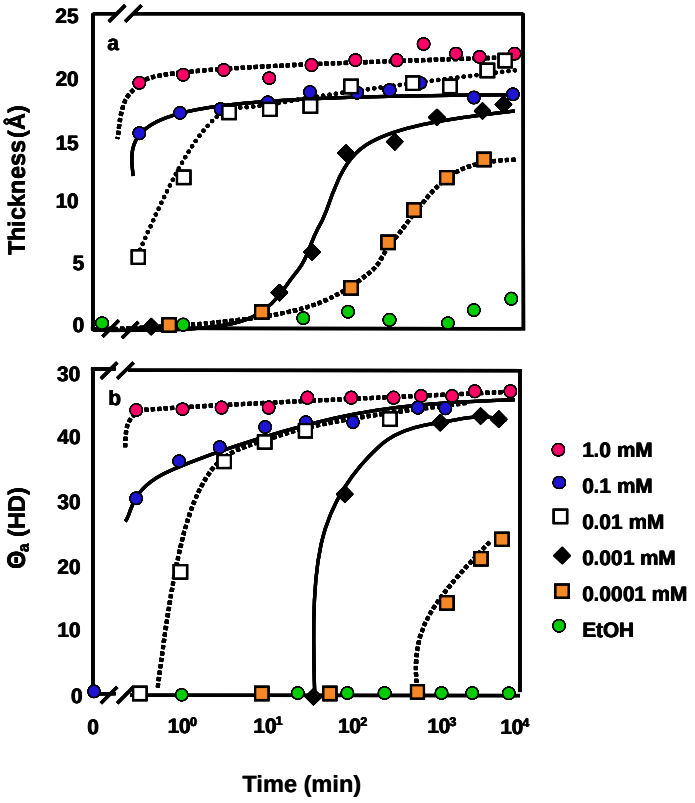

Figure I-8: Kinetics of adsorption of octadecanethiol from ethanol as a function of concentration: (a) ellipsometric thickness, (b) advancing contact angles. Reproduced from [24]

Bain *et al.* also studied the influence of chain length and contaminants on the kinetics of formation of alkanethiol monolayers. Comparing the kinetics for octadecanethiol and decanethiol, it was found that assembly is more rapid for the longer chain, as shown in Figure I-9, and this was attributed to a stronger van der Waal's interaction.

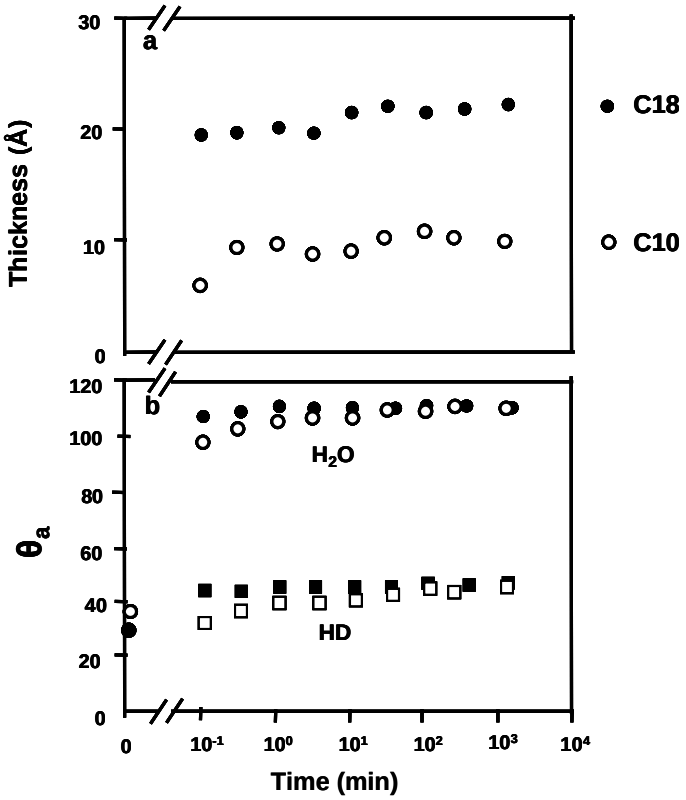

Figure I-9: Kinetics of adsorption of octadecanethiol (solid symbols) and decanethiol (open symbols) from ethanol onto gold. (a) Ellipsometric thickness. (b) Advancing contact angles (○,●) water, (□,■) hexadecane. Reproduced from [24]

Ellipsometry measurements of the thickness of a film formed on a contaminated gold substrate showed slower kinetics, compared to the clean surface, during the initial phase but an identical limiting thickness at the end of the process (Figure I-10).

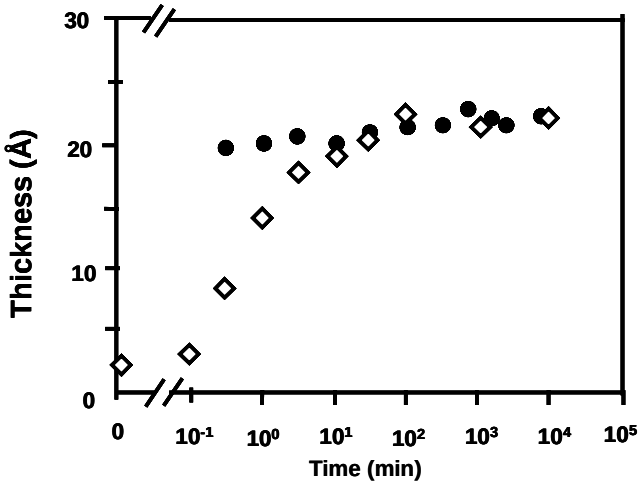

Figure I-10: Effect of contamination on kinetics of adsorption of octadecanethiol: (●) "clean" gold, (◊) gold with a preformed monolayer of propanethiol. Reproduced from [24]

This ‘slowing down’ is linked to a more difficult adsorption of the surfactant molecules on the gold surface, which must first displace the contaminant molecules before organising in the ordered SAM.

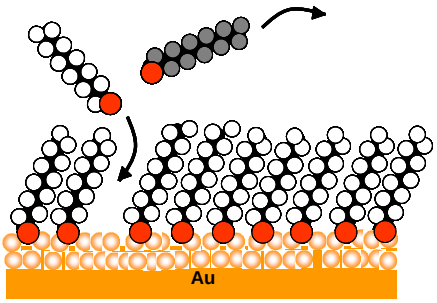

Figure I-11: Displacement of contaminant molecule by a self-assembling molecule. Reproduced from [25]

The monolayer made of organosulfur compounds is obtained through chemisorption, in other words the surfactant adheres to the surface through the formation of a chemical bond. The sp^3 binding mode of the surfactant molecules to Au (111) hollow sites induces a surface-S-C angle of 104° [1] which causes the chain to be tilted with respect to the surface. For alkane thiol molecules on gold, the extended alkyl chains orient around 30° from the normal. [4, 26, 27]

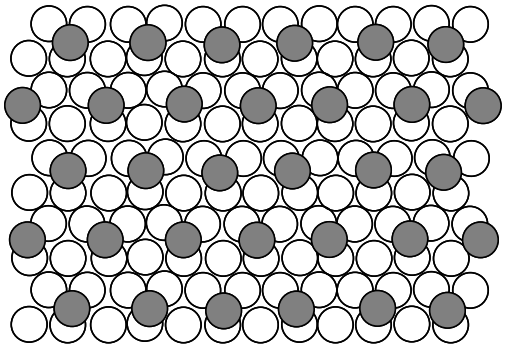

Figure I-12: Hexagonal coverage scheme for alkanethiols on Au(111). Reproduced from [1]

The sulfur atoms of the alkanethiol in an ordered film bind to the hollow sites on a Au(111) surface, shown as shaded circles in Figure I-12. The hollow sites are arranged in a hexagonal shape leading to an area per molecule of 21.4 $Å^2$, which corresponds to a packing density of 4.67 molecules/nm^2. [28]

Although the structure and configuration of the monolayer [29] is thermodynamically stable and has a low defect density, self-assembled monomolecular layers are still not perfect.

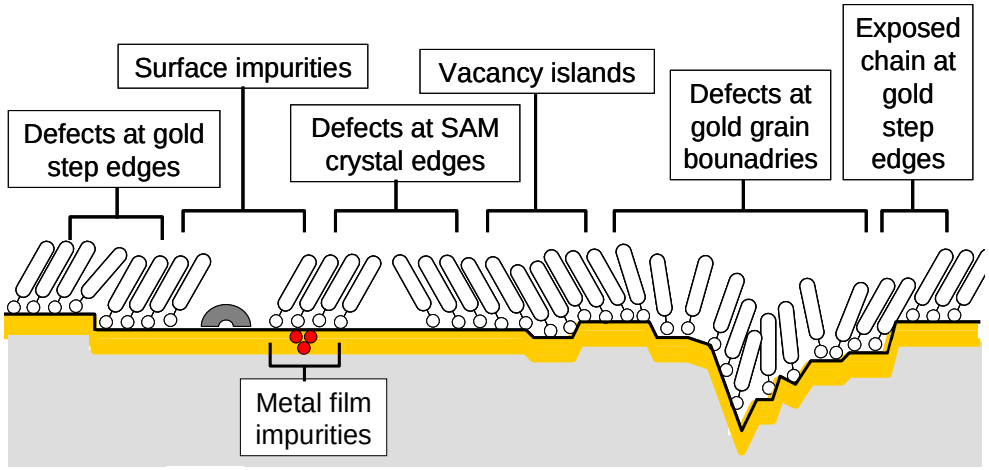

Figure I-13: Schematic illustration of some of the intrinsic and extrinsic defects found in SAMs formed on polycrystalline substrates. The dark line at the metal-sulfur interface is a visual guide for the reader and indicates the changing topography of the substrate itself. Reproduced from [29]

A SAM essentially duplicates the relief of its substrate and as such any defects are also reproduced by the self-assembling molecules (Figure I-13). Impurities on the substrate and in the surfactant solution can cause further defects by preventing adsorption of molecules at sites they occupy. When binding sites remain unoccupied it is also possible to obtain 'pinhole' vacancies. Nevertheless, the defect density can be considered as insignificantly low after cleaning by immersion for at least 24h. [23] Despite the presence of defects, which are smaller than a few molecular diameters, SAMs are considered highly organised from a surface-science perspective. [2]

As a consequence of their monomolecular thickness, high degree of order, stability, simplicity and flexibility with respect to functionalisation, SAMs are being widely exploited in the ever expanding field of nanotechnology and this will be described in the following section.

III) Self-Assembled Monolayer Applications

The diverse range of potential surface-groups, which impart chemical functionality to a SAM, offers appealing technological applications that cover many fields.

SAMs are ubiquitous in chemical applications with their use in heterogeneous catalysis [30] being of particular note. When immobilised at the surface of a SAM, catalytically active species can be oriented in such a way that a particular surface is presented to the reactants for example. A second example of immobilisation was demonstrated by Wang *et al.* who employed SAMs to organise carbon nanotubes into well-ordered patterns. [31] SAMs have also been employed extensively for the production of electronic components based on a monomolecular thick assembly where they act as a junction between two electrodes. [32] In an industry where miniaturisation is at the forefront of technological advancement, SAMs are also being studied as potential transistors. [33, 34] These highly versatile systems not only pass electric current but can be designed to create it when photoactive functional groups are introduced at the surface as demonstrated by Kondo and Uosaki. [35] SAMs have also proven to be suitable model surfaces for the study of wetting and the surface tension of liquids. Bain and Whitesides [36] used mixed SAMs obtained from decanethiol-based self-assembling molecules with both carboxylic acid and methyl surface groups to study wettability. They demonstrated that wettability is dependent on the composition of the surfactant solution (i.e. the ration of acid to methyl group functionality) as well as the pH of the aqueous solution used for measuring the contact angle. SAMs have also had an impact in lubrication applications where they provide a low friction surface for sliding parts [37] and as a means to provide a protective layer against corrosion.[38-40] It is clear, from the relatively few examples given, that SAMs have a diverse range of applications and this is exemplified more so in life sciences.

These highly packed and organized unimolecular layers provide a membrane-like environment, which has led to important breakthroughs in nanotechnological applications as biocompatible materials and supports that enable manipulation of cells and proteins. By modifying the surface group of the self-assembling molecule, the chemical and physical properties of biological interfaces can be easily adapted. Today, SAMs are used to provide biocompatibile layers on implant surfaces [41] which significantly improves tolerance by the body. They are also useful as an immobilising surface that enables the study of the function of individual components within complex biological systems. [42] For instance, this approach has attracted interest in genomics, by providing a platform for the study of protein sequences, and similarly in proteomics, which differentiates the proteins of a biological system. [43] In Life Sciences a challenging and important target is the selective immobilisation of proteins for their detection. This can be realised by employing immunosensors that are covered by SAMs for transducing antigen-antibody interactions directly into physical signals.[44] Prominent

examples of this technology include the immunosensor elaborated by Scheller and co-workers for the detection of cocaine [45] and the system developed by Ryan and co-workers for identification of the common nosocomial pathogen *Staphylococcus aureus*. [46] Selective immobilisation can be achieved by the inclusion of well-known receptor molecules in the organic packed layer which encourage coupling between complementary reactive groups [47] as illustrated by Mrksich and co-workers (reproduced in Figure 14 below).

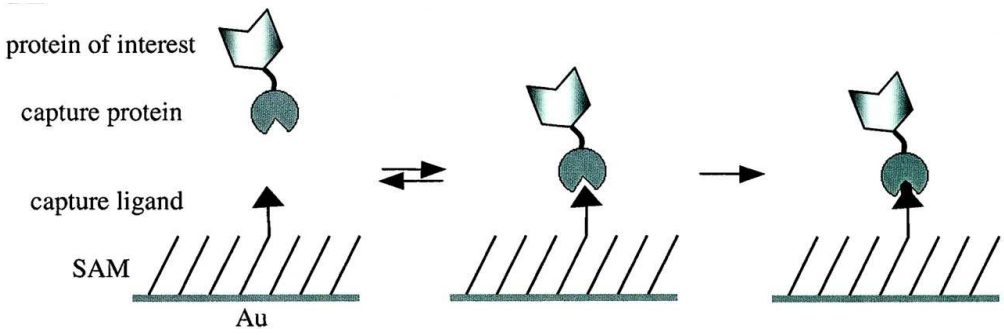

Figure I-14: Strategy for protein immobilization. The protein of interest is fused to a capture protein, which specifically binds a capture ligand of the substrate to give covalent immobilisation of proteins while maintaining activity and orientation. The density of immobilized proteins can be controlled by adjusting the density of the ligand. . Reproduced from [48]

The necessity for such "inclusion", to facilitate selective adsorption, means that the monolayer is not composed of a unique self-assembling molecule and is therefore a mixed SAM. [49] The receptor molecules regulate selective adsorption of the protein whilst the layer formed by the major surfactant must possess protein repelling properties.

This non-specific repulsion of proteins is required in other fields, such as biomedicine where applications include the prevention of protein folding (on the door handles in hospitals), and the limitation of interaction between a modern medicine tool and blood components. SAMs based on phosphorylcholine-terminated thiol (Figure I-15) and oligo(phosphorylcholine)-terminated thiol, [50, 51] or alkanethiolates with mannitol groups [52] are examples of monolayers that exhibit a strong protein-phobic surface.

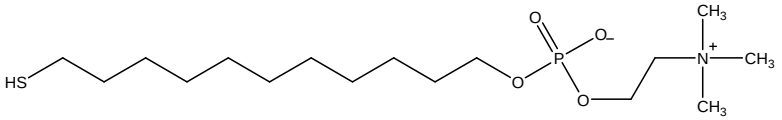

Figure I-15: Phosphorylcholine-terminated thiol used as SAM constituent by Rao and co-workers

Although not unique in their ability to resist the adsorption of proteins (eg [53]), oligo(ethylene glycol) based SAMs have attracted the most attention and this will be described in more detail in the following section.

IV) Oligoethylene Glycol Self-Assembled Monolayers and Proteins

Recognition of foreign materials by a living body can be suppressed by preventing the adsorption of proteins at its surface, which in turn will negate a biochemical response that would otherwise lead to rejection. A major step forward in the search for increased biocompatibility of medical devices, such as implants, was the modification of their surfaces by an ultrathin, polymeric film of poly(ethylene)glycol. Poly(ethylene glycol) (PEG) has been of great interest in the preparation of protein-resistant surfaces because of its ability to effectively reduce or prevent non-specific protein adsorption. [54, 55]

In an attempt to understand the physical mechanisms of the protein resistance displayed by PEG polymer surfaces, Harder and co-workers studied the interaction of proteins with oligo(ethylene glycol) terminated alkanethiol SAMs on gold. These short chain PEG-type systems were used as models because of the relative ease with which they can be characterised. [56] Oligo(ethylene glycol) SAMs were found to be very efficient for repelling proteins. [15, 57] As SAMs have a reproducible structure, the addition of oligo(ethylene glycol) (OEG) alkanethiol based monolayers to a surface became one of the most attractive means to render a biomaterial more resistant to the non-specific adsorption of proteins. The crucial step in elucidating the mechanism of protein resistance from the OEG based alkanethiol SAM lies in understanding the interaction of the surface with water. [6]

Dahint and co-workers compared the protein-resistance of methoxy-tri(ethylene glycol)-terminated (EG_3-OMe) undecanethiol self-assembled monolayers prepared on gold and silver. While the treated gold surface expresses a strong repulsion towards proteins, the silver surface was found to adsorb variable amounts of biomacromolecules. The distinctly different behaviour of the two systems can be attributed to the observed conformation of OEG on gold and silver as illustrated below. [56]

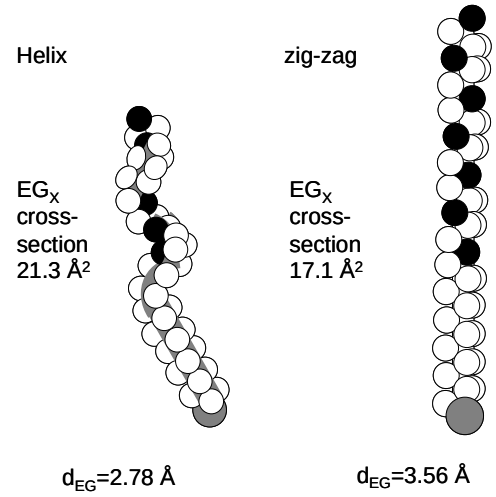

Figure I-16: Molecular cross-sections for the helical EG$_x$-OMe on gold with a ~30° tilt of the alkyl chain and a perpendicular orientation of "zig-zag" EGx-OMe on silver. Reproduced from [56]

The OEG tails adopt a helical conformation on gold as opposed to an "all trans" orientation that occurs on silver. Dahint and co-workers speculated that the helical monolayer prevents protein adsorption through its ability to bind water strongly. A stable interfacial water layer develops, as represented on the left of Figure I-17, that was believed to be responsible for preventing biomolecule adsorption.

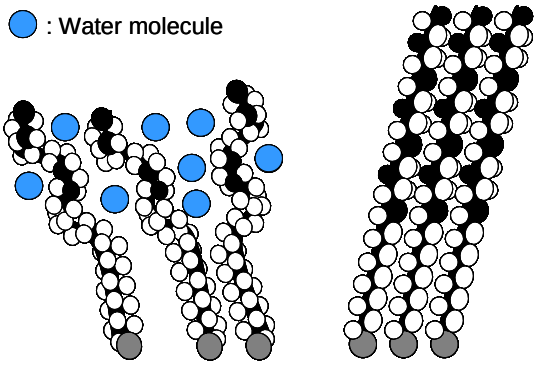

Figure I-17: Illustration of a water layer present only on a helical monolayer

This water layer does not form on silver because the more densely packed SAM resists the penetration of water molecules (as shown on the right of Figure I-17). This assumption was confirmed by the calculations conducted by Grunze and co-workers. [37] More precise calculations conducted by Whitesides and co-workers predicted the OEG conformers where water molecules can bind. [58]

Grunze and co-workers discovered that the interaction between proteins and surfaces can be easily explored using scanning force microscopy (SFM) with a fibrinogen-functionalised probe (Figure I-18). [60]

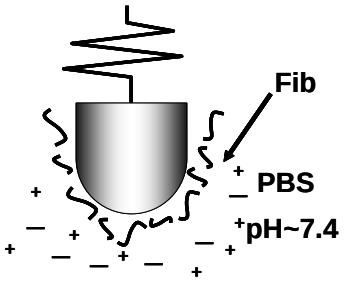

Figure I-18: Fibrinogen functionalised probe used for the SFM study of the resistance of OEG-terminated SAM. Reproduced from [60]

This technique was adapted to the study of protein mimics, i.e. the surface-protein interaction of methoxy-tri(ethylene glycol)-terminated undecanethiol self-assembled monolayers prepared on gold and silver, by utilizing a charged and hydrophobic probe. The forces measured with a hydrophobic probe (attraction or repulsion) were found to correlate with the protein adsorption properties of the films (adsorption or resistance to adsorption). [60, 61] The force experienced by the probe from the modified gold surface was thus repulsive whilst it was attractive from the treated silver interface.

Further measurements were performed with the helical OEG terminated SAM to elucidate the forces which intervene between the functionalised probe and the monolayer. Hähner *et al.* modulated the environment in which the force spectroscopy measurements were performed by changing the ionic strength of the liquid media. [62] The observed correlation between repulsive force and salt concentration provided evidence for the existence of electrostatic interactions. This electrostatic repulsion is seen as a key factor responsible for the repulsion of negatively charged proteins in aqueous media. However, the gold based SAMs described by Whitesides are non-ionic in nature but still display efficient protein repulsion. This raises the question as to the origin of this surface charge that must be present in the gold system but not when SAMs are formed on silver as previously discussed. Grunze *et al.* postulated that the negative charge arises from the adsorption of hydroxide ions from solution as an extension to the theory concerning water binding. [62, 63]

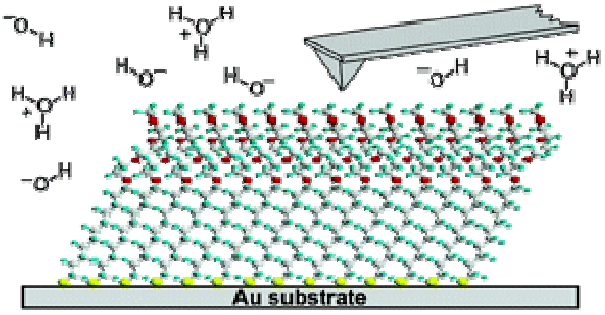

Figure I-19: Hydroxide ion formation conferring the negative charge to the SAM. Reproduced from [62]

The hydrophobicity of the substrate represents another important parameter that influences the interaction of proteins from a surface. A terminal alkyl moiety can be introduced additionally on top of the OEG units of the surfactant molecules to enhance hydrophobicity. Whitesides and co-workers studied mixed SAMs of varying composition prepared from a mixture of dodecanethiol and oligo(ethylene glycol)-terminated alkanethiol. The hydrophilicity of the mixed SAMs was measured by water contact angle and it was shown that the protein adsorption increases with the hydrophobicity of the substrate. [57, 64] The extent of protein adsorption will therefore be dictated by the balance between opposing electrostatic repulsions and hydrophobic attractions.

Grunze *et al.* [63] measured the electrical potential of SAMs prepared from methoxy(triethylene glycol) and poly(ethylene glycol) with 44 ethylene glycol units. The electrical potential was found to be negative for all surfaces leading to an electrostatic repulsion of negatively charged proteins. In spite of this repulsion, protein adsorption was still observed on certain surfaces providing further evidence that additional factors can play an important role in the protein resistance of some SAMs. This can be used to design biointerfaces, in particular those with switching properties and this will be described in the following section.

V)Dynamic Self-Assembled Monolayers

Langer *et al.* generated a (16-Mercapto)hexadecanoic acid (MHA) self-assembled monolayer with a low density and measured the water contact angle as a function of potential difference at constant temperature. [65] A striking difference was noticed in the wettability of the surface

with a change in the cosine of the contact angle when applying a positive and a negative potential. The cosine of the receding contact angle was ~0.7 while applying 80 mV and ~0.9 while applying -300 mV. Moreover, this switch occurs without changing the chemical identity of the monolayer. Langer *et al.* had predicted that these reversibly switchable surfaces could be applied in the field of interfacial engineering. Subsequently, Kong *et al.* explored these results by studying a low density SAM using the substrate as a biointerface. [66]

The low density SAM was prepared in two steps. First a gold substrate was immersed into a solution of a cyclodextrin-wrapped alkanethiolate leading to a SAM as presented in Figure I-20 (top left). Subsequently the desired SAM was obtained by removing the space-filling groups (cyclodextrin) with ethanol. Measurements were carried out in aqueous solution at pH=7.4, therefore the top of the self-assembling molecule was a negatively charged carboxylated group. Depending on the applied electric potential this top group experienced either an attraction or a repulsion by the charged substrate. Thus, each chain either pointed outwards from the surface (as shown on top of the middle of Figure I-20) or was bended (as shown at the bottom of the middle of Figure I-20). As the negatively charged head group exposure could be tailored by the sign of the applied electric potential, the adsorption of positively charged proteins like streptavidin was controlled as well (as shown on the right of the following figure).

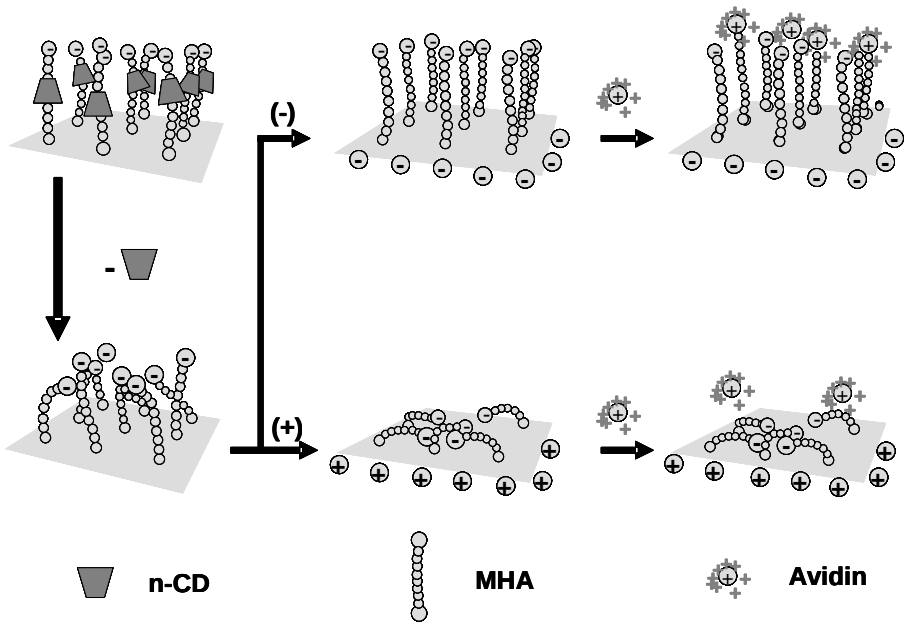

Figure I-20: The idealized illustration of the SAM used by Kong and co-workers, the transition at applied potentials and the subsequent protein assembly. Reproduced from [66]

This protein assembly control can be used for life-science devices to study proteins or biofouling but its extension to the study of systems *in vivo* is not so straightforward.

Grunze *et al.* [67] studied mixed SAMs created from a mixture of two surfactants: hexa(ethylene glycol)-terminated undecanethiol and dodecanethiol in a ratio of 95:5.

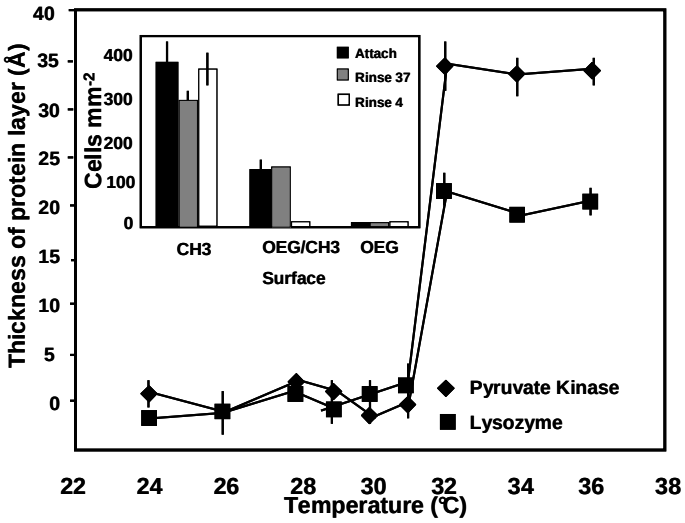

Figure I-21: Adsorption of two proteins on the mixed SAM as a function of temperature, as measured by ellipsometry of dry samples. Inset: Number of bacterial cells attached to an alkanethiol SAM, the mixed SAM, and an hexa(ethylene glycol) based SAM after 2h attachment at 37° and rinsing either 37 or 4 °C. Reproduced from [67]

The quantity of bioadhesion was a function of temperature (RT – 37°C) and this was correlated to corresponding changes in SAM structure that in turn influence its interaction with proteins.

This project was focused on the possibility to control the amount of proteins which adsorb on a self-assembled monolayer in a liquid environment. New surface-active molecules were designed and synthesized based on previous force studies performed with AFM and published in the literature. [62] AFM measurements carried out with certain SAMs showed that the strength of the interaction occurring between a partially negatively charged surface and a hydrophobic tip depends on the ionic strength of the liquid environment. When the SAM was an alkanethiol film the force showed a pure hydrophobic attraction while the interaction between an OEG-terminated SAM and a hydrophobic tip was repulsive and of electrostatic origin. It was moreover observed that the latter interaction can be modified by an external parameter: the range of the interaction could be changed by changing the ionic strength of the liquid environment. The idea of this project was to prepare a SAM that combines hydrophobic attraction and electrostatic repulsion. Functionalizing an alkanethiol with an OEG group

should allow the resulting SAM to exert both a hydrophobic attraction and an electrostatic repulsion. As the electrostatic force depends on the ion concentration, the resulting overall force can be modified by the external parameter allowing a switch from repulsion to attraction. The force experienced by the hydrophobic tip was studied in liquids of varying ion concentration to check if the switch can be observed. As some proteins are partially negatively charged and have hydrophobic moiety, the interaction of such proteins with the surface are expected to be similar to the one with the tip leading to a possible reversible adsorption of proteins on the surface.

VI) Literature

1. A. Ulman, *Chem. Rev.*, 1996, **96**, 1533-1554.
2. A. Ulman, *An Introduction to Ultrathin Organic Fims from Langmuir-Blodgett to Self-Assembly*, Academic Press, San Diego, 1991.
3. W. C. Bigelow, D. L. Pickett and D. C. Zisman, *Journal of Colloid Science*, 1946, **1**, 513-538.
4. R. G. Nuzzo and D. L. Allara, *J. Am. Chem. Soc.*, 1983, **105**, 4481-4483.
5. S. Dutta, M. Perring, S. Barret, M. Mitchell, P. J. A. Kenis and N. B. Bowden, *Langmuir*, 2006, **22**, 2146-2155.
6. R. Basu, J.-C. Lin, C.-Y. Kim, M. J. Schmitz, L. Y. Nathan, J. A. Kellar, M. J. Bedzyk and M. C. Hersam, *Langmuir*, 2007, **23**, 1905-1911.
7. M. E. McGovern, K. M. R. Kallury and M. Thompson, *Langmuir*, 1994, **10**, 3607-3614.
8. N. Tillman, A. Ulman and J. F. Elman, *Langmuir*, 1990, **6**, 1512-1518.
9. A. Ulman, *Adv. Mater.*, 1990, **2**, 573-582.
10. R. Romeo, G. Arena, L. M. Scolaro, M. R. Plutino, G. Bruno and F. Nicolo, *Inorg. Chem.*, 1994, **33**, 4029-4037.
11. C. N. Suzenik, N. Balachander, L. A. Culp, K. Lewandowska and K. Merrit, *Journal of Biomedical Materials Research*, 1990, **24**, 1307-1323.
12. C. T. Vogelson, A. Keys, C. L. Edwards and A. R. Barron, *J. Mater. Chem.*, 2003, **13**, 291-296.
13. D. LI, X. Yu and Y. Dong, *Applied Surface Science* 2007, **253**, 4182-4187.

14. P. E. Laibinis and G. M. Whitesides, *J. Am. Chem. Soc.*, 1992, **114**, 9022-9028.
15. P. E. Laibinis, G. M. Whitesides, D. L. Allara, Y.-T. Tao, A. N. Parikh and R. G. Nuzzo, *J. Am. Chem. Soc.*, 1991, **113**, 7152-7167.
16. M. Yu, D. P. Woodruff, C. J. Satterley, R. G. Jones and V. R. Dhanak, *J. Phys. Chem. B*, 2007, **111**, 10040-10048.
17. M. M. Walczak, C. Chung, S. M. Stole, C. A. Widrig and M. D. Porter, *J. Am. Chem. Soc.*, 1991, **113**, 2370-2378.
18. X. Jiang, D. A. Bruzewick, M. M. Thant and G. M. Whitesides, *Anal. Chem.*, 2004, **76**, 6116-6121.
19. J. C. Love, D. B. Wolfe, R. Haasch, M. L. Chabinyc, K. E. Paul, G. M. Whitesides and R. G. Nuzzo, *J. Am. Chem. Soc.*, 2003, **125**, 2597-2609.
20. http://www.omicron.de/index2.html?/rom/formation_of_iron_oxide_nanoparticles_and_thin_films_on_au_111_/index.html~Omicron.
21. J. C. Love, L. A. Estroff, J. K. Kriebel, R. G. Nuzzo and G. M. Whitesides, *Chem. Rev.*, 2005, **105**, 1103-1169.
22. W. Senaratne, L. Andruzzi and C. K. Ober, *Biomacromolecules*, 2005, **6**, 2427-2448.
23. S. Xu, S. J. N. Crucho-Dupeyrat, J. C. Garno, G.-Y. Liu, G. K. Jennings, T.-H. Yong and P. E. Laibinis, *J. Chem. Phys.*, 1998, **108**, 5002-5012.
24. C. D. Bain, E. B. Troughton, Y.-T. Tao, J. Evall, G. M. Whitesides and R. G. Nuzzo, *J. Am. Chem. Soc.*, 1989, **111**, 321-335.
25. http://csacs.mcgill.ca/images/Axe1.jpg.
26. P. Fenter, A. Eberhardt, K. S. Liang and P. Eisenberger, *J. Chem. Phys.*, 1997, **106**, 1600-1608.
27. M. D. Porter, T. B. Bright, D. L. Allara and C. E. D. Chidsey, *J. Am. Chem. Soc.*, 1987, **109**, 3559-3568.
28. S. Herrwerth, W. Eck, S. Reinhardt and M. Grunze, *J. Am. Chem. Soc.*, 2003, **125**, 9359-9366.
29. Y. Xia, X.-M. Zhao and G. M. Whitesides, *Microelectronics Engineering*, 1996, **32**, 255-268.
30. S. Berner, S. Biela, G. Ledung, A. Gogoll, J.-E. Backvall, C. Puglia and S. Oscarsson, *Journal of Catalysis*, 2006, **244**, 86-91.
31. Y. Wang, D. Maspoch, S. Zou, G. C. Schatz, R. E. Smalley and C. A. Mirkin, *PNAS*, 2006, **103**, 2026-2031.

32. H. B. Akkerman and B. de Boer, *J. Phys. : Condens. Matter.*, 2008, **20**.
33. M. McDowell, I. G. Hill, J. E. McDermott, S. L. Bernasek and J. Schwartz, *Applied Physics Letters*, 2006, **88**.
34. D. K. Aswal, S. Lenfant, D. Guerin, J. V. Yakhmi and D. Vuillaume, *Analytica Chimica Acta*, 2006, **568**, 84-108.
35. T. Kondo and K. Uosaki, *Journal of Photochemistry and Photobiology C: Photochemistry Reviews*, 2007, **8**, 1-17.
36. C. D. Bain and G. M. Whitesides, *Langmuir*, 1989, **5**, 1370-1378.
37. A. Lio, D. H. Charych and M. Salmeron, *J. Phys. Chem. B*, 1997, **101**, 3800-3805.
38. O. Azzaroni, M. Cipollone, M. E. Vela and R. C. Salvazerra, *Langmuir*, 2001, **17**, 1483-1487.
39. G. Brunoro, A. Frignani, A. Colledan and C. Chiavari, *Corrosion Science*, 2003, **45**, 2219-2231.
40. F. Zucchi, V. Grassi, A. Frignani and G. Trabanelli, *Corrosion Science*, 2004, **46**, 2853-2865.
41. M. Kalltorp, S. Oblogina, S. Jacobson, A. Karlsson, P. Tengvall and P. Thomsen, *Biomaterials*, 1999, **20**, 2123-2137.
42. G. MacBeath, *Nature Biotechnology*, 2001, **19**, 828-829.
43. S. Fields, *Science*, 2001, **291**, 1221-1224.
44. S. Hleli, C. Martelet, A. Abdelghani, F. Bessueille, A. Errachid, J. Samitier, H. C. W. Hays, P. A. Millner, N. Burais and N. Jaffrezic-Renault, *Materials Scence and Engineering C*, 2006, **26**, 322-327.
45. J. Halamek, A. Makower, P. Skladal and F. W. Scheller, *Biosensors and Bioelectronics*, 2002, **17**, 1045-1050.
46. A. Subramanian, J. Irudayaraj and T. Ryan, *Sensors and Actuators B*, 2006, **114**, 192-198.
47. M. T. Cygan, G. E. Collins, T. D. Dunbar, D. L. Allara, C. G. Gibbs and C. D. Gutsche, *Anal. Chem.*, 1999, **71**, 142-148.
48. C. D. Hodneland, Y.-S. Lee, D.-H. Min and M. Mrksich, *PNAS*, 2002, **99**, 5048-5052.
49. C. Boozer, Q. Yu, S. Chen, C.-Y. Lee, J. Homola, S. S. Yee and S. Jiang, *Sensors and Actuators B*, 2003, **90**, 22-30.
50. V. A. Tegoulia and W. Rap, *Langmuir*, 2001, **17**, 4396-4404.
51. S. Chen, L. Liu and S. Jiang, *Langmuir*, 2006, **22**, 2418-2421.
52. Y.-Y. Luk, M. Kato and M. Mrksich, *Langmuir*, 2000, **16**, 9604-9608.

53. E. Ostuni, R. G. Chapman, M. N. Linang, G. Meluleni, G. Pier, D. E. Ingber and G. M. Whitesides, *Langmuir*, 2001, **17**, 6336-6343.
54. P. Kinshott and H. J. Griesser, *Current Opinion in Colloid and Interface Science*, 1999, **4**, 403-412.
55. M. N. Mar, B. D. Ratner and S. S. Yee, *Sensors and Actuators B*, 1999, **54**, 125-131.
56. P. Harder, M. Grunze, R. Dahint, G. M. Whitesides and P. E. Laibinis, *J. Phys. Chem. B*, 1998, **102**, 426-436.
57. K. L. Prime and G. M. Whitesides, *J. Am. Chem. Soc.*, 1993, **115**, 10714-10721.
58. R. L. C. Wang, H. J. Kreuzer and M. Grunze, *Phys. Chem. Chem. Phys.*, 2000, **2**, 3613-3622.
59. M. Zolk, F. Eisert, J. Pipper, S. Herrwerth, W. Eck, M. Buck and M. Grunze, *Langmuir*, 2000, **16**, 5849-5852.
60. K. Feldman, G. Hähner, N. D. Spencer, P. Harder and M. Grunze, *J. Am. Chem. Soc.*, 1999, **121**, 10134-10141.
61. C. Dicke and G. Hähner, *J. Phys. Chem. B*, 2002, **106**, 4450-4456.
62. C. Dicke and G. Hähner, *J. Am. Chem. Soc.*, 2002, **124**, 12619-12625.
63. Y.-H. M. Chan, R. Schweiss, C. Werner and M. Grunze, *Langmuir*, 2003, **19**, 7380-7385.
64. C. Pale-Grosdemange, E. S. Simon, K. L. Prime and G. M. Whitesides, *J. Am. Chem. Soc.*, 1991, **113**, 12-20.
65. J. Lahann, S. Mitragoti, T.-N. Tran, H. Kaido, J. Sundaram, I. S. Choi, S. Hoffer, G. A. Somorjai, R. Langer , *Science*, 2003, **299**, 371-374
66. Y. Liu, L. Mu, B. Liu, S. Zhang, P. Yang and J. Kong, *Chem.Comm.*, 2004, 1194-1195.
67. S. Balamurugan, L. K. Ista, J. Yan, G. P. Lopez, J. Fick, M. Himmelhaus and M. Grunze, *J. Am. Chem. Soc.*, 2005, **127**, 14548-14549.

Chapter 2

Experimental Techniques used for Surface Characterisation and Surface Property Study

This thesis describes the work carried out with newly synthesized ultrathin films. It is consequently essential to initially have a complete characterization of these surfaces. The principle of each employed surface analysis technique is described in this chapter. These techniques include X-ray Photoelectron Spectroscopy (XPS), ellipsometry, and contact angle measurements. In addition to surface characterization, this work aims to determine one particular surface property concerning the interactions between the synthetic organic surfaces and hydrophobic particles. This study involves an Atomic Force Microscope (AFM) performing so-called force-distance curves which will also be explained in this section.

I) X-ray Photoelectron Spectroscopy

X-Ray Photoelectron Spectroscopy (XPS) is an important experimental approach for defining the nature of solid surfaces. It is a powerful analytical tool for determining the surface compositions of flat samples within approximately the first 20 Å of the surface. [1] This non destructive technique enables the presence of all the expected elements, except hydrogen and helium, to be checked and a possible contamination by unforeseen atoms to be detected. [2] Information about the chemical and electronic states of the elements can also be determined,

which explains why ESCA (Electron Spectroscopy for Chemical Analysis) is another designation for this analysis. [3] In addition to the qualitative study, the relative amounts of the chemical elements of the sample, and thus the empirical formula of the sample are provided, [4] as well as surface coverage quantification. [5, 6]

1) Basic Principles

This technique exploits the photoelectric effect represented in Figure II-1. The photoelectric effect is the generation of electrons, called photoelectrons, after irradiating the target sample with X-rays.

The photoelectrons are collected and their kinetic energy is measured with a spectrometer.

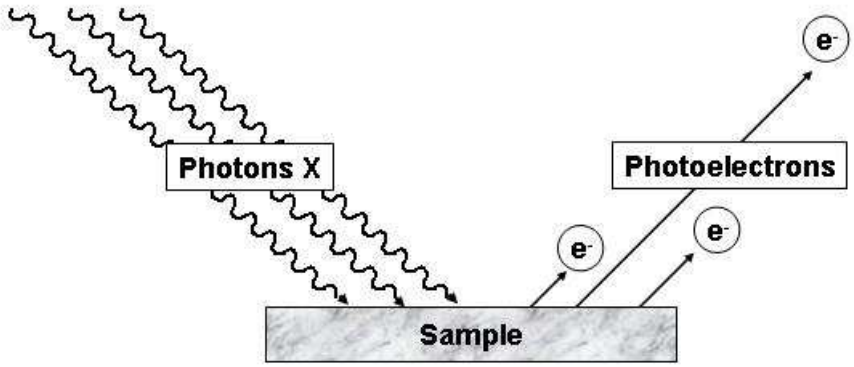

Figure II-1: Representation of the photoelectric effect. Inspired from [7]

The sample is irradiated with X-rays whose energy is known. The incident photon energy is then transmitted to the photoelectron in the form of kinetic energy. If the X-ray energy, or frequency, is high enough, an electron is emitted from the material. The emission of an electron, bonded to the atom with certain energy, leads to the ionization of this atom. This process can be represented by the equation:

Equation II-1: $A + E_{Photon} \rightarrow A^{+} + e^{-}$

where A is the atom and A^+ the ion resulting from the electron ejection, E_{Photon} is the energy of a photon which is equal to hν (h is Planck constant, 6.62×10^{-34}J.s, and ν is the frequency in Hertz, Hz, of the radiation) according to the Einstein relation.
The energy conservation principle gives:

Equation II-2: $$E(A)+h\nu=E(A^+)+KE$$

where E(A) and $E(A^+)$ are the energies of the neutral atom and of the ion respectively, and KE is the emitted electron energy which is only kinetic energy. The difference in energy between the neutral and the ionized state of the atom equals the binding energy of the emitted electron, BE. The kinetic energy of photoelectrons is thus given by: [4]

Equation II-3: $$KE=h\nu-BE$$

Knowing the photon energy and measuring the kinetic energy of the photoelectrons allows the binding energies of the electron orbitals in atoms to be measured. The atomic core levels of each element have a defined binding energy BE whose measurements were performed and gathered to give a binding energy database. The XPS analysis gives a spectrum of peaks which are assigned to an element using the database. The energy distinction in the photoelectron peaks providing from atoms with different electronic state allows the chemical analysis.

Quantitative analysis is achieved by measuring and comparing the photoelectron peak intensity (height or, preferably, the area).

2) Instrumentation

Any XPS instrument, schematised in Figure II-2, has three essential components: an X-ray source, an energy analyser, and an electron detector. A vacuum chamber is also necessary as measurements are performed under ultrahigh vacuum.

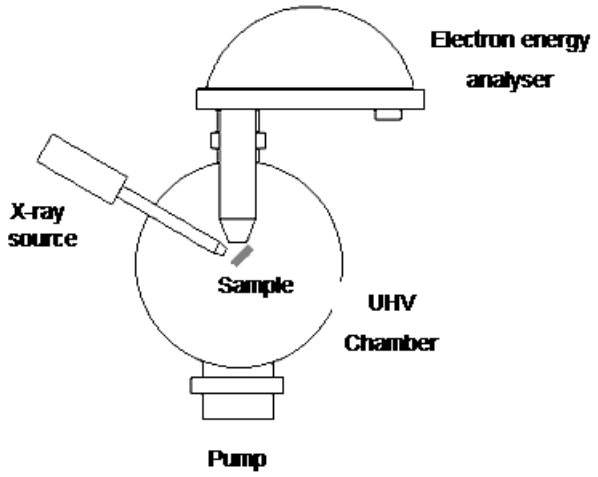

Figure II-2: Representation of the main components of a XPS experiment

i). X-ray Source

X-ray production starts with the creation of electron vacancies in the inner shells of a metal by bombarding the metallic anode with accelerated electrons. As shown in Figure II-3, charged particles, called thermions, are produced by heating a metal filament (known as the Edison or Richardson effect). Using a tungsten filament for instance, electrons are formed and then accelerated by a high voltage (10-100 kV). The electron bombardment leads to the ejection of inner electrons of the target metal which is commonly magnesium or aluminium.

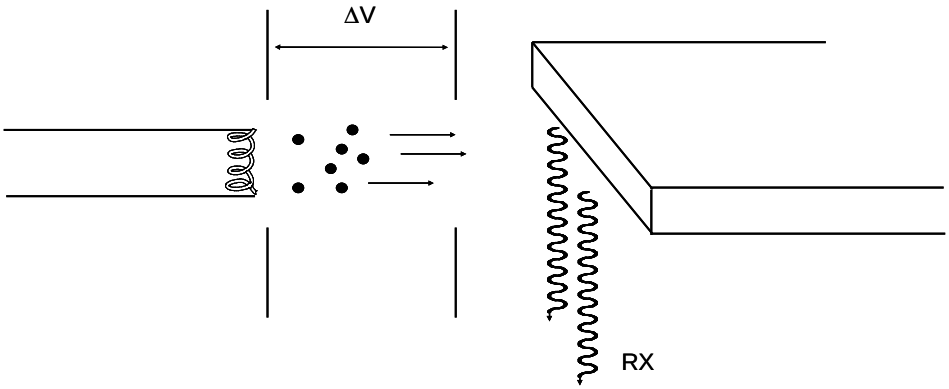

Figure II-3: Schematic of the X-ray source

Vacancies are filled by electrons from higher energy levels falling to occupy it producing X-rays whose frequency depends on the energy difference of the levels between which the transition takes place ($\Delta E=h\nu$).

The most common X-ray lines are the AlKα and MgKα whose photon energy is 1486.6 eV and 1253.6 eV respectively.

Some XPS machines use monochromatized radiation to reduce the line width, to remove unwanted peaks, and to improve the resolution of spectra. [4] This can be achieved using a quartz crystal as shown in Figure II-4.

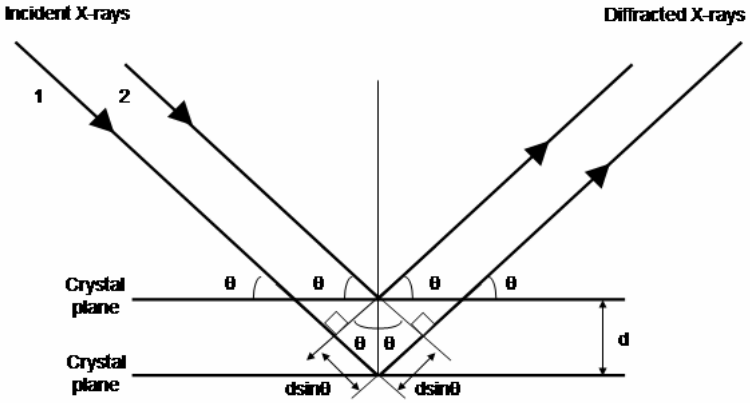

Figure II-4: Representation of diffraction of X-rays at a quartz crystal used to obtain monochromated X-rays. Reproduced from [8]

The thickness of the quartz layer d is determined by Bragg's equation:

$n\lambda=2d\sin\theta$

Where n is the diffraction order, λ the wavelength and θ the Bragg angle. θ is the angle between the surface and the incident beam. X-rays can be reflected on the two planes of the crystal, producing a difference in the path length $2d\sin\theta$. To have constructive interference, this distance must be a whole number multiple of the wavelength.

The X-rays are now focused on the sample leading to photoelectrons whose energy is analyzed.

The photoelectric electrons escape from the sample with too high a speed to allow a high resolution analysis. [8] It is thus necessary to retard them before they enter the analyzer using transfer lenses, either electrostatic or magnetic. Retarded electrons enter the analyzer which selects electrons according to their kinetic energy. The main analyzer for XPS is the hemispherical sector analyzer, HSA.

ii). Energy Analyser

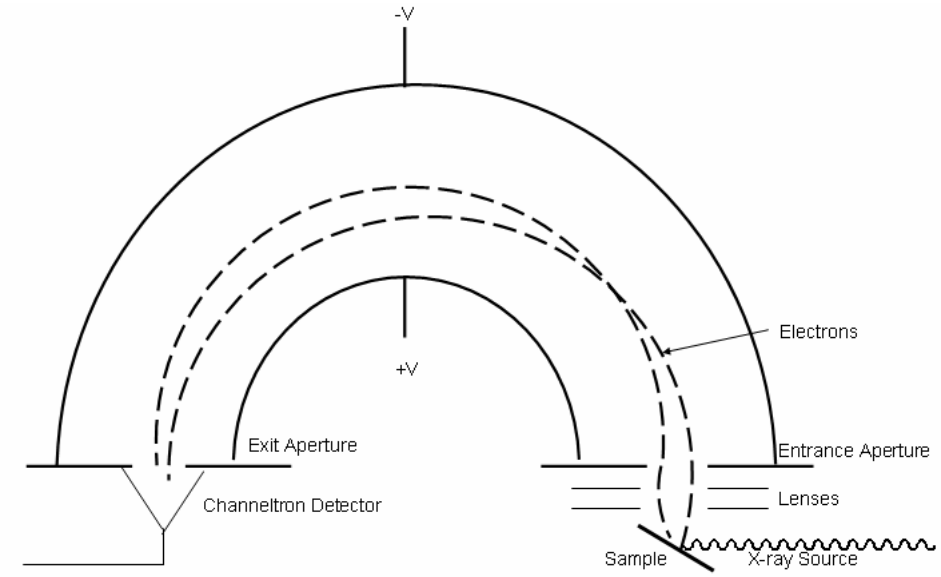

Figure II-5: Electrostatic deflection analyser: Hemispherical Analyzer. Reproduced from [4]

A potential is applied between two concentric hemispherical electrodes, so that the outer one is more negative than the inner one. Retarded electrons enter the HSA tangentially between the two hemispheres and they will be able to reach the detector without striking the walls of the electrodes if their energy E obeys:

Equation II-4: $E = ke\Delta V$

with E, the electron kinetic energy, e the charge of an electron, ΔV the potential difference between the hemispheres, and k, the spectrometer constant

Electrons with a higher or lower kinetic energy than keΔV will strike the outer or inner hemisphere respectively.

Thanks to the HSA only electrons with a kinetic energy in a certain range will arrive at the detector. To obtain a measurable current in order to count the electrons for each kinetic energy, an electron multiplier is used. The arriving electrons are first accelerated to enter a funnel-shaped collector. This tube is curved so that the electrons can strike the internal walls and emit secondary electrons through a phenomenon that resembles the photoelectric effect, but with electrons as incident particles.

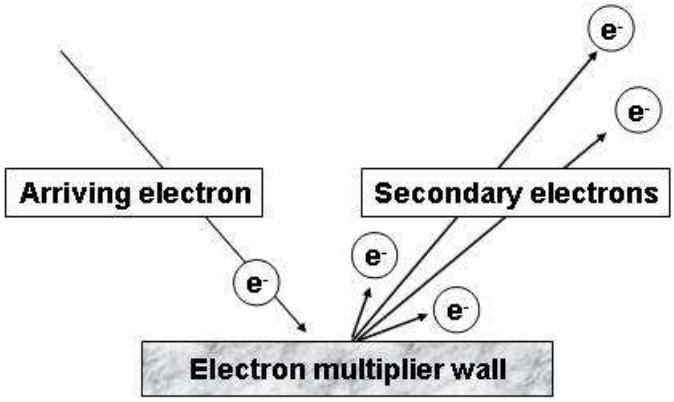

Figure II-6: Electron multiplier

Secondary electrons are accelerated and then this event repeats itself many times and thus, the amplification can reach 10^8.

The number of electrons reaching the detector with a certain kinetic energy is then measured. The counts-kinetic energy or counts-binding energy graph can therefore be plotted allowing a qualitative analysis by comparing the peak energies with database values and a quantitative study by comparing the area under the peaks corresponding to each element after subtracting the background.

3) Experimental

X-ray Photoelectron spectra were obtained using a VG Escalab II (VG Scientific Ltd., UK) and Al Kα radiation (1486.6 eV). During the analysis, the pressure in the test chamber was kept around 2×10^{-10} mbar. The detector had a takeoff angle of 90° to the surface. CasaXPS (Casa Software Ltd., UK) was the software used for the analysis.

II) Ellipsometry

Ellipsometry is a surface analytical technique allowing the measurement of optical constants (refraction and extinction coefficients) and thickness of thin layers. [9, 10]

In addition, information about roughness, alloy ratio, crystallinity of films or depth profile of material properties can also be provided by this technique.

1) Basic Principles

The physical phenomenon used in ellipsometry, illustrated in Figure II-7, is the reflection of polarised light on the sample surface leading to a change in the polarization state of the light which is linked to the physical properties of the material.

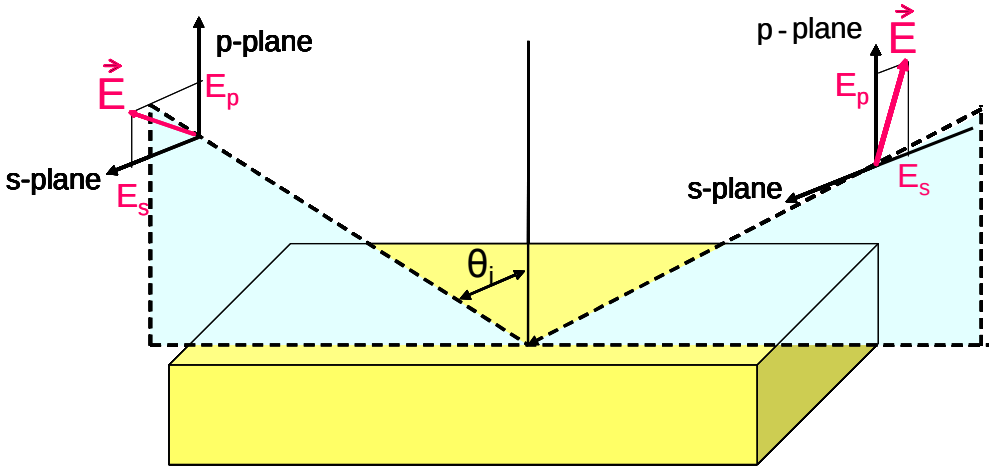

Fig II-7: Schematic of the geometry of an ellipsometry experiment

This polarisation state change, gives the fundamental equation of ellipsometry:

Equation II-5: $$\rho = \frac{r^p}{r^s} = \tan\Psi e^{j\Delta}$$

where Δ is the phase difference between the p and s waves before and after the reflection. The p-s coordinate system consists of the s-direction, taken perpendicular to the direction of propagation and parallel to the sample surface, and the p-direction perpendicular to the direction of propagation and contained in the plane of incidence.

Ψ is linked to reflection coefficients with:

Equation II-6: $\tan\Psi = \frac{\left|r^p\right|}{\left|r^s\right|}$

where r^p and r^s are the reflection coefficients which will be explained through an example. Both Δ and Ψ are measured by an analyser.

Considering the reflection of the light on a large sample, like in Figure II-7, two states of the light, before and after reflection, can be represented. In the most general case, the polarisations are elliptic.

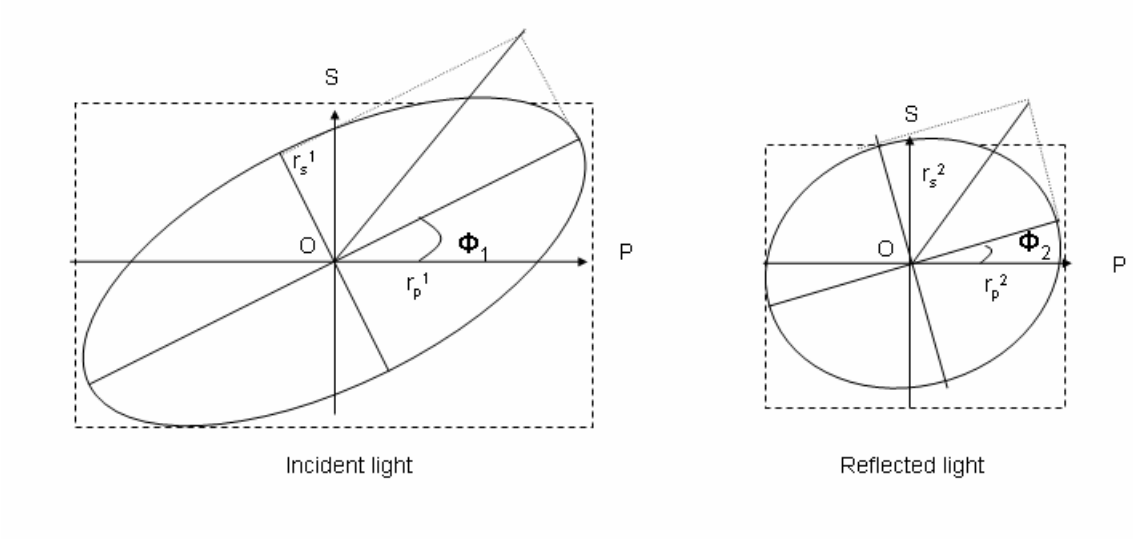

Figure II-8: Elliptic polarisation state of the incident and reflected light

r_s^1 and r_p^1 are the components of the incident light parallel and perpendicular to the plane of incidence, in media 1(air) and r_s^2 and r_p^2 are the components of the light after reflection on media 2(the material of the sample). Φ_1 and Φ_2 are called the azimuth angles of the ellipses.
The incident light state is known and the reflected wave is decomposed by an analyser allowing the calculation of reflection coefficients defined by:

Equation II-7: $r_{12}^p = \frac{n_2\cos\phi_1 - n_1\cos\phi_2}{n_2\cos\phi_1 + n_1\cos\phi_2}$

And

Equation II-8: $r_{12}^s = \frac{n_1\cos\phi_1 - n_2\cos\phi_2}{n_1\cos\phi_1 + n_2\cos\phi_2}$

where n_1 and n_2 are the refraction indices of the air and the material constituting the substrate, respectively.

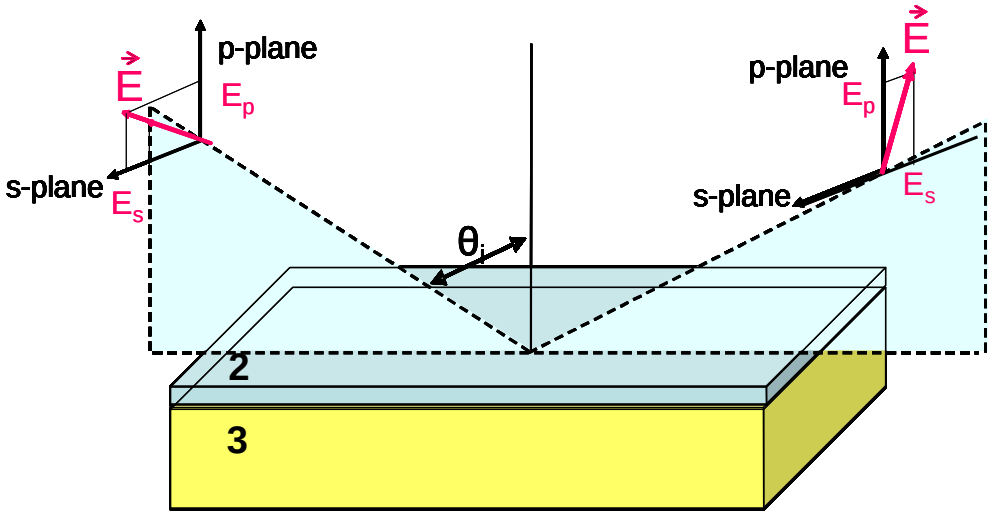

Fig II-9: Schematic of the geometry of an ellipsometry experiment on a sample with a thin layer

With a thin layer of thickness d of a material 2 on top of a thick layer of 3, represented in Figure II-9, the dephasing β between parallel or perpendicular component before and after the reflection is:

$$\textbf{Equation II-9:}\quad \beta = 2\pi\left(\frac{d}{\lambda}\right)n_2\cos\phi_2$$

and

$$\textbf{Equation II-10:}\quad r^p = \frac{r_{12}^p + r_{23}^p \exp(-j2\beta)}{1 + r_{12}^p r_{23}^p \exp(-j2\beta)},$$

$$\textbf{Equation II-11:}\quad r^s = \frac{r_{12}^s + r_{23}^s \exp(-j2\beta)}{1 + r_{12}^s r_{23}^s \exp(-j2\beta)}$$

where r^s_{23} and r^p_{23} are the reflection coefficients for the 2-3 interface.

Measuring Ψ and Δ and solving the fundamental equation of ellipsometry allows the calculation of two parameters, namely the refraction index n_2 and the thickness d of the thin

layer. Ellipsometry measurements were performed to determine the thickness of our self-assembled monolayers. The optical measurement gives the polarization states Ψ and Δ but not the desired parameter directly. An "inverse modelling problem" had to be solved to obtain this thickness. Thus, a model was built representing the sample with its different layers. Ψ and Δ were evaluated from the model giving a fit which was compared to the measured data. This estimation was performed changing the model itself, modifying the thickness until experimental curves and fit were overlaid. The thickness of the layer was the one giving the best fit.

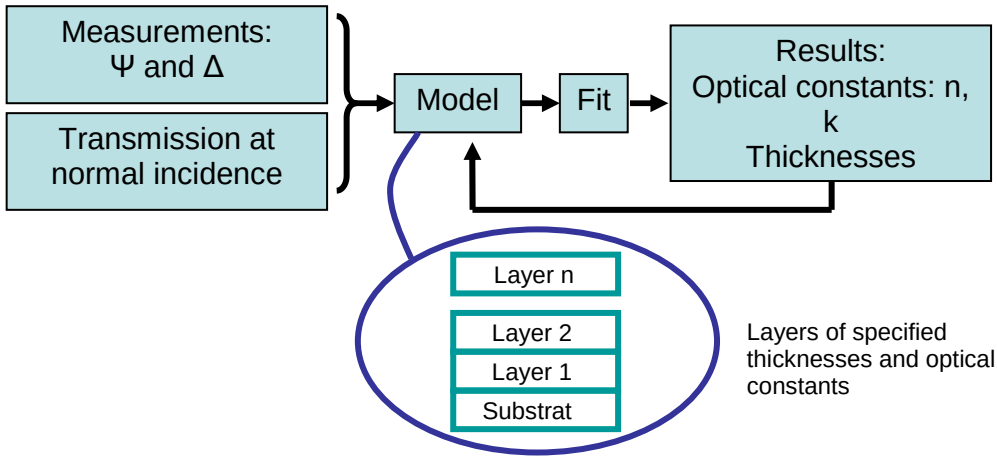

Figure II-10: Ellipsometry analysis principle

Unfortunately, this analysis would only be this simple if the SAM thickness were the only unknown parameter influencing the estimation of Ψ and Δ. The SAMs were on a substrate made of silica covered with titanium and gold. If each layer of the substrate were perfectly defined, it would be possible to estimate its contribution on Ψ and Δ and obtain the SAM thickness easily. To perfectly define the substrate layers, the thickness as well as the optical constants had to be measured. Some data banks exist containing optical parameters for materials and the thickness given by the supplier could be used. However, the titanium and gold optical values in the data banks were obtained for thick samples while the layers on the silica wafers were thin and obtained by evaporation. As the density of the layers could have been different from the nominal bulk values their optical parameters could be different as well leading to a poor estimate of Ψ and Δ. Moreover, the thickness value is probably different from one wafer to another but also from one point to another on the same wafer, due to the thermal evaporation deposition process. This technique consists of evaporating the material to

be deposited by heating it under vacuum. The solid material is put in a crucible at the centre of the vacuum chamber. Its vapour flow, from the crucible to the target (the wafer) is conical; this could explain why the condensed layer could be thicker in the middle of the wafer than close to the edges.

The first step consisted of perfectly defining the substrate layer by layer. It was necessary to fully characterize titanium and gold and to define the substrate with the two layers before adding and characterising the SAM.

A titanium layer was evaporated on a piece of silica and on a quartz disc, whose optical parameters and thickness were already known. Measurements were repeated on several substrates in order to enhance the precision of the characterisation data.

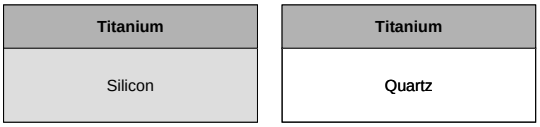

Figure II-11: Samples used for the titanium layer characterisation

Ellipsometry measurements were performed to determine the optical constants of the material and the thickness of this layer. These measurements were made at several angles of incidence (45°, 50°, 55°, 60°, 65°, 70°, and 75°) to acquire the large amount of data necessary for complete characterization. As quartz is transparent, a transmission measurement was carried out to give supplementary data.

As a result, the refractive index, the extinction coefficient, transmission (Figure 12) and the thickness were found. As curves and fit were similar for the two samples (on silica and quartz), only the results on quartz will be presented here.

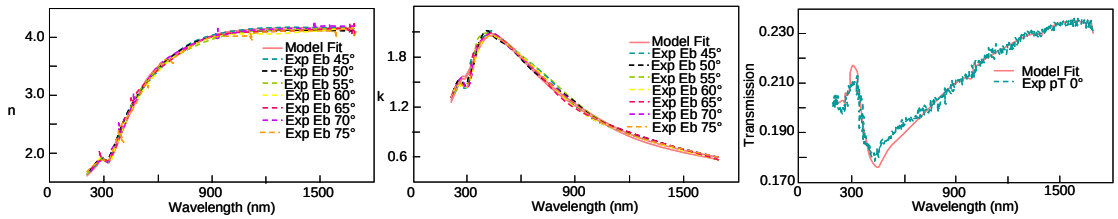

Figure II-12: Refractive index, extinction coefficient and transmission of titanium on a quartz disc

The model of a titanium layer, with the properties found on silica or quartz gave a fit of Ψ and Δ (Figure 13) similar to the experimental values. Therefore, the material could be considered to be fully characterized.

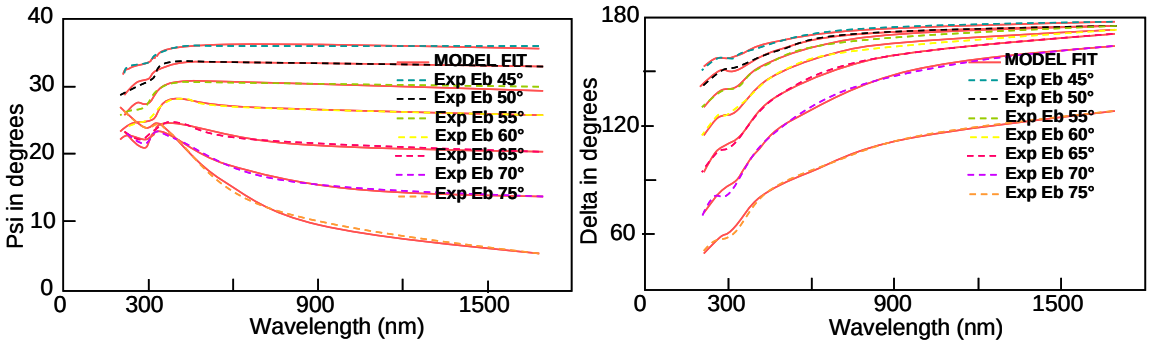

Figure II-13: psi and delta for titanium on a quartz disc

The same measurements were performed for a gold layer.

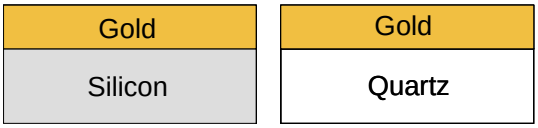

Figure II-14: Samples used for the gold layer characterisation

Hence, the refractive index, extinction coefficient and transmission (Figure 15), and the thickness were all known. The material is fully characterized allowing the thickness to be determined.

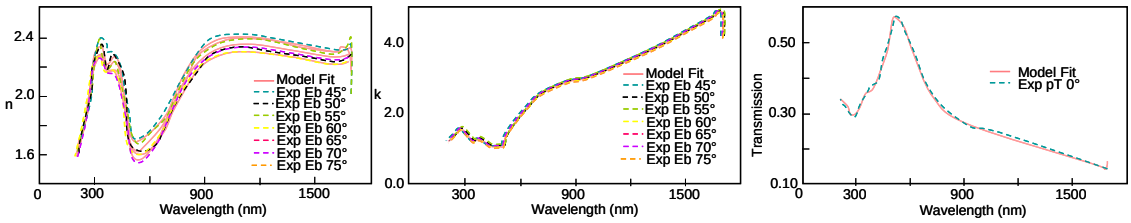

Figure II-15: Refractive index, extinction coefficient, and transmission for gold on a quartz disc

As for titanium, the fit found for Ψ and Δ (Figure 16) confirmed that the material was well characterized.

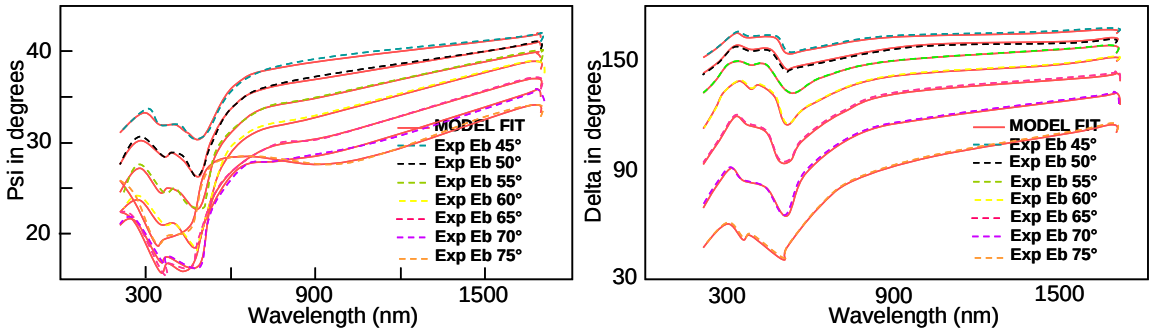

Figure II-16: Psi and delta for gold on a quartz disc

A gold layer was deposited on the sample with the titanium layer in order to characterize the adhesion promoter.

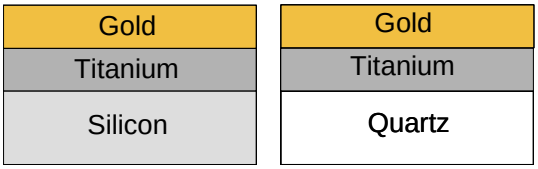

Figure II-17: Samples used for the substrate (titanium and gold layers) characterisation

As the titanium layer thickness and the optical parameters were known for both materials, only the thickness of the gold layer was missing. As shown by the fit for Ψ and Δ (Figure 18) the whole substrate was then fully characterized.

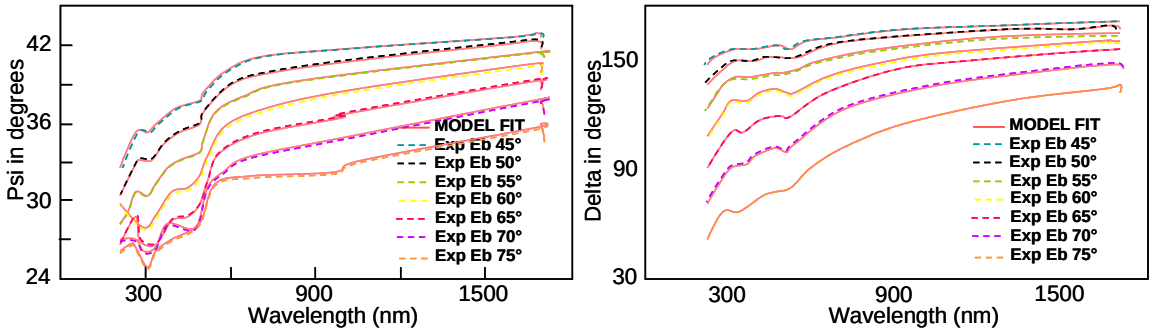

Figure IIV-18: Psi and delta for the substrate (titanium and gold) on a quartz disc

2) Instrumentation

An ellipsometer, represented in Figure II-19, has a light source, polariser(s), and a detector.

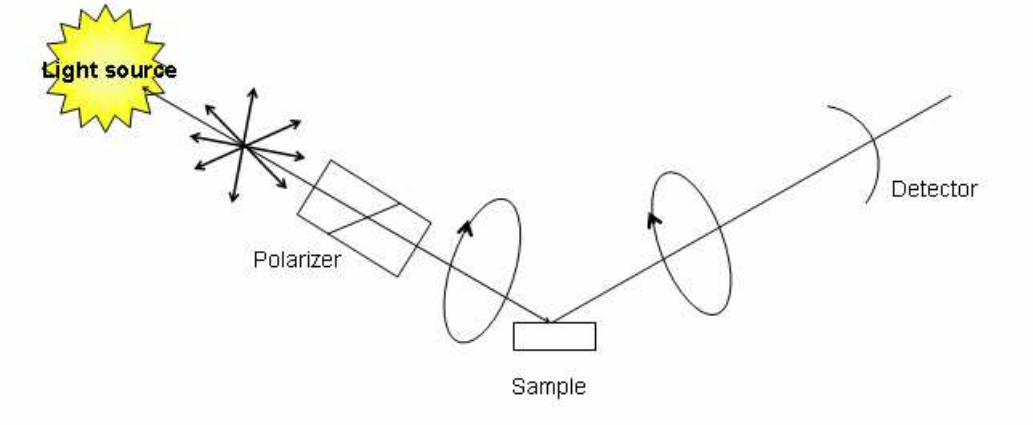

Figure II-19: Common optical components of an ellipsometer

The light source can be a laser if the ellipsometer is for single-wavelength measurements, or several sources (for instance a deuterium, xenon, and silicon lamp) can be utilized to match the desired range of wavelengths.

A polarizer is placed after the light source to set the polarization state of the incident light. The elliptic reflected light goes through the detector where the polarisation state difference from the incident light is determined. The M-2000 ellipsometer uses a silicon CCD detector.

3) Experimental

Ellipsometry measurements were performed with an M-2000DI^{TM} spectroscopic ellipsometer (J. A. Woollman Co., Inc., USA). The integrated data acquisition software is WASE32$^{®}$.

III) Contact Angle

The contact angle measurement is a straightforward way to estimate properties of a surface, to determine the nature of the solid, or to detect a coating or contamination of the surface, by observing the shape of a solvent droplet resting on the solid surface.

1) Basic Principles

The interaction between the substrate and a solvent is evaluated via the contact angle formed by a droplet of this solvent on the surface. The contact angle θ is the angle between the tangent of a liquid droplet measured at the three phase boundary and the surface of the solid on which the droplet is deposited. Its measurement is important in surface characterization but the practical use is limited to macroscopic dimensions, linked to the droplet size.

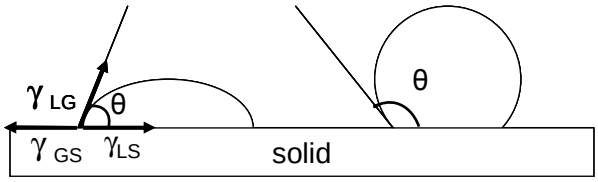

Figure II-20: Contact angle representation

The shape of the droplet depends on the Young-Laplace equation:

Equation II-12: $\gamma_{LS} + \gamma_{LG}\cos\theta - \gamma_{GS} = 0$

where γ_{LS}, γ_{LG}, and γ_{GS} are the interfacial energies of the liquid/vapour, solid/vapour, and solid/liquid phases respectively. It defines the wetting phenomenon. A low value of θ shows that the liquid wets or spreads on the surface while the wetting is poor for a high value of θ. If the liquid is water, contact angle measurement allows the hydrophilic or hydrophobic properties of the surface to be determined. It is also possible to calculate the surface free energy when several liquids with known surface tensions are used.

2) Instrumentation

A light source illuminates the sample surface placed on the sample holder, as well as the droplet applied by a microsyringe. Magnifying lenses allow the observation of the liquid droplet and a line drawn on a rotating part of the goniometer is positioned at the tangent line of the droplet at the three phase boundary. The inclination angle is then measured with a fixed scale inscribed on another piece of the goniometer.

3) Experimental

In this work, advancing deionised water contact angles were measured with a G10 goniometer microscope (KRÜSS GmbH, Hamburg, Germany). Droplets were dispensed from a microburette and measurements were taken under ambient conditions.

IV) Atomic Force Microscopy

To give some background about Scanning Probe Microscopy's (SPM), its history started with the first Scanning Tunnelling Microscope (STM) constructed by Gerd Binnig and Heinrich Rohrer (Nobel Prize in physics in 1986) in the IBM laboratories in Zurich. [11] The STM concept, based on the tunnelling effect, allows the study of a material surface at an atomic scale, opening the possibility of imaging conductive sample surfaces.

In order to image insulating surfaces, several Scanning Probe Microscopes were subsequently developed [12] among them, the Atomic Force Microscope (AFM). Atomic Force Microscopy was introduced by Binnig *et al* in 1986. [13, 14] AFM, in contrast to STM, can study and image both conductors and insulating materials with atomic resolution.

1) Instrumentation

The sample holder depends on the environment in which measurements are performed. The sample is either maintained with clips for experiments in air, or put in a liquid cell and covered with a solution for manipulations in liquid.

The tip, typically composed of silicon (Si) or silicon nitride (Si_3N_4), is mounted at the end of a cantilever.

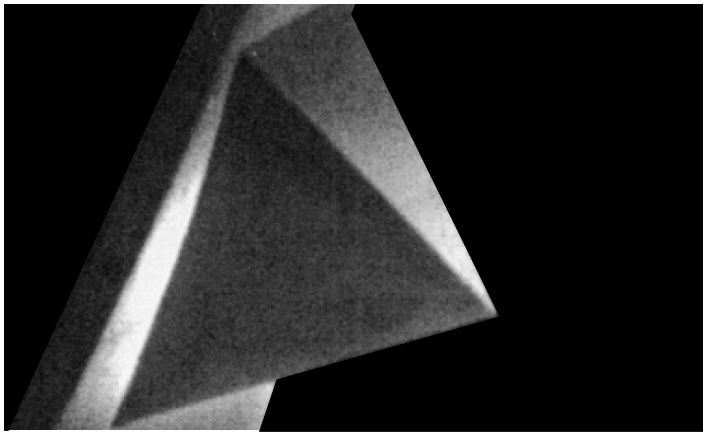

Figure II-21: Scanning electron microscopy image of a gold-coated cantilever with attached probe. The inset shows a high magnification view of the area near the end of the tip. Reproduced from [15]

As shown in Figure II-22, several techniques to measure the cantilever deflection exist: [16] They comprise a capacity measurement, [17] an STM which detects the cantilever position, or a fiber interferometer. [18]

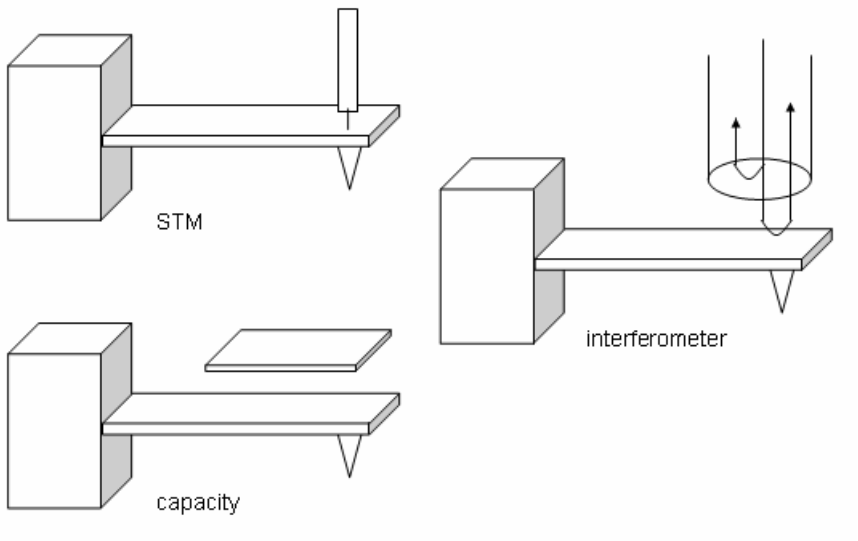

Figure II-22: Different ways to detect the cantilever deflection

The most common method uses the optical reflection of a laser beam off the back of the cantilever, made reflective beforehand by being coated with a gold layer for instance. Deflections of the cantilever cause the reflected laser beam to change its angle. The motion of the reflected laser beam is detected by a four quadrant photodiode hit by the reflected laser beam. When the laser spot moves from the central position, a voltage difference is created, which reports the cantilever deflection.

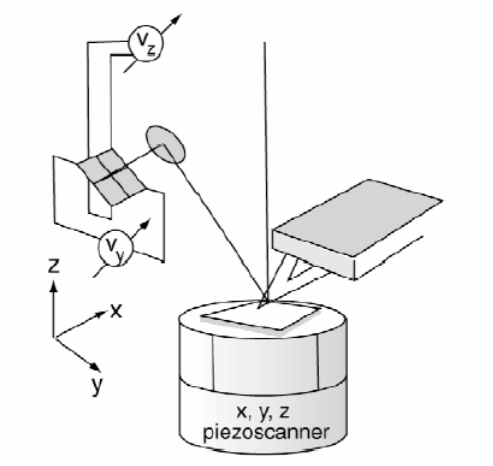

Figure II-23: Schematic of an atomic force microscopy and direct surface measurements. Reproduced from [19]

The photodiode is linked to a piezoelectric positioner in order to maintain the cantilever deflection constant when the surface is imaged or to control the distance between the sample and the tip during force measurements by controlling the voltage on the photodiode.

2) Basic Principles

i). Imaging

Instead of the tunnelling current, AFM uses the interaction forces between the probing tip mounted on a cantilever and the sample surface via the measurement of the cantilever deflection, resulting from the interaction between the surface and the tip. While the tunnelling current was kept constant during the STM surface scanning, it is the AFM cantilever

deflection, which is maintained constant with the feedback loop recording the vertical tip displacements.

a. Forces

If measurements were performed in ambient conditions, ambient humidity could give rise to a thin water layer on the sample surface. When the tip would be close to the surface, water molecules would attract it. [16, 20, 21] In our project, as all AFM measurements were performed in aqueous solution, the capillary force does not act on the tip. Operation in liquid has other advantages: the total force exerted on the tip is reduced, avoiding damage of sensitive samples, and biological environments can be reproduced. Chemical, repulsive, and van der Waals interactions can also be sensed by the AFM probe, [16] but focus is particularly directed on electrostatic double-layer and hydrophobic forces because they are the main interactions acting between our SAMs and the tip.

b. Electrostatic Force

As explained in the previous chapter, OEG-terminated alkanethiol SAMs adsorb hydroxide ions from solution leading to a negative charge of the surface. When the sample is put into an electrolyte solution, compensating counterions are attracted by the surface. Counterions attracted by the sample to re-establish the electroneutrality close to it can be divided into two layers. One layer is composed of fixed counterions linked to the surface forming the Stern layer. The other layer, the diffuse layer, is made of mobile counterions close to the surface. The limit between the Stern layer and the diffuse layer is called the Helmholtz plane. These two layers constitute the electric double layer. Thus, the counterion concentration is high close to the surface and decreases progressively further from the surface until reaching the bulk concentration. Moreover, near the surface, there is a co-ion deficit as well; they are repelled from the surface by electrostatic forces. The density of both counterions and co-ions decays or increases, respectively, exponentially with distance from the surface, described by the Boltzman distribution: [22]

Equation II-13: $\rho = \rho_0 \exp\left(-\frac{ze\psi}{kT}\right)$

where ρ is the number density of ions of valence z, ρ_0 is the ionic concentration in the bulk and ψ is the electrostatic potential.

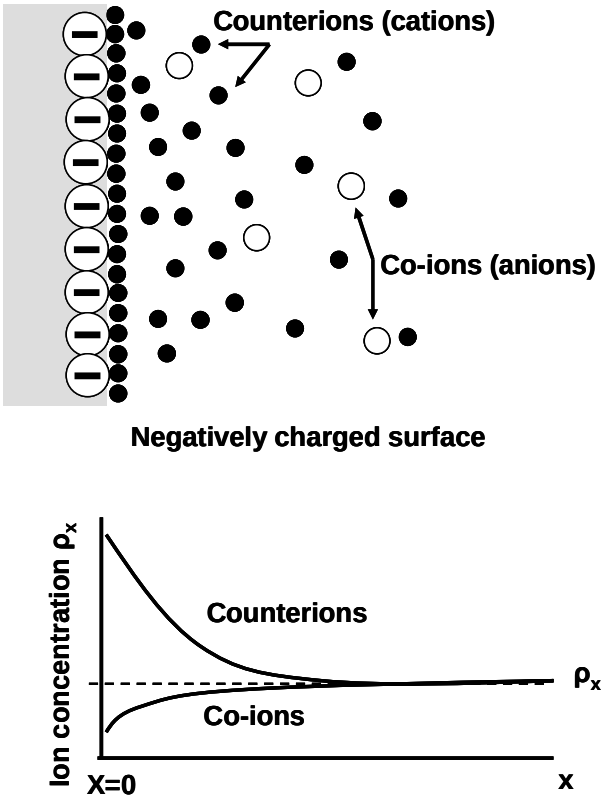

Figure II-24: Near a charged surface there is an accumulation of counterions (ions of opposite charge to the surface charge) and a depletion of co-ions, shown graphically for a 1:1 electrolyte, where ρ_∞ is the electrolyte concentration in the bulk or 'reservoir' at x = ∞. Reproduced from [22]

The concentration difference between anions and cations creates an electric potential which equals Ψ_0 at the sample surface and linearly decreases to ζ at the Helmoltz plane as represented in Figure II-25. Beyond this plane, the electric potential decreases exponentially according to the Gouy-Chapman theory: [22]

Equation II-14: $\Psi_x = \zeta \exp[-\kappa x]$

where Ψ_x is the electric potential at a distance x from the surface, ζ is the electric potential on the Helmoltz plane and κ^{-1} is the exponential decay length or the so-called Debye length (this is the distance from the surface where electroneutrality is reached in the solution). The electric double layer thickness is influenced by the ionic strength C of the solution which was considered to be equal to the ion concentration in this study, and the nature of the electrolyte. The higher the ionic strength, the more compressed the electrical double layer will be. The relation between the Debye length and the ion concentration can be obtained from the Grahame equation and is given by: [23]

Equation II-15: $\kappa^{-1} = 0.304/\sqrt{C}$ nm

for 1:1 electrolytes, e.g. NaCl

Equation II-16: $\kappa^{-1} = 0.176/\sqrt{C}$ nm

for 2:1 electrolytes, e.g. K_2CO_3

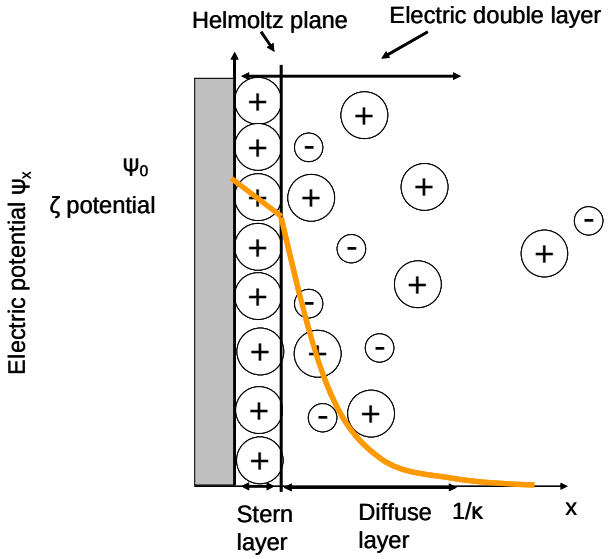

Figure II-25: Schematic representation of the electric double layer and of the evolution of the electric potential as a function of the distance from the surface

The potential difference gives rise to the electrostatic double-layer force. The intensity of this interaction appearing in an aqueous salt solution between a charged sphere, with radius R, and a flat surface in case of constant charge densities is described by the expression:

Equation II-17: $$F_{el} = \frac{2\pi R}{\kappa \varepsilon \varepsilon_0}\left[\left(\sigma_1^2 + \sigma_2^2\right)2e^{-2\kappa x} + 2\sigma_1\sigma_2 e^{-\kappa x}\right]$$

where ε_0 is the permittivity of free space, ε is the dielectric constant of the electrolyte solution, σ_1 and σ_2 are the surface charge densities of the sphere and the surface, and x is the distance between the two bodies.

c. Hydrophobic Force

The stable network of water molecules held together by hydrogen bonds is disrupted by the intrusion of hydrophobic solutes. A special type of hydration, the hydrophobic hydration takes place when such molecules are added to water.

The molecular mechanism of this hydration is an arrangement of molecules that maximizes the number of hydrogen bonds. By introducing a hydrophobic particle in water, some hydrogen bonds are destroyed which is energetically unfavourable. [22] Water forms a clathrate around the hydrophobic material. A clathrate is a cage where the network of hydrogen bonds between water molecules is optimized. The arrangement of water molecules surrounding the solute is more orderly than the water environment and therefore induces a decrease in entropy. Quasi-crystalline structure with 4 hydrogen bonds per water molecule compared to ~3.5 in water environment explains the large decrease in entropy which dominates the hydrophobic hydration. [23] Despite the high degree of structuring observed in the clathrates, the introduction of a hydrophobic material disrupts the initial structure of the solvent. Water is excluded from the equilibrium and naturally tends to minimize the disruption until a new state of equilibrium is reached. When two clathrates meet, they quickly merge and combine their content in a hydrophobic cluster. This phenomenon is called coalescence. As the surface of this cluster is smaller than the surface of the two initial structures, a significant number of water molecules are released into the solvent. The new cluster can capture other clathrates and thus become increasingly large. Each merging reduces the total area of clathrate and hence the number of water molecules trapped in these structures. This allows water to reach a new equilibrium where the surface in contact with the hydrophobic material is as small as possible. This clustering increases with increasing temperature, showing that this phenomenon is entropy-driven. The decrease in entropy when

two hydrophobic molecules are inserted into water is lower when hydrophobic solute molecules are close together compared to when they are separated. The interaction between hydrophobic molecules or surfaces comes from the preferential orientation of water molecules in the hydration layer and the polarization propagates step by step over a large range through layers of water increasingly remote. Once brought together into clusters, the hydrophobic molecules are held together by van der Waals interactions. [24]

ii). Force Spectroscopy

While the forces acting on the cantilever deflection allow topographic measurements, the actual study of those interactions is possible with force-versus-distance curves. Those curves represent the force felt by the tip as a function of the distance from the surface when the probe is brought close to a sample surface and then pulled away. However, what is actually measured with the AFM is the cantilever deflection-versus-piezo displacement.

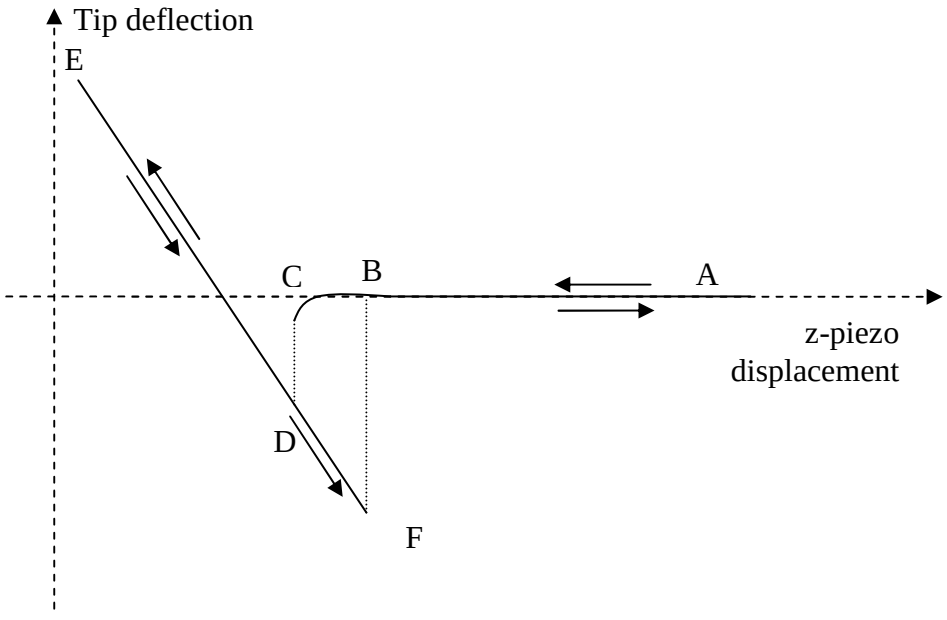

Figure II-26: Cantilever deflection versus z-piezo displacement curve

At the beginning of the force spectroscopy measurement, the tip is too far from the surface to feel any interaction with it. The cantilever is not deflected and is in its rest position (A on the

figure). A piezo movement over the direction normal to the surface reduces the distance between the probe tip and the substrate. When this distance equals the range of an interaction exerted by the surface, (B on the figure) the tip will experience this force and the cantilever will bend either toward or away from the surface, depending on whether the interaction is attractive or repulsive. The cantilever deflection δ is therefore either negative or positive respectively. Consequently, two forces act on the tip: the force produced by the surface and the elastic force of the cantilever given by Hooke's law

Equation II-18: $F = -k\delta$

where k is the cantilever spring constant. When the tip is in equilibrium, these two forces are equal. The force felt by the tip is simply obtained by multiplying the deflection by the spring constant. It is now possible to plot force-versus-piezo displacement curves. When the force gradient overcomes k, there is a "jump-to-contact" (as shown in C in Figure II-26). While the tip and the surface are in contact, in D on the figure, the piezo is still moving. This contact gives the zero distance between the tip and the surface. Force-versus-distance curves can now be plotted. The cantilever deflection is linear because the tip and the surface are in contact. In E, the sample is now withdrawn. The deflection will follow the line from E to D where the tip "jumps-out-of-contact". The "jump-to-contact" and the "jump-out-of-contact" points are different, due to adhesion between the probe tip and the surface. Finally the tip is back in its rest position.

3) Experimental

The Atomic Force Microscope used in this study was a PicoSPM II (Molecular Imaging, Phoenix, AZ, USA) with an interchangeable nose scanner. It was equipped with a video system and a liquid cell. The AFM probes were provided by Veeco and made of silicon nitride. The model which was used was DNP whose nominal radius and spring constant values were 20-40 nm and 0.06 and 0.12 $N.m^{-1}$. These values were not calibrated as only relative measurements were carried out. These tips were made hydrophobic by covering them with 5nm of titanium and 50 nm of gold. A dodecanethiol SAM was then added by immersion in solution. For measurements under different ionic conditions several aqueous solutions were

prepared. The most concentrated was first obtained dissolving KNO_3 in deionised water with resistivity ~18MΩ/cm. Dilutions by a factor of ten gave the other solutions. The tip, along with the surface, was dried between each measurement. Measurements were started from the least concentrated solution and then progressed toward the most concentrated one. A customised MATLAB routine was employed to convert measured cantilever deflection versus piezo displacement curves into force-distance curves according to a procedure described in the literature with 'zero distance' corresponding to a hard-wall potential.[25] These curves were fitted with exponentials and the decay length was determined.

V) Literature

1. D. M. Hercules, L. E. Cox, S. Onisick, G. D. Nichols and J. C. Carver, *Anal. Chem.*, 1973, **45**, 1973-1975.
2. G. Ertl and J. Kuppers, *Energy Electrons and Surface Chemistry*, VCH, Weinheim (Federal Republic of Germany) 1985.
3. A. Shchukarev, *Advances in colloid and interface science*, 2006, **122**, 149-157.
4. C. R. Brundle, J. C. A. Evans and S. Wilson, *Encyclopedia Of Materials Characterization*, Manning Publications Co., Greenwich, 1992.
5. A. Lapicki, F. Sakamoto and A. Sandhu, *Japanese Journal of Applied Physics* 2007, **46**, L49-L52.
6. M. Janghorbani, M. Vulli and K. Starke, *Anal. Chem.*, 1975, **47**, 2200-2208.
7. H. H. Willard, L. L. Merritt Jr., J. A. Dean and F. A. Settle Jr., *Instrumental Methods of Analysis*, seventh edition edn., Wadsworth publishing company, Belmont California.
8. J. F. Watts and J. Wolstenholme, *AN Introduction to Surface Analysis by XPS and AES*, John Wiley & Sons Ltd, Chichester, West Sussex, 2003.
9. R. M. A. Azzam and N. M. Bashara, *Ellipsometry and Polarized Light*, North-Holland Personal Library, Amsterdam, 1977.
10. H. G. Tompkins, *A User's Guide to Ellipsometry*, Academic Press, Inc., San Diego, 1993.
11. G. Binnig, H. Rohrer, C. Gerber and W. E., *physical review letters*, 1983, **50**.
12. L. A. Bottomley, *Anal. Chem.*, 1998, **70**, 425R-475R.

13. G. Binnig, H. Rohrer, C. Gerber and E. Weibel, *Physical review letters*, 1983, **50**, 120-123.
14. G. Binnig, C. F. Quate and C. Gerber, *Phys. Rev. Lett.*, 1986, **56**, 930.
15. A. Noy, C. D. Frisbie, L. F. Rozsnyai, W. M. S. and C. M. Lieber, *J. Am. Chem. Soc.*, 1995, **117**, 7943-7951.
16. Y. Seo and W. Jhe, *Rep.Prog. Phys.*, 2008, **71**.
17. G. Neubauer, S. R. Cohen, G. M. McClelland, D. Horne and C. M. Mate, *Rev. Sci. instrum*, 1990, **61**, 2296-2308.
18. C. M. Mate, G. M. McClelland, R. Erlandsson and S. Chiang, *Physical Review Letters*, 1987, **59**, 1942-1945.
19. J. Ralston, I. Larson, M. W. Rutland, A. A. Feiler and M. Kleijn, *Pure Appl. Chem.* , 2005, **77**, 2149-2170.
20. J. Colchero, A. Storch, M. Luna, J. Gomez Herrero and A. M. Baro, *Langmuir*, 1998, **14**, 2230-2234.
21. T. Stifter, O. Marti and B. Brushan, *Physical Review B*, 2000, **62**, 13667-13673.
22. J. Israelachvili, *Intermolecular and Surface Forces*, Second Edition edn., Academic Press, San Diego, 1992.
23. A. J. Stone, The Theory of Intermolecular Forces, Clarendon Press, Oxford, 1997.
24. P. W. Atkins, Physical Chemistry, Oxford University Press, Oxford, 1998.
25. W. A. Ducker, T. J. Senden and R. M. Pashley, *Nature*, 1991, **353**, 239.

Chapter 3

Synthesis of Trifluoro Alkyl Oligo(Ethylene Glycol)-terminated Alkanethiols and Self-Assembled Monolayer Preparation

Monolayers have been used to observe a reversible adsorption of proteins by playing on external parameters which were not easily modified in a living media [1] or with mixed self-assembled monolayers. [2] It can be difficult to precisely know the proportion of molecules adsorbed on the surface from a solution whose ratio is known because each self-assembling molecule has its own adsorption kinetics. In addition, the film may not be homogeneous and have regions with only one molecule. This thesis describes work carried out with the objective to obtain the same dynamic property with a self-assembled monolayer made from a single surfactant molecule. The switch is envisaged by modifying the forces acting between the surface and proteins thanks to a modification of an external parameter which is easy to set up.

I) Self-Assembling Molecule Design

The design of the new self-assembling molecule was based on previous force studies. Force-distance curves were determined for an hexadecanethiol film as well as for a tri(ethylene glycol)-terminated hexadecanethiol film employing a functionalised tip. The tip was made hydrophobic by covering the silicon nitride tip with a thin gold layer and adding an

alkanethiol SAM. Measurements were performed in a liquid environment. They were performed in aqueous KNO_3 solutions with concentration ranging from 0.1 mM to 0.1 M. The most concentrated solution was obtained by diluting salt into deionised water. The other solutions were obtained by iterative tenfold dilutions. The solution order followed for force-distance measurements is the opposite of the solution preparation order: SFM experiments were first carried out in the most diluted solution before moving to solutions with progressively higher salt concentrations. As shown in Figure III-1, the interaction between the hydrophobized tip and the hexadecanethiol SAM was attractive under any KNO_3 concentration.

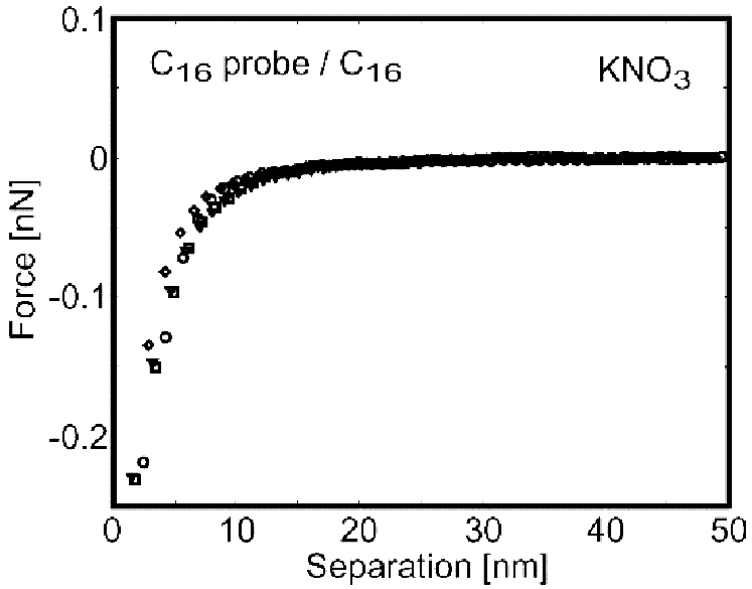

Figure III-1: Force-distance curves observed with hexadecane thiol SAM under KNO3 aqueous solutions (◊, 0.1 M; ○, 0.01 M;▼, 1mM; □, 0.1 mM) . Reproduced from [3]

Moreover, the range of this attractive force was constant when changing the ionic strength of the liquid used in the liquid cell. The nature of this interaction was hydrophobic.

The same process was followed for the study with the tri(ethylene glycol) functionalised hexadecanethiol SAM.

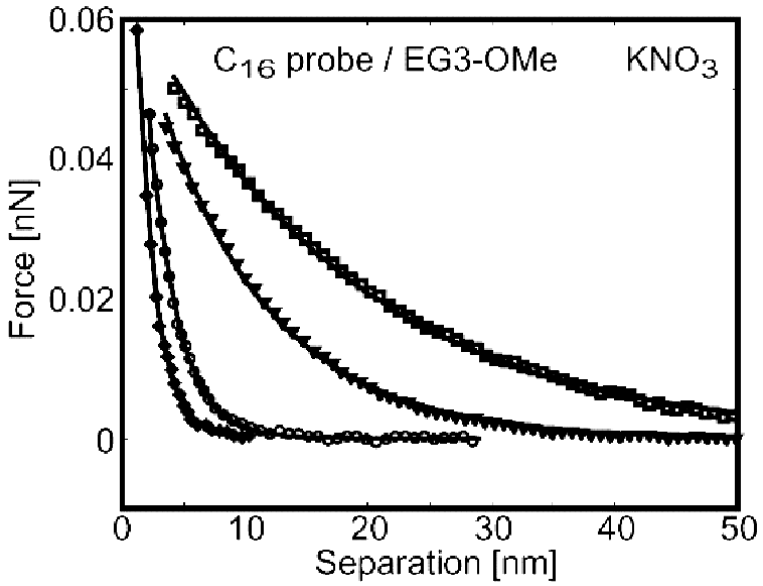

Figure III-2: Force-distance curves observed with tri (ethylene glycol) functionalised hexadecanethiol terminated with a methyl group SAM under KNO3 aqueous solutions (◊, 0.1 M; ○, 0.01 M;▼, 1mM; □, 0.1 mM) . Reproduced from [3]

The profile of the curves is significantly different. The force is now repulsive. The hydrophobic tip approaching the surface is repelled. Contrary to the hydrophobic interaction, this repulsive force strongly depends on the ionic strength. The main difference is the range of the force; it decreases while the ionic strength increases. It was shown that the interaction is of electrostatic nature. [3] This electrostatic repulsion suggests that the surface is charged. The charge on both the tip and the SAM was proved to come from the adsorption of hydroxyl ions from the solution. [4]

The designed molecule was a combination of the two previous ones. The new molecule consists of three parts: an alkane thiol chain ensuring assembly of stable films on gold substrate, an oligo(ethylene glycol) block and a short hydrophobic terminus. Rather than an alkyl end, a trifluoroalkane moiety was chosen for the terminus. The aim of this combination was that the force felt by the tip during force-distance measurements with the SAMs would be the sum of the interactions separately measured with the two previous surfaces for each ionic strength. It is possible to represent graphically the sum of the force-versus-distance curves measured with the hexadecanethiol and the tri(ethylene glycol) functionalised hexadecanethiol SAMs according to the range and intensity of measured forces.

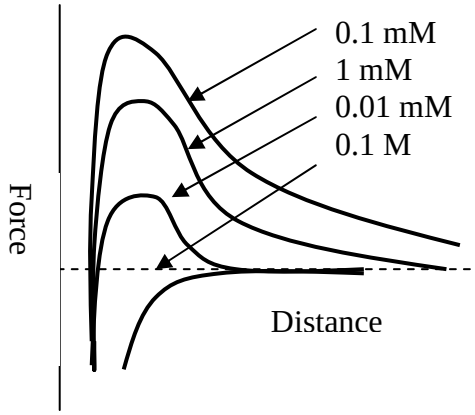

Figure III-3: Sum of the force-distance curves observed with tri (ethylene glycol) functionalised hexadecanethiol terminated with a methyl group and hexadecanethiol SAMs under KNO_3 aqueous solutions (◊, 0.1 M; ○, 0.01 M; ▼, 1mM; □, 0.1 mM)

The sum of the force-distance curves obtained by the two films separately represents what can be expected as force-distance curves measured with the combination molecule. Figure III-3 shows that the tip approaching the surface would be first repelled at lower ionic strength whereas it would be directly attracted under the highest ionic strength. Modifying the ionic strength, it would be possible to observe a switch between repulsion and attraction of the probe by the same surface.

The basic molecule chosen is (1-mercaptoundec-11-yl)tri(ethylene glycol) 3,3,3-trifluoropropyl ether:

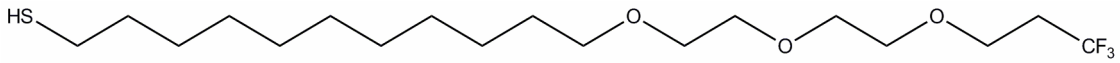

Figure III-4: (1-mercaptoundec-11-yl)tri(ethylene glycol) 3,3,3-trifluoropropyl ether

Two interactions were brought into play. The presence of oligo-ethylene glycol (OEG) groups provided the electrostatic repulsion and the hydrophobic top created an attraction. It was expected that the number of OEG groups influenced the intensity and range of the repulsive force. In the same way, the length of the hydrophobic moiety could have some influence on the hydrophobic attraction.

The influence of the number of ethylene glycol groups and the length of the hydrophobic end were studied. To this end, six molecules were synthesised:

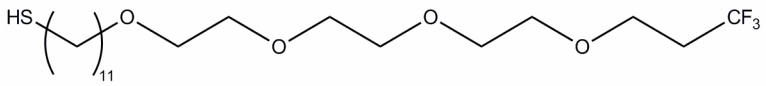

(1-mercaptoundec-11-yl)tri(ethylene glycol) 3,3,3-trifluoropropyl ether: molecule 1

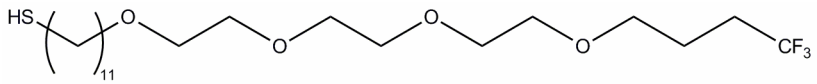

(1-mercaptoundec-11-yl)tri(ethylene glycol) 3,3,3-trifluorobutyl ether: molecule 2

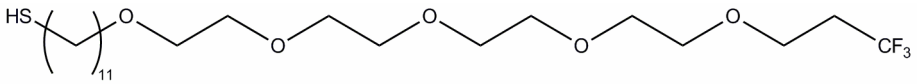

(1-mercaptoundec-11-yl)tetra(ethylene glycol) 3,3,3-trifluoropropyl ether: molecule 3

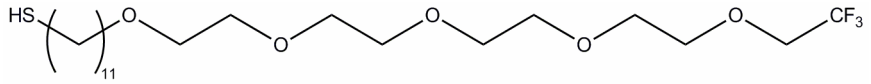

(1-mercaptoundec-11-yl)tetra(ethylene glycol) 2,2,2-trifluoroethyl ether: molecule 4

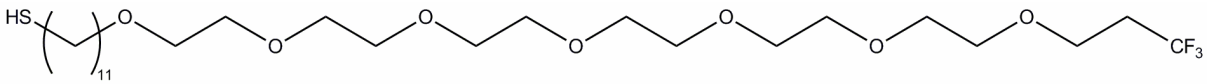

(1-mercaptoundec-11-yl)hexa(ethylene glycol) 3,3,3-trifluoropropyl ether: molecule 5

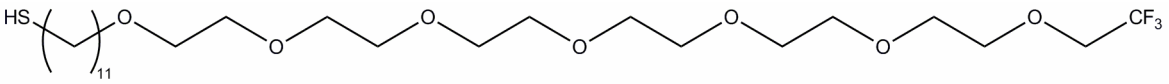

(1-mercaptoundec-11-yl)hexa(ethylene glycol) 2,2,2-trifluoroethyl ether: molecule 6

Figure III-5: Six synthesized (1-mercaptoundec-11-yl)poly(ethylene glycol) 3,3,3-trifluoroalkyl ether molecules

II) Self-Assembling Molecule synthetic pathway

These molecules were not commercially available. Therefore, their preparation was attempted according to the method illustrated in Scheme 1.

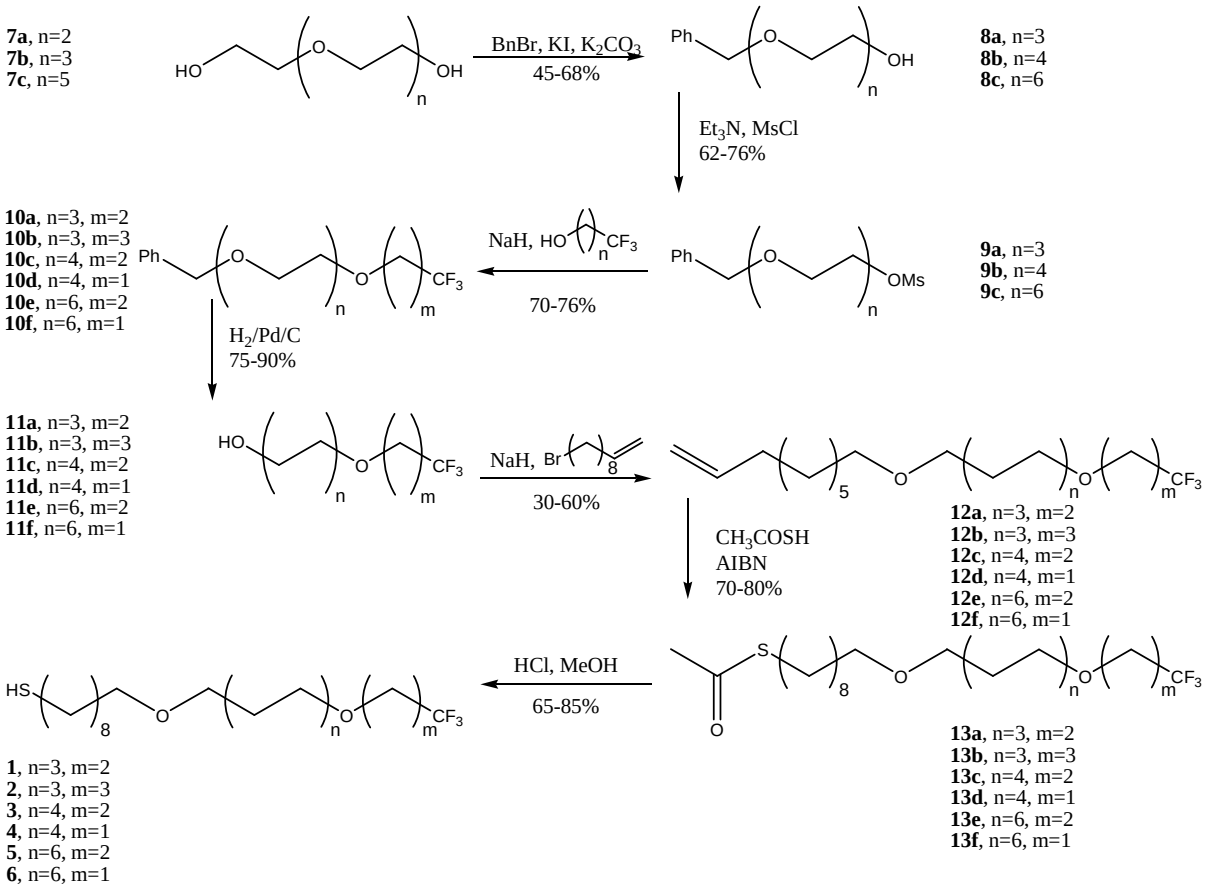

Scheme 1: Synthetic pathway for the synthesis of (1-mercaptoundec-1-11-yl)poly(ethylene glycol) trifluoroalkyl ether

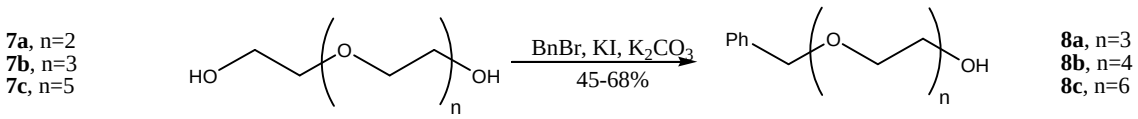

Scheme 2: First step of the synthesis of (1-mercaptoundec-1-11-yl)poly(ethylene glycol) trifluoroalkyl ether

First, tri (tetra or hexa) (ethylene glycol) was monoprotected as the benzyl ether [5]. This nucleophilic substitution of bromine by the alcohol was very sluggish. The reaction was tried in other solvents and adding crown-ether but no improvement was observed.

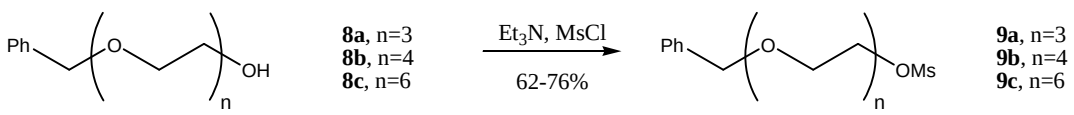

Scheme 3: Second step of the synthesis of (1-mercaptoundec-1-11-yl)poly(ethylene glycol) trifluoroalkyl ether

The mesylation [6] of the alcohol is followed by a nucleophilic substitution of mesylate by trifluoro propanol (or ethanol or butanol). [7]

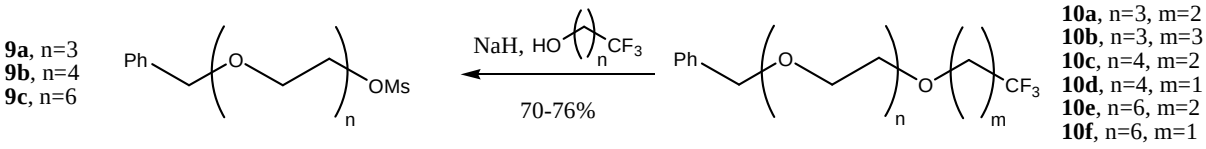

Scheme 4: Third step of the synthesis of (1-mercaptoundec-1-11-yl)poly(ethylene glycol) trifluoroalkyl ether

Next, the benzyl ether was hydrogenolysed [8] in order to obtain the trifluoro alcohol **11**. In an attempt to improve the rate of reaction, other solvents (eg. THF rather than methanol) and catalysts (eg. $Pd(OH)_2$ rather than Pd/C) were employed. However under modified conditions the reaction rate was unchanged.

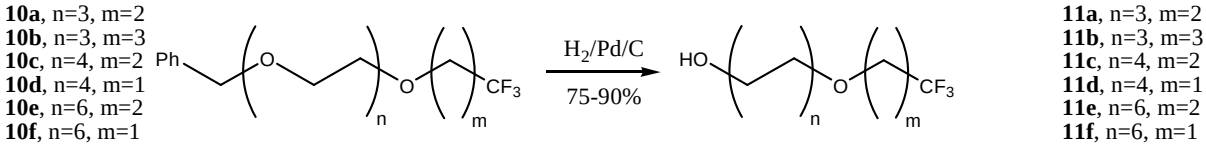

Scheme 5: Fourth step of the synthesis of (1-mercaptoundec-1-11-yl)poly(ethylene glycol) trifluoroalkyl ether

The next step was a nucleophilic substitution reaction with bromo-undecene.[9] However the yield was quite low. An improvement was achieved using 2.5 equivalents of bromo-undecene rather than 2 but the yield remained low.

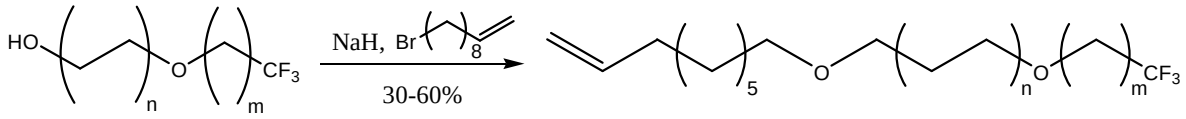

11a, n=3, m=2
11b, n=3, m=3
11c, n=4, m=2
11d, n=4, m=1
11e, n=6, m=2
11f, n=6, m=1

12a, n=3, m=2
12b, n=3, m=3
12c, n=4, m=2
12d, n=4, m=1
12e, n=6, m=2
12f, n=6, m=1

Scheme 6: Fifth step of the synthesis of (1-mercaptoundec-1-11-yl)poly(ethylene glycol) trifluoroalkyl ether

Whitesides *et al.* [9] have synthesised molecules similar to our target molecules. Their methodology was follown for the last three steps.

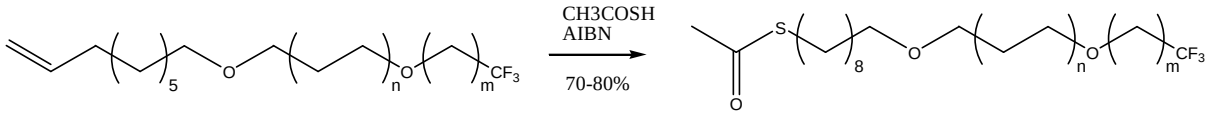

12a, n=3, m=2
12b, n=3, m=3
12c, n=4, m=2
12d, n=4, m=1
12e, n=6, m=2
12f, n=6, m=1

13a, n=3, m=2
13b, n=3, m=3
13c, n=4, m=2
13d, n=4, m=1
13e, n=6, m=2
13f, n=6, m=1

Scheme 7: Sixth step of the synthesis of (1-mercaptoundec-1-11-yl)poly(ethylene glycol) trifluoroalkyl ether

The addition of thiolacetic acid [9] was carried out as described by Whitesides and coworkers, using a UV lamp and a UV-transparent reaction vessel (made of quartz). Subsequently, the reaction was found to be just as successful using ordinary borosilicate glassware. This prompted speculation that the radical initiation was being caused by heat rather than photoionisation. Indeed, the lamp emitted considerable heat. Consequently, the radical addition was performed in borosilicate glass flask plunged into a hot oil bath.

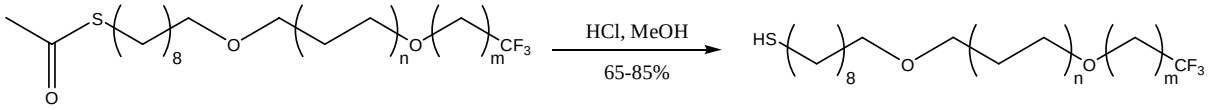

13a, n=3, m=2
13b, n=3, m=3
13c, n=4, m=2
13d, n=4, m=1
13e, n=6, m=2
13f, n=6, m=1

1, n=3, m=2
2, n=3, m=3
3, n=4, m=2
4, n=4, m=1
5, n=6, m=2
6, n=6, m=1

Scheme 8: Seventh step of the synthesis of (1-mercaptoundec-1-11-yl)poly(ethylene glycol) trifluoroalkyl ether

Methanolysis of the thioacetate gave the desired target molecule. This reaction was operationally simple because the reactant was merely dissolved and refluxed, then HCl as well as methanol were evaporated under vacuum.

III) Surface Preparation

SAMs were prepared from the synthesised thiols as well as from commercially available dodecanethiol (Aldrich, +98%) and octadecanethiol (Fluka, ≥95%). These alkanethiol SAMs

were mainly used as reference for some measurements (XPS and ellipsometry). 1 mM solutions were prepared. The in-house synthesised thiols were dissolved in dimethylformamide (Aldrich, 99.8%), while the commercial alkanethiols are dissolved in ethanol (VWR BDH Prolabo, ethyl alcohol absolute). A gold coated Si wafer (5 nm evaporated titanium as adhesion promoter, and 100 nm evaporated gold layer, Georg Albert PVD, Heideberg, Germany), which was stored under vacuum in a dessicator, was cut into pieces immediately before being immersed into the solution for 12-16 hours. The substrates were then rinsed with ethanol and dried with nitrogen.

IV) Experimental Part: Synthesis of Self-Assembling Molecules

1) General Methods

All reagents of synthetic grade were used as supplied. If further purification or drying were required the procedures used are detailed in Armarego and Perrin, "Purification of laboratory chemicals" 4th ED.

Room temperature refers to 20–25ºC. Reaction progress was monitored by thin layer chromatography (TLC) performed using Merck, Kieselgel 60 plates. Column chromatography was performed using Merck Kieselgel 60 silica gel (230 – 400 nm mesh).

Nuclear magnetic resonance (NMR) spectra were measured using a Bruker Av-300 or a Varian Unity Plus 300 operating at 300 MHz for ^{1}H NMR, 75 MHz for ^{13}C NMR, 282 MHz for ^{19}F NMR. All chemical shifts (δ) are reported in parts per million (ppm) and are quoted relative to the residual proton peak of $CDCl_3$. Coupling constants (J) are given in Hertz (Hz) and represent $^{3}J_{H,H}$ unless otherwise stated. Spectral coupling patterns are designated as follows; s: singlet; d: doublet; t: triplet; q: quartet; m: multiplet and br: broad signal.

2) Synthesis of (1-mercaptoundec-11-yl)tri(ethylene glycol) 3,3,3-trifluoropropyl ether (**1**)

i). Triethylene glycol monobenzyl ether (8a) [5]

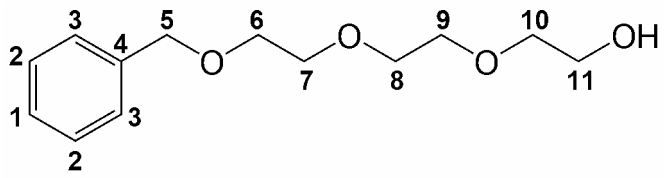

Figure III-6: Triethylene glycol monobenzyl ether

Anhydrous potassium carbonate (0.36 mol, 50 g), potassium iodide (6 mmol, 1 g) and benzyl bromide (0.1 mol, 17.1 g) were added to a solution of triethylene glycol **(7a)** (0.2 mol, 30 g) in dry acetone (200 mL). The solution was refluxed for 71 h. The mixture was cooled down to room temperature and filtered through sintered glass. After acetone removal under reduced pressure the residue was dissolved in diethyl ether (30 mL). The organic layer was washed with water (30 mL), brine (30 mL) and dried over magnesium sulfate. Diethyl ether was removed under vacuum. The product was purified over silica (eluent: cyclohexane:ethyl acetate, 4:6) and was obtained as a yellow oil (14.73g, 61% yield). $\boldsymbol{\delta_H}$ 2.59 (1H, br, **11**-O*H*), 3.58–3.76 (12H, m, **6**-H, **7**-H, **8**-H, **9**-H, **10**-H, and **11**-H), 4.58 (2H, s, **5**-H), 7.28–7.38 (5H, m, **1**-H, **2**-H, and **3**-H); $\boldsymbol{\delta_C}$ 61.5 (1C, **11**), 69.2, 70.2, 70.4, 70.5, 72.4, 73.1 (6C, **5**, **6**, **7**, **8**, **9**, and **10**), 127.5, 127.6, 128.2 (5C, **1**, **2**, and **3**), 138.0 (1C, **4**); $\boldsymbol{\nu_{MAX}}$***(film)/cm*$^{-1}$ 699.39, 740.41 (Ar); 1099.55, 1351.10, 1454.44 (C-O-C); 2867.94 (C-H); 3030.54, 3062.98, 3087.76 (Ar); 3446.43 (O-H); ***HRMS m/z (****ES+)*: $[MNa]^+$ 263.1262, calculated 263.1259.

ii). 2-(2-(2-benzyloxyethoxy)ethoxy)ethyl methanesulfonate (9a) [6]

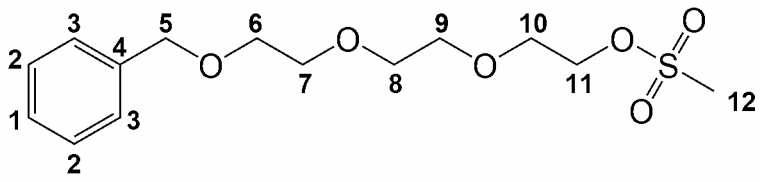

Figure III-7: 2-(2-(2-(benzyloxy)ethoxy)ethoxy)ethyl methanesulfonate (9a)

Triethylamine (0.067 mol, 6.93 g) and mesyl chloride (0.061 mol, 2.69 g) were added to a solution of **(8a)** (0.030 mol, 7.26 g) in dichloromethane (300 mL). Then, the mixture was stirred at 0 ºC under nitrogen for 2 h.

The reaction was quenched with 30 mL of water. The phases were separated. The aqueous layer was extracted with dichloromethane and the combined organic layers were washed with water and brine, and dried over $MgSO_4$.

Dichloromethane was evaporated under vacuum. The product was purified over silica (eluent: hexane:ethyl acetate, 5:5) and isolated as a pale yellow oil (7.12 g, 72% yield).

The methanesulfonic acid 2-[2-(2-benzyloxy-ethoxy)-ethoxy]-ethyl ester was stored under nitrogen. $\boldsymbol{\delta_H}$ 3.04 (3H, s, **12**-H), 3.60–3.71, 3.75–3.81 (4H, m, **10**-H, and **11**-H), 4.57 (2H, s, **5**-H), 7.28–7.39 (5H, m, **1**-H, **2**-H, and **3**-H); $\boldsymbol{\delta_C}$ 37.3 (1C, **12**), 60.0, 68.6, 69.1, 69.2, 70.2, 70.3, and 72.8 (7C, **5**, **6**, **7**, **8**, **9**, **10**, and **11**), 127.3, 127.4, 128.1 (5C, **1**, **2**, and **3**), 137.9 (1C, **4**); $\boldsymbol{\nu_{MAX}(film)/cm^{-1}}$ 701.12, 737.70 (Ar); 810.77 (-SO_2-); 1101.72 (C-O-C); 1175.83 (-SO_2-); 1352.91, 1454.73 (C-O-C); 2870.86 (C-H); 3029.05, 3062.76 (Ar); ***HRMS m/z (ES+)***: $[MNa]^+$ 341.1031, calculated 341.1035.

iii). Triethylene glycol benzyl 3,3,3-trifluoropropyl ether (10a)[7]

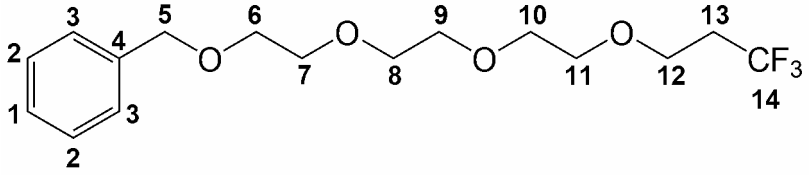

Figure III-8: Triethylene glycol benzyl 3,3,3-trifluoropropyl ether

Sodium hydride (0.048 mol, 1.16 g) was added to a solution of 3,3,3-trifluoropropan-1-ol (0.0438 mol, 5 g) in dry tetrahydrofuran (400 mL). The mixture was stirred for 30 min under nitrogen at room temperature. **(9a)** (0.021 mol, 6.97 g) was then added and the solution was refluxed for 26 h. After cooling, a few drops of isopropanol and water were added to hydrolyse the excess sodium hydride. Tetrahydrofuran was removed *in vacuo* and, the residue was dissolved in diethyl ether (40mL). The organic layer was washed with brine (3 times 30 mL) and dried over magnesium sulfate. The product was recovered as light brown oil (5.39 g, 74% yield). $\boldsymbol{\delta_H}$ 2.84 (2H, tq, $^3J_{H,F}$: 10.8, $^3J_{H,H}$: 6.8, **13**-H) 3.57–3.72 (14H, m, **6**-H, **7**-H, **8**-H, **9**-H, **10**-H, **11**-H and **12**-H), 4.55 (2H, **5**-H), 7.28–7.37 (5H, m, **1**-H, **2**-H and **3**-H); $\boldsymbol{\delta_C}$ 34.4 (1C, q, $^2J_{C,F}$: 28.6, **13**), 64.1 (1C, q, $^3J_{C,F}$: 3.3, **12**), 69.4, 70.4, 70.5, 70.6, 70.7, 72.5, 73.2 (7C, **5**, **6**, **7**, **8**, **9**, **10**, and **11**), 127.6, 127. 6, 127.7, 127.8, 128.4 (5H, **1**, **2**, and **3**), 138.3 (1C, **4**); $\boldsymbol{\delta_F}$ -65.17 (t, $^1J_{C,F}$: 10.8, **14**-F); $\boldsymbol{\nu_{MAX}}$***(film)/cm*$^{-1}$ 699.15, 739.26 (Ar); 844.84, 1004.91, 1145.02, 1256.22 (CF_3); 1351.47, 1454.58 (C-O-C); 2869.11 (C-H); 3031.19, 3064.20, 3088.41 (Ar); ***HRMS m/z (****ES+)*: $[MNa]^+$ 359.1454, calculated 359.1446.

iv). Triethylene glycol mono(3,3,3-trifluoropropyl) ether (11a) [8]

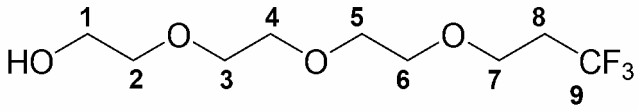

Figure III-9: Triethylene glycol mono(3,3,3-trifluoropropyl) ether

(10a) (0.016 mol, 5.39 g) was added to a suspension of palladium on charcoal (10% weight) (0.675 mmol, 71.8 mg of palladium) in ethanol (200 mL). The reaction mixture was left to stir for 36 hours under hydrogen pressure of 20 bar at room temperature. The solution was filtered through celite. Ethanol was evaporated under vacuum and the product was purified over silica (eluent: hexane: ethyl acetate: 60/40) to give the product as pale orange oil (3.86 g, 85% yield). $\boldsymbol{\delta_H}$ 2.33 (2H, tq, $^3J_{H,F}$: 10.8, $^3J_{H,H}$: 6.8, **8**-H), 3.09 (1H, br, **1**-OH), 3.48–3.65 (14H, m, **1**-H, **2**-H, **3**-H, **4**-H, **5**-H, **6**-H, and **7**-H); $\boldsymbol{\delta_C}$ 34.0 (1C, q, $^2J_{C,F}$: 28.2, **8**), 61.3 (1C, **1**), 63.8 (1C, q, $^3J_{H,H}$: 3.5, **7**), 70.0, 70.2, 70.4, 72.3 (5C, m, **2**, **3**, **4**, **5**, and **6**), 125.9 (1C, q, J: 276.8, **9**); $\boldsymbol{\delta_F}$ -65.4 (s, decoupling); $\boldsymbol{\nu_{MAX}}$***(film)/cm*$^{-1}$ 837.35, 1005.63, 1150.87, 1256.83 (CF_3); 1351.65,

1443.39 (C-O-C); 2879.18 (C-H); 3447.88 (O-H); ***HRMS m/z (ES+)***: $[MNa]^+$ 269.0970, calculated 269.0977.

v). Triethylene glycol 3,3,3-trifluoropropyl undec-10-enyl ether (12a)[9]

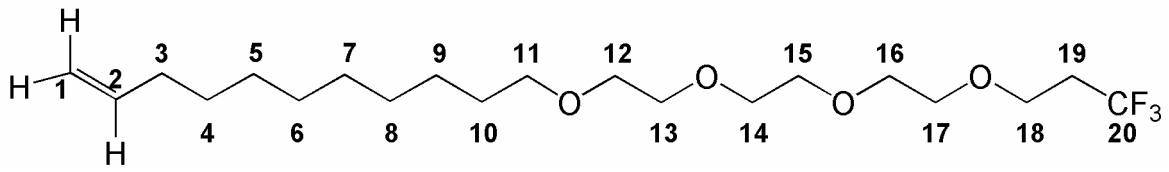

Figure III-10: Triethylene glycol 3,3,3-trifluoropropyl undec-10-enyl ether

Sodium hydroxide (20.4 mmol, 490 mg) was added to a solution of the **(11a)** (3.86 g, 15.7 mmol) in tetrahydrofuran (350 mL) and the mixture was stirred 30 minutes. Then 11-bromoundec-1-ene (39.2 mmol, 9.14 g) was added to the solution. The mixture was refluxed for 26 hours. Then the solution was cooled and quenched with isopropanol and water. THF was removed and the organic layer was washed with water (30 mL), and brine (twice 30 mL), and dried over magnesium sulfate. The product is purified over silica (eluent: hexane: ethyl acetate: 80/20) and isolated as colourless oil (4.45 mmol, 2.11 g, 34% yield). $\boldsymbol{\delta_H}$ 1.18–1.41 (12H, m, **4**-H, **5**-H, **6**-H, **7**-H, **8**-H and **9**-H), 1.51 (2H, t, $^3J_{H,H}$: 6.8, **10**-H), 1.97 (2H, q, $^3J_{H,H}$: 7.0, **3**-H), 2.35 (2H, tq, $^4J_{H,F}$: 10.8, $^3J_{H,H}$: 6.8, **18**-H), 3.38 (2H, t, $^3J_{H,H}$: 6.8, **11**-H), 3.48–3.68 (14H, m, **12**-H, **13**-H, **14**-H, **15**-H, **16**-H, **17**-H, and **18**-H), 4.86 (1H, d, $^3J_{H,H}$: 10.2, **1**-$H_{\mathbf{a}}$), 4.92 (1H, d, $^3J_{H,H}$: 17.1, **1**-$H_{\mathbf{b}}$), 5.72–5.88 (1H, m, **2**-H); $\boldsymbol{\delta_C}$ 25.9, 28.7, 28.9, 29.2, 29.2, 29.3, 29.4 (7C, **4**, **5**, **6**, **7**, **8**, **9**, and **10**), 33. 6 (1C, **3**), 34.1 (1C, q, $^2J_{C,F}$: 28.2, **19**), 63. 9 (1C, q, $^3J_{C,F}$: 3.3, **18**), 66.4, 69.6, 69.8, 70.3, 70.4, 70.4, 71.2 (7C, **11**, **12**, **13**, **14**, **15**, **16**, and **17**), 113.9 (1C, **1**), 125.9 (1C, q, $^1J_{C,F}$: 276.5, **20**), 138.9 (1C, **2**); $\boldsymbol{\delta_F}$ -65.4 (t, $^3J_{F,H}$: 10.8); $\boldsymbol{\nu_{MAX}}$***(film)/cm***$^{-1}$ 994.14, 1122.50, 1255.35 (CF_3); 1351.06, 1440.56 (C-O-C); 1640.76 ($CH=CH_2$); 2855.77, 2927.02 (C-H); 3077.05 ($=CH_2$); ***HRMS m/z (ES+)***: $[MNa]^+$ 399.2720, calculated 399.2722.

vi). Triethylene glycol 10-acetylthiodecyl 3,3,3-trifluoropropyl ether (13a)[9]

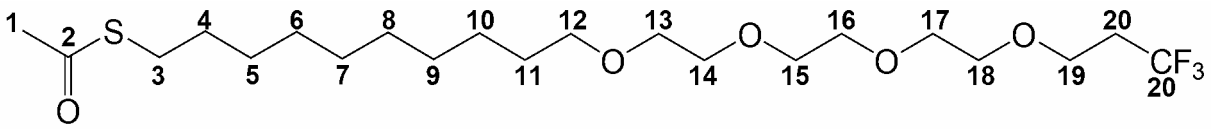

Figure III-11: Triethylene glycol 10-acetylthiodecyl 3,3,3-trifluoropropyl ether

Thioacetic acid (17.8 mmol, 1.35 g) and AIBN (25 mg) were added to a solution of **(12a)** (4.45 mmol, 2.11 g) in methanol (50 mL). The reaction solution was plunged into a preheated oil bath and refluxed for 2 hours under nitrogen atmosphere. The mixture was concentrated under vacuum and purified by chromatography over silica giving colourless and malodorous oil (1.69 g, 79 % yield). $\boldsymbol{\delta_H}$ 1.19 (1H, t, $^3J_{H,H}$: 7.1, **3**-H), 1.22–1.36 (14H, m, **6**-H, **7**-H, **8**-H, **9**-H, **10**-H, **11**-H, and **12**-H), 1.48–1.60 (4H, m, **4**-H, and **12**-H), 2.30 (3H, s, **1**), 2.40 (2H, tq, $^3J_{H,F}$: 10.8, $^3J_{H,H}$: 6.9, **21**-H), 2.84 (2H, t, $^3J_{H,H}$: 7.4, **13**-H), 3.42 (2H, t, $^3J_{H,H}$:6.8, **20**-H), 3.54–3.65 (12H, m, **14**-H, **15**-H, **16**-H, **17**-H, **18**-H, and **19**-H); $\boldsymbol{\delta_C}$ 26.0, 28.7, 29.0, 29.0, 29.4, 29.4, 29.5, 29.5 (10C, **3**, **4**, **5**, **6**, **7**, **8**, **9**, **10**, **11**, and **12**), 30.5 (1C, **1**), 34.3 (1C, q, $^2J_{C,F}$: 28.1, **21**), 64.0 (1C, q, $^3J_{C,F}$: 3.6, **20**), 66.5, 69.2, 69.9, 70.4, 70.5, 70.6, 71.4 (7C, **13**, **14**, **15**, **16**, **17**, **18**, and **19**); $\boldsymbol{\delta_F}$ -65.3 (3F, t, $^3J_{F,H}$:10.8, **22**-F); $\boldsymbol{\nu_{MAX}}$***(film)/cm*** $^{-1}$ 627.49 (-S-); 840.71, 1005.10, 1135.13, 1255.84 (CF_3); 1352.92, 1442.05 (C-O-C); 1693.72 (C=O); 2856.62, 2927.34 (C-H); ***HRMS m/z (****ES+)*: $[MNa]^+$ 497.2526, calculated 497.2525.

vii). (1- mercaptoundec-11-yl)tri(ethylene glycol) 3,3,3-trifluoropropyl ether (1)[9]

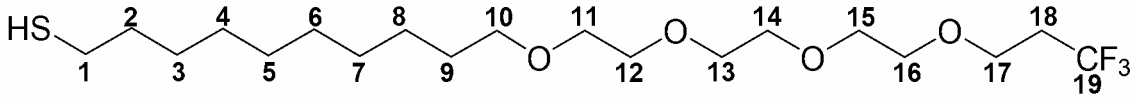

Figure III-12: (1-mercaptoundec-11-yl)tri(ethylene glycol) 3,3,3-trifluoropropyl ether

(13a) was dissolved in HCl/methanol solution (60 mL, 1.25 mol.L^{-1}). The mixture was refluxed overnight, concentrated and purified over silica (eluent: hexane, ethylacetate: 80/20)

to give the thiol as colourless oil (2.82 mmol, 1.22 g, 79% yield). δ_H 1.24–1.39 (14H, m, **3**-H, **4**-H, **5**-H, **6**-H, **7**-H, **8**-H, and **9**-H), 1.43 (1H, s, S-H), 1.53–1.67 (4H, m, **2**-H, and **10**-H), 2.43 (2H, tq, $^3J_{H,F}$: 10.8, and $^3J_{H,H}$: 6.8, **19**-H), 2.53 (2H, dt, $^3J_{H,H}$: 7.10, $^3J_{H,H}$: 7.49, **1**-H) , 3.45 (2H, t, $^3J_{H,H}$: 6.9, **11**-H), 3.56–3.68 (12H, m, **12**-H, **13**-H, **14**-H, **15**-H, **16**-H, and **17**-H), 3.71 (2H, t, $^3J_{H,H}$: 6.8, **18**-H); δ_C 24.5, 25.9, 26.8, 28.2, 28.9, 29.4, 29.4, 29.5, 33.9 (10C, **1**, **2**, **3**, **4**, **5**, **6**, **7**, **8**, **9**, and **10**), 34.2 (1C, q, $^2J_{C,F}$: 28.2, **19**), 64.0 (1C, q, $^3J_{C,F}$: 3.5, **18**), 69.9, 70.4, 70.5, 70.5, 71.4, (7C, **11**, **12**, **13**, **14**, **15**, **16**, and **17**), 126.0 (1C, q, $^1J_{C,F}$: 126.2, **20**); δ_F -65.3 (3F, t, $^3J_{F,H}$:10.8, **20**-F); ν_{MAX}*(film)/cm*$^{-1}$ 636.19, 657.91 (S-C); 839.33, 1005.05, 1150.29, 1255.62 (CF_3); 1350.77, 1442.24 (C-O-C); 2855.94, 2926.77 (C-H); ***HRMS m/z (****ES+)*: $[MNa]^+$ 455.2420, calculated 455.2419.

3) Synthesis of (1-mercaptoundec-11-yl)tri(ethylene glycol) 4,4,4-trifluorobutyl ether (**2**)

i). Triethylene glycol benzyl 4,4,4-trifluorobutyl ether (10b)[7]

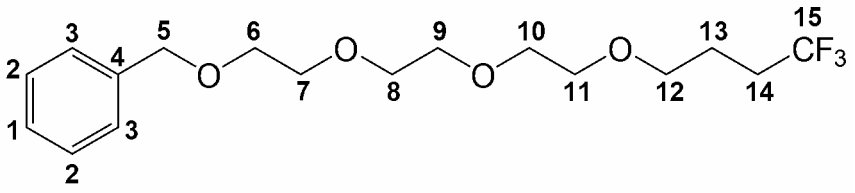

Figure III-13: Triethylene glycol benzyl 4,4,4,-trifluorobutyl ether

δ_H 1.74–1.89 (2H, m, **13**-H), 2.1–2.29 (2H, m, **14**-H), 3.46–3.72 (14H, m, **6**-H, **7**-H, **8**-H, **9**-H, **10**-H, **11**-H and **12**-H), 4.57 (2H, **5**-H), 7.27–7.38 (5H, m, **1**-H, **2**-H and **3**-H); δ_C 22.2 (1C, q, $^2J_{C,F}$: 2.8, **13**), 30.5 (1C, q, $^3J_{C,F}$: 29.1, **14**), 69.2, 69.3, 70.0, 70.4, 70.5, 73.0 (8C, **5**, **6**, **7**, **8**, **9**, **10**, **11** and **12**), 127.2 (1C, q, $^1J_{C,F}$: 276.1, **15**), 127.4, 127. 6, 128.2, 129.9, 132.8 (5H, **1**, **2**, and **3**), 138.1 (1C, **4**); δ_F -66.8 (t, $^1J_{C,F}$: 11.1, **14**-F); ν_{MAX}*(film)/cm*$^{-1}$ 699.13, 738.55 (Ar); 833.92, 1029.40, 1112.71, 1254.26 (CF_3); 1388.88, 1454.31 (C-O-C); 2867.81 (C-H); 3031.44, 3064.50, 3088.49 (Ar); ***HRMS m/z (****ES+)*: $[MNa]^+$ 373.1598, calculated 373.1603.

ii). Triethylene glycol mono(4,4,4-trifluorobutyl)ether (11b)[8]

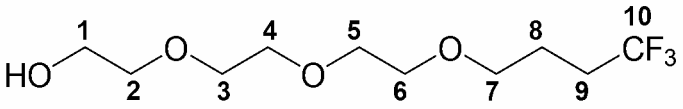

Figure III-14: Triethylene glycol mono(4,4,4-trifluorobutyl)ether

δ_H 1.72–1.84 (2H, m, **8**-H), 2.06–2.24 (2H, m, **9**-H), 2.91 (1H, br, **1**-OH), 3.43–3.73 (14H, m, **1**-H, **2**-H, **3**-H, **4**-H, **5**-H, **6**-H, and **7**-H); δ_C 22.2 (1C, q, $^2J_{C,F}$: 2.9, **8**), 30.5 (1C, q, $^2J_{C,F}$: 28.9, **9**), 61.5, 69.2, 70.0, 70.2, 70.3, 70.5, 72.4 (7C, **2**, **3**, **4**, **5**, **6**, and **7**), 125.2 (1C, q, J: 274.6, **10**); δ_F -66.9 (t, $^1J_{C,F}$: 11); ν_{MAX}*(film)/cm*$^{-1}$ 833.68, 935.36, 1157.96, 1256.07 (CF_3); 1454.83 (C-O-C); 2865.78 (C-H); 3449.62 (O-H); ***HRMS m/z*** *(ES+)*: $[MNa]^+$ 283.1128, calculated 283.1133.

iii). Triethylene glycol 4,4,4-trifluorobutyl undec-10-enyl ether (12b)[9]

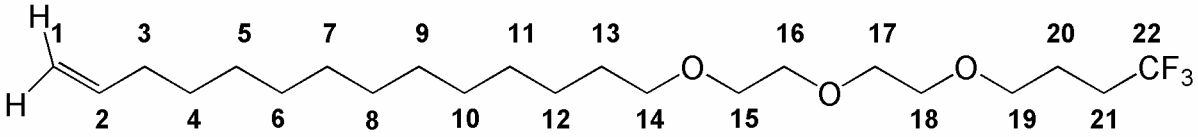

Figure III-15: Undec-11-enyl trifluoropropyl triethylene glycol

δ_H 1.22–1.40 (12H, m, **4**-H, **5**-H, **6**-H, **7**-H, **8**-H and **9**-H), 1.51–1.62 (2H, m, **10**-H), 1.76–1.88 (2H, m, **19**-H), 1.97–2.08 (2H, m, **3**-H), 2.10–2.27 (2H, m, **20**-H), 3.39–3.70 (16H, m, **11**-H, **12**-H, **13**-H, **14**-H, **15**-H, **16**-H, **17**-H, and **18**-H), 4.89–5.03 (2H, m, **1**-H_a, and **1**-H_b), 5.81 (1H, tdd, $^3J_{H,Hb}$: 16.9, $^3J_{H,Ha}$: 10.2, $^3J_{H,H}$: 6.7, **2**-H); δ_C 22.2 (1C, q, $^3J_{C,F}$: 2.7, **19**), 25.9, 28.7, 28.9, 29.3, 29.3, and 33.6 (8C, **3**, **4**, **5**, **6**, **7**, **8**, **9**, and **10**), 30.5 (1C, q, $^2J_{C,F}$: 28.9, **20**), 66.4, 69.2, 69.7, 69.9, 70.0, 70.4, 70.5, and 71.3 (8C, **11**, **12**, **13**, **14**, **15**, **16**, **17** and **18**), 113.9 (1C, **1**), 127.1 (1C, q, $^1J_{C,F}$: 276.4, **21**), 139.0 (1C, **2**); δ_F -66.9 (t, $^3J_{F,H}$: 11.0); ν_{MAX}*(film)/cm*$^{-1}$ 1031.41, 1121.92, 1254.19 (CF_3); 1351.28, 1454.61 (C-O-C); 1640.92 ($CH=CH_2$); 2857.53, 2927.67 (C-H); 3077.30 ($=CH_2$); ***HRMS m/z*** *(ES+)*: $[MNa]^+$ 413.2879, calculated 413.2879.

iv). Triethylene glycol 10-acetylthiodecyl 4,4,4-trifluorobutyl ether (13b)[9]

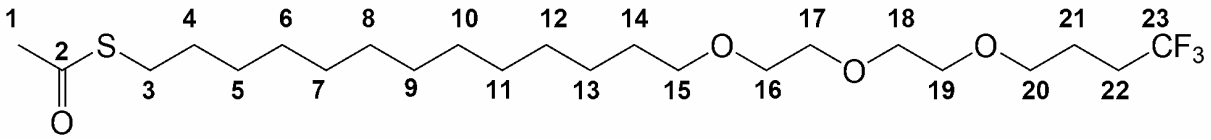

Figure III-16: Triethylene glycol 10-acetylthiodecyl 4,4,4-trifluorobutyl ether

δ_H 1.21–1.31 (14 H, m, **5**-H, **6**-H, **7**-H, **8**-H, **9**-H, **10**-H, and **11**-H), 1.49–1.59 (4 H, m, **4**-H, and **12**-H), 1.75–1.86 (2H, m, **21**-H), 2.07–2.26 (2H, m, **22**-H), 2.29 (3H, s, **1**-H), 2.83 (2H, t, $^3J_{H,H}$: 7.3, **3**-H), 3.42 (2H, t, $^3J_{H,H}$: 6.8, **13**-H), 3.46–3.66 (14H, m, **14**-H, **15**-H, **16**-H, **17**-H, **18**-H, **19**-H, and **20**-H); δ_C 22.2, 26.0, 28.7, 29.0, 29.0, 29.4, 29.4, 29.5, 29.5 (10C, **3**, **4**, **5**, **6**, **7**, **8**, **9**, **10**, **11**, and **12**), 30.6 (1C, q, **23**), 34.3 (1C, q, $^2J_{C,F}$: 28.9, **21**), 66.5 (1C, **22**), 69.2, 69.7, 69.9, 70.1, 70.4, 70.5, and 71.4 (9C, **13**, **14**, **15**, **16**, **17**, **18**, **19**, **20**, and **21**), 127.2 (1C, q, $^1J_{C,F}$: 276.4, **24**), 196.0 (1C, **2**); δ_F -66.8 (3F, t, $^3J_{F,H}$:11.0, **24**-F); ν_{MAX}*(film)/cm*$^{-1}$ 634.28 (-S-); 834.47, 994.76, 1120.09, 1254.00 (CF_3); 1351.20, 1454.90 (C-O-C); 1640.84 (C=O); 2859.49, 2935.18 (C-H); ***HRMS m/z (****ES+)*: $[MNa]^+$ 511.2679, calculated 511.2681.

v). (1-mercaptoundec-11-yl)tri(ethylene glycol) 3,3,3-trifluorobutyl ether (2)[9]

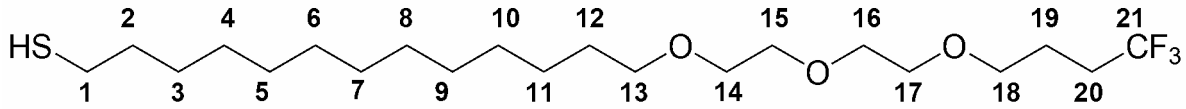

Figure III-17: (1-mercaptoundec-11-yl)tri(ethylene glycol) 3,3,3-trifluorobutyl ether

δ_H 1.15–1.37 (15H, m, **4**-H, **5**-H, **6**-H, **7**-H, **8**-H, **9**-H, and **10**-H, a triplet with $^3J_{H,H}$: 7.7 in the multiplet for S-H), 1.50–1.65 (4H, m, **3**-H, and **11**-H), 1.76–1.89 (2H, m, **20**-H), 2.06–2.28 (2H, m, **21**-H), 2.50 (2H, td, $^3J_{H,H} \approx {}^3J_{H,H}$ (through S atom): 7.7, **1**-H), 3.43 (2H, t, $^3J_{H,H}$**:** 6.7, **12**-H), 3.50 (2H, t, $^3J_{H,H}$**:** 6.2, **19**-H), 3.54–3.69 (12 H, m, **13**-H, **14**-H, **15**-H, **16**-H, **17**-H, and **18**-H); δ_C 22.3 (1C, q, $^3J_{C,F}$: 2.8), 24.6, 26.0, 28.3, 29.0, 29.4, 29.5, 29.5, 34.0 (10 C, **1**, **2**, **3**, **4**, **5**, **6**, **7**, **8**, **9**, and **10**), 30.6 (1C, q, $^2J_{C,F}$: 28.8, **20**), 69.3, 69.8, 70.0, 70.1, 70.5, 70.6, and 71.5 (8C, **11**, **12**, **13**, **14**, **15**, **16**, **17**, and **18**), 127.2 (1C, q, $^1J_{C,F}$: 276.4, **21**) δ_F -66.8 (3F, t,

$^{3}J_{F,H}$:11.0, **21**-F); ***ν_{MAX}(film)/cm^{-1}*** 660.04 (S-C); 868.31, 1029.83, 1121.97, 1253.88 (CF_3); 1351.18, 1452.55 (C-O-C); 2859.94, 2936.20 (C-H); ***HRMS m/z (ES+)***: $[MNa]^+$ 447.2750, calculated 447.2756.

4) Synthesis of (1-mercaptoundec-11-yl)tetra(ethylene glycol) 3,3,3-trifluoropropyl ether (**3**)

i). Tetra ethylene glycol monobenzyl ether (8b)[5]

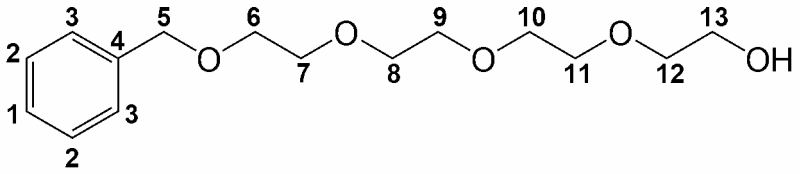

Figure III-18: Tetra ethylene glycol monobenzyl ether

δ_H 3.03 (1H, s br, O-H), 3.56–3.73 (16H, m, **6**-H, **7**-H, **8**-H, **9**-H, **10**-H, **11**-H, **12**-H, and **13**-H), 4.58 (2H, s, **5**-H), 7.28–7.37 (5H, m, **1**-H, **2**-H, and **3**-H); ***δ_C*** 61.4, 69.2, 70.1, 70.4, 70.4, 70.6, 72.4, 73.0, and 73.3 (9C, **5**, **6**, **7**, **8**, **9**, **10**, **11**, **12**, and **13**), 127.4, 127.6, and 128.2 (5C, **1**, **2**, and **3**), 138.0 (1C, **4**); ***ν_{MAX}(film)/cm^{-1}*** 699.21, 738.66 (Ar); 1102.20, 1357.65, 1454.22 (C-O-C); 2868.85 (C-H); 3030.15, 3063.44, 3087.58 (Ar); 3439.71 (O-H); ***HRMS m/z (ES+)***: $[MNa]^+$ 307.1512, calculated 307.1521.

ii). 2-(2-(2-(2-benzyloxyethoxy)ethoxy)ethoxy)ethyl methanesulfonate (9b)[6]

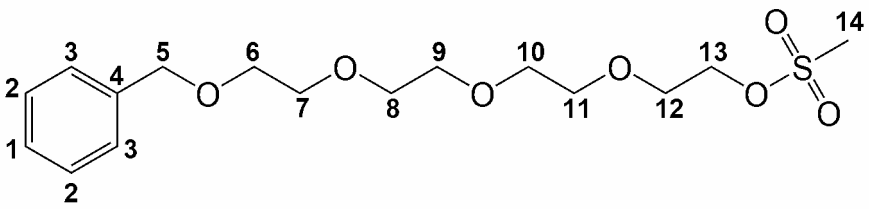

Figure III-19: 2-(2-(2-(2-benzyloxyethoxy)ethoxy)ethoxy)ethyl methanesulfonate

δ_H 3.02 (3H, s, **14**-H), 3.59–3.68 (12H, m, **6**-H, **7**-H, **8**-H, **9**-H, **10**-H, and **11**-H), 3.69–3.74, and 4.29–4.36 (4H, m, **12**-H, and **13**-H), 4.54 (2H, s, **5**-H), 7.27–7.35 (4H, m, **1**-H, **2**-H, and **3**-H); δ_C 37.2 (1C, **14**), 68.6, 69.1, 70.1, 70.2, 72.7 (9C, **5**, **6**, **7**, **8**, **9**, **10**, **11**, **12**, and **13**), 128.0, 128.1, 128.7 (5C, **1**, **2**, and **3**), 137.9 (1C, **4**); ν_{MAX}***(film)/cm***$^{-1}$ 700.56, 740.92 (Ar); 806.54 (-SO_2-); 1105.91 (C-O-C); 1175.21 (-SO_2-); 1352.52, 1454.84 (C-O-C); 2869.48 (C-H); 3028.98, 3062.70 (Ar); ***HRMS m/z (****ES+)*: $[MNa]^+$ 385.1304, calculated 385.1297.

iii). Tetraethylene glycol benzyl 3,3,3-trifluoropropyl ether (10c)[7]

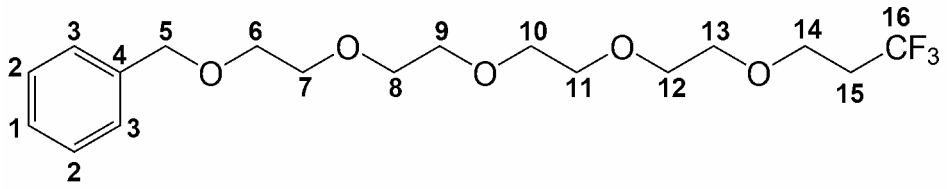

Figure III-20: Tetraethylene glycol benzyl 3,3,3-trifluoropropyl ether

δ_H 1.79 (1H, s br, O-H), 2.42 (tq, $^3J_{H,F}$: 10.9, $^3J_{H,H}$: 6.8, **15**-H), 3.59–3.73 (18H, m, **6**-H, **7**-H, **8**-H, **9**-H, **10**-H, **11**-H, **12**-H, **13**-H, and **14**-H), 4.57 (2H, s, 5-H), 7.26–7.38 (5H, m, 1-H, 2-H, and 3-H); δ_C 34.0 (1C, q, $^2J_{C,F}$: 28.2, **15**), 63.7 (1C, q, $^3J_{C,F}$: 3.6, **14**), 69.1, 70.1, 70.2, 70.3, 70.3, and 72.8 (9C, **5**, **6**, **7**, **8**, **9**, **10**, **11**, **12**, and **13**), 125.9 (1C, $^1J_{C,F}$: 276.7, **16**), 127.2, 127.3, 128.0 (5C, **1**, **2**, and **3**), 138.0 (1C, **4**); δ_F -65.24 (t, $^1J_{C,F}$: 10.8, **16**-F); ν_{MAX}***(film)/cm***$^{-1}$ 699.20, 738.88 (Ar); 848.03, 1004.69, 1144.58, 1256.00 (CF_3); 1351.56, 1454.55 (C-O-C); 2868.64 (C-H); 3031.09, 3063.91, 3088.27 (Ar); ***HRMS m/z (****ES+)*: $[MNa]^+$ 403.1706, calculated 403.1708.

iv). Tetraethylene glycol mono(3,3,3-trifluoropropyl)ether (11c)[8]

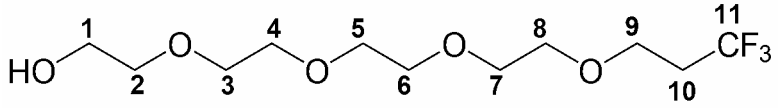

Figure III-21: Tetraethylene glycol mono(3,3,3-trifluoropropyl)ether

δ_H 2.43 (2H, tq, $^{3}J_{H,F}$: 10.8, $^{3}J_{H,H}$: 6.8, **11**-H), 3.59–3.76 (18H, m, **1**-H, **2**-H, **3**-H, **4**-H, **5**-H, **6**-H, **7**-H, **8**-H, **9**-H, and **10**-H); ***δ_C*** 34.0 (1C, q, $^{2}J_{C,F}$: 28.3, **11**), 61.3 (1C, **1**), 63.8 (1C, q, $^{3}J_{H,H}$: 3.5, **7**), 70.0, 70.2, 70.3, 72.3, 70.3 (7C, m, **2**, **3**, **4**, **5**, **6**, **7**, and **8**), 125.9 (1C, q, J: 276.5, **12**); ***δ_F*** -65.3 (3F, t, $^{1}J_{C,F}$: 10.8); ***ν_{MAX}(film)/cm⁻¹*** 838.34, 1005.46 1146.22, 1256.74 (CF_3); 1351.14, 1443.49 (C-O-C); 2879.89 (C-H); 3458.17 (O-H); ***HRMS m/z (ES+)***: $[MNa]^+$ 313.1237, calculated 313.1239.

v). Tetraethylene glycol 3,3,3-trifluoropropyl undec-10-unyl ether (12c)[9]

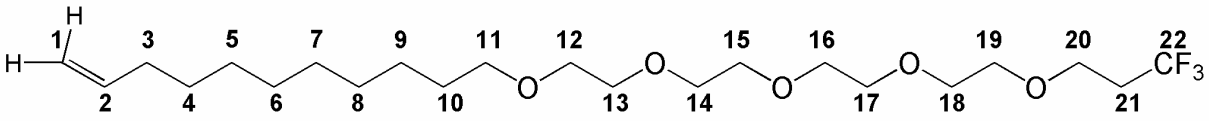

Figure III-22: Tetrathylene glycol 3,3,3-trifluoropropyl undec-10-wnyl ether

δ_H 1.21–1.41 (12H, m, **4**-H, **5**-H, **6**-H, **7**-H, **8**-H and **9**-H), 1.51–1.64 (2H, m, **10**-H), 1.95–2.14 (2H, m, **3**-H), 2.43 (2H, tq, $^{4}J_{H,F}$: 10.8, $^{3}J_{H,H}$: 6.8, **23**-H), 3.45 (2H, t, $^{3}J_{H,H}$: 6.8, **11**-H), 3.55–3.71 (18H, m, **12**-H, **13**-H, **14**-H, **15**-H, **16**-H, **17**-H, **18**-H, **19**-H, and **20**-H), 4.90–5.04 (2H, m, **1**-H), 5.81 (1H, tdd, $^{3}J_{H,Hb}$: 17, $^{3}J_{H,Ha}$: 10.2, $^{3}J_{H,H}$: 6.7); ***δ_C*** 26.0, 28.8, 29.0, 29.3, 29.4, 29.4, 29.5, 33.7 (8C, **3**, **4**, **5**, **6**, **7**, **8**, **9**, and **10**), 34.3 (1C, q, $^{2}J_{C,F}$: 28.3, **21**), 64.0 (1C, q, $^{3}J_{C,F}$: 3.6, **20**), 70.0, 70.4, 70.5, 70.6, 71.4 (9C, **11**, **12**, **13**, **14**, **15**, **16**, **17**, **18**, and **19**), 114.0 (1C, **1**), 126.0 (1C, q, $^{1}J_{C,F}$: 276.0, **22**), 139.1 (1C, **2**); ***δ_F*** -65.3 (t, $^{3}J_{F,H}$: 10.8); ***ν_{MAX}(film)/cm⁻¹*** 993.09, 1121.72, 1257.73 (CF_3); 1351.03, 14250.35 (C-O-C); 1640.71 ($CH=CH_2$); 2855.94, 2926.77 (C-H); 3076.90 ($=CH_2$); ***HRMS m/z (ES+)***: $[MNa]^+$ 465.2801, calculated 465.2804.

vi). Tetraethylene glycol 10-acetylthiodecyl 3,3,3-trifluoropropyl ether (13c)[9]

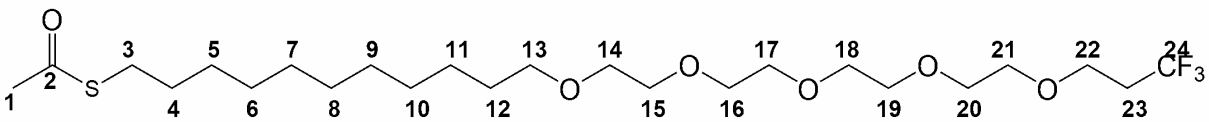

Figure III-23: Tetraethylene glycol 10-acetylthiodecyl 3,3,3-trifluoropropyl ether

δ_H 1.23–1.30 (12H, m, 6-H, 7-H, 8-H, 9-H, 10-H, and 11-H), 1.52–1.61 (6H, m, 4-H, 5-H, and 12-H), 2.32 (3H, s, 1-H), 2.42 (2H, tq, $^3J_{H,F}$: 10.8, $^3J_{H,H}$: 6.8, 23-H), 2.86 (2H, t, $^3J_{H,H}$:6.8, 3-H), 3.44 (2H, t, $^3J_{H,H}$:6.8, 13-H), 3.54–3.73 (18, m, **14**-H, **15**-H, **16**-H, **17**-H, **18**-H, **19**-H, **20**-H, **21**-H, and **22**-H); δ_C 26.0, 28.7, 29.0, 29.0, 29.4, 29.4, 29.4, and 29.5 (10C, **3**, **4**, **5**, **6**, **7**, **8**, **9**, and **10**), 34.3 (1C, q, $^3J_{C,F}$: 28.2, **23**), 64.0 (1C, q, $^3J_{C,F}$: 3.5, **22**), 69.9, 70.4, 70.5, 70.6, and 71.4 (9C, **13**, **14**, **15**, **16**, **17**, **18**, **19**, **20**, and **21**), 126.0 (1C, q, $^3J_{C,F}$:276.9, **24**), 196.0 (1C, **2**); δ_F -65.3 (3F, t, $^3J_{F,H}$:10.8, **22**-F); ν_{MAX}***(film)/cm^{-1}*** 627.84 (-S-); 841.58, 1005.04, 1135.93, 1255.78 (CF_3); 1352.96, 1441.76 (C-O-C); 1693.70 (C=O); 2856.59, 2926.82 (C-H); ***HRMS m/z (****ES+)*: [MNa]$^+$ 541.2787, calculated 541.2787.

vii). (1-mercaptoundec-11-yl)tetra(ethylene glycol) 3,3,3-trifluoropropyl ether (3)[9]

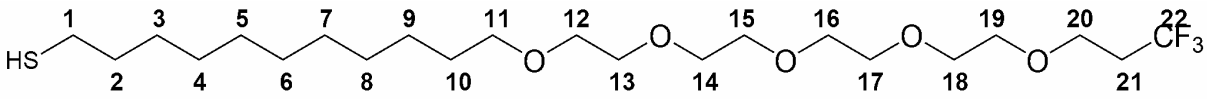

Figure III-24: (1-mercaptoundec-11-yl)tetra(ethylene glycol) 3,3,3-trifluoropropyl ether

δ_H 1.15–1.39 (15H, m, **3**-H, **4**-H, **5**-H, **6**-H, **7**-H, **8**-H, **9**-H, and S-H), 1.47–1.62 (4H, m, **2**-H, and **10**-H), 2.26–2.52 (4H, m, **1**-H, and **21**-H), 3.40 (2H, t, $^3J_{H,H}$: 3.40, **11**-H), 3.50–3.70 (18H, m, **12**-H, **13**-H, **14**-H, **15**-H, **16**-H, **17**-H, **18**-H, **19**-H, and **20**-H); δ_C 24.5, 25.9, 28.2, 28.9, 29.3, 29.4, 29.5, 32.8, 33.9, and 34.0 (10C, **1**, **2**, **3**, **4**, **5**, **6**, **7**, **8**, **9**, and **10**), 34.2 (1C, q, $^2J_{C,F}$: 28.1, **21**), 63.9 (1C, q, $^3J_{C,F}$: 3.6, **20**), 69.9, 70.4, 70.4, 70.5, 71.3 (8C, **11**, **12**, **13**, **14**, **15**, **16**, **17**, and **18**), 126.0 (1C, q, $^1J_{C,F}$: 277.0, **22**); δ_F -65.3 (3F, t, $^3J_{F,H}$:10.8, **22**-F); ν_{MAX}***(film)/cm^{-1}*** 657.73 (S-C); 842.51, 1004.91, 1148.59, 1255.80 (CF_3); 1351.01, 1439.67 (C-O-C); 2856.45, 2927.02 (C-H); ***HRMS m/z (****ES+)*: [MNa]$^+$ 499.2685, calculated 499.2681.

5) Synthesis of (1-mercaptoundec-11-yl)tetra(ethylene glycol) 2,2,2-trifluoroethyl ether (**4**)

i). Tetraethylene glycol benzyl 2,2,2-trifluoroethyl ether (10d)[7]

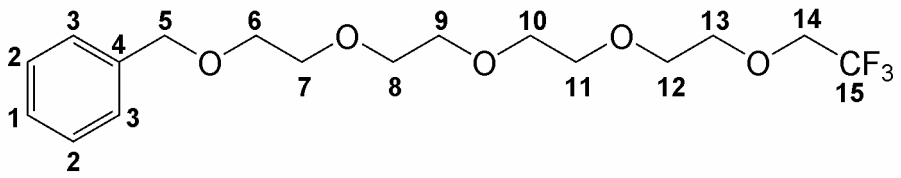

Figure III-25: Tetraethylene glycol benzyl 2,2,2-trifluoroethyl ether

δ_H 3.81–3.82 (16H, m, **6**-H, **7**-H, **8**-H, **9**-H, **10**-H, **11**-H, **12**-H, and **13**-H), 3.91 (2H, q, $^3J_{H,F}$: 8.8, **14**-H), 4.58 (2H, s, **5**-H), 7.28–7.39 (5H, m, **1**-H, **2**-H, and **3**-H); δ_C 68.5 (1C, q, $^2J_{C,F}$: 33.8, **14**), 69.3, 70.4, 70.5, 70.5, 71.7, and 73.0 (9C, **5**, **6**, **7**, **8**, **9**, **10**, **11**, **12**, and **13**), 123.9 (1C, $^1J_{C,F}$: 279.9, **15**), 127.4, 127.6, 128.2 (5C, **1**, **2**, and **3**), 138.1 (1C, **4**); δ_F -74.71 (t, $^1J_{C,F}$: 8.8, **15**-F); ν_{MAX}*(film)/cm*$^{-1}$ 699.14, 739.35 (Ar); 965.47, 1152.07, 1279.34 (CF_3); 1351.05, 1454.58 (C-O-C); 2869.87 (C-H); 3031.67, 3064.85, 3089.06 (Ar); ***HRMS m/z*** *(ES+)*: $[MNa]^+$ 389.1552, calculated 389.1553.

ii). Tetraethylene glycol mono (2,2,2-trifluoroethyl) ether (11d)[8]

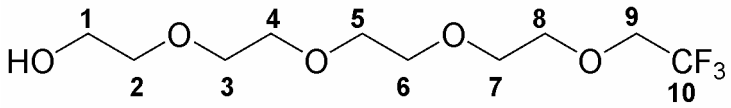

Figure III-26: Tetraethylene glycol mono(2,2,2-trifluoroethyl) ether

δ_H 2.10 (1H, s br,), 3.58–3.84 (16H, **1**-H, **2**-H, **3**-H, **4**-H, **5**-H, **6**-H, **7**-H, and **8**-H), 3.92 (2H, q, $^3J_{H,F}$: 8.8, **9**-H); δ_C 61.4 (1C, **1**), 68.5 (1C, q, $^3J_{H,H}$: 33.8, **9**), 70.1, 70.3, 70.4, 70.4, 71.7, 72.4 (7C, m, **2**, **3**, **4**, **5**, **6**, **7**, and **8**), 123.9 (1C, q, J: 279.7, **10**); δ_F -74.7 (t, $^3J_{H,F}$: 8.8); ν_{MAX}*(film)/cm*$^{-1}$ 886.48, 965.69, 1156.36, 1279.92 (CF_3); 1350.79, 1457.32 (C-O-C); 2877.33 (C-H); 3446.23 (O-H); ***HRMS m/z*** *(ES+)*: $[MNa]^+$ 299.1082, calculated 299.1078.

iii). Tetraethylene glycol 2,2,2-trifluoroethyl undec-10-enyl ether (12d)[9]

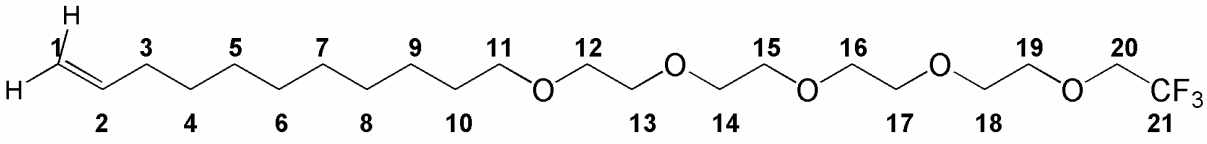

Figure III-27: Tetraethylene glycol 2,2,2-trifluoroethyl undec-10-enyl ether

δ_H 1.14–1.63 (16H, m, **3**-H, **4**-H, **5**-H, **6**-H, **7**-H, **8**-H, **9**-H and **10**-H), 1.94–2.06 (2H, m, **10**-H), 3.41 (2H, t, $^3J_{H,H}$: 6.8, **11**-H), 3.51–3.78 (16H, m, **12**-H, **13**-H, **14**-H, **15**-H, **16**-H, **17**-H, **18**-H and **19**-H), 3.88 (2H, q, $^3J_{H,F}$: 8.9, **20**-H), 4.86–4.99 (2H, m, **1**-H_a, and 1-H_b), 5.77 (1H, tdd, $^3J_{H,\ Hb}$: 17.0, $^3J_{H,\ Hb}$: 10.3, $^3J_{H,\ H}$: 6.6, **2**-H); δ_C 25.9, 28.8, 29.0, 29.3, 29.3, 29.4, 29.5 (7C, **4**, **5**, **6**, **7**, **8**, **9**, and **10**), 33. 7 (1C, **3**), 69.1 (1C, q, $^2J_{C,F}$: 33.9, **20**), 69.9, 70.4, 70.5, 70.5, 70.6, 71.4, 71.8 (9C, **11**, **12**, **13**, **14**, **15**, **16**, **17**, **18**, and **19**), 114.0 (1C, **1**), 123.9 (1C, q, $^1J_{C,F}$: 279.2, **20**), 139.0 (1C, **2**); δ_F -74.8 (t, $^3J_{F,H}$: 8.8); ν_{MAX}*(film)/cm*$^{-1}$ 966.08, 1120.17, 1280.04 (CF_3); 1351.27, 1459.54 (C-O-C); 1640.87 ($CH=CH_2$); 2857.42, 2927.59 (C-H); 3077.06 ($=CH_2$); ***HRMS m/z (****ES+)*: $[MNa]^+$ 451.2659, calculated 451.2647.

iv). Tetraethylene glycol 10-acetylthiodecyl 2,2,2-trifluoroethyl ether (13d)[9]

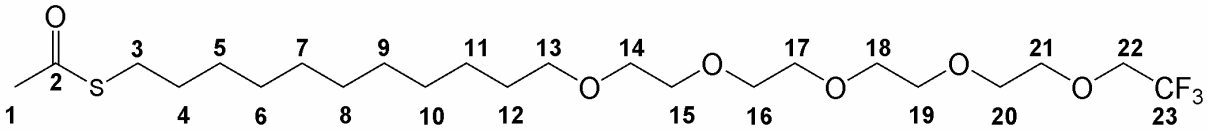

Figure III-28: Tetraethylene glycol 10-acetylthiodecyl 2,2,2-trifluoroethyl ether

δ_H 1.20–1.66 (18H, m, **4**-H, **5**-H, **6**-H, **7**-H, **8**-H, **9**-H, **10**-H, **11**-H, and **12**-H), 2.36 (3H, s, **1**-H), 2.87 (2H, t, $^3J_{H,H}$: 7.4, **3**-H), 3.45 (2H, t, $^3J_{H,H}$: 6.8, **13**-H), 3.52–3.83 (16H, m, **14**-H, **15**-H, **16**-H, **17**-H, **18**-H, **19**-H, **20**-H and **21**-H), 3.90 (2H, q, $^3J_{H,F}$: 8.8, **22**-H); δ_C 25.9, 28.7, 28.9, 29.0, 29.3, 29.3, 29.4, 29.5, 30.5 (10C, **1**, **3**, **4**, **5**, **6**, **7**, **8**, **9**, **10**, and **11**), 68.6 (1C, q, $^2J_{C,F}$: 33.8, **21**), 69.9, 70.5, 70.6, 71.4, 71.8 (9C, **12**, **13**, **14**, **15**, **16**, **17**, **18**, **19**, and **20**), 123.9 (1C,

22), 195.8 (1C, **2**); δ_F -74.7 (3F, t, $^3J_{F,H}$: 8.8, **22**-F); ν_{MAX}*(film)/cm*$^{-1}$ 627.51 (-S-); 827.76, 964.91, 1154.86, 1279.86 (CF_3); 1354.17, 1460.23 (C-O-C); 1693.27 (C=O); 2856.75, 2927.76 (C-H); ***HRMS m/z (****ES+)*: $[MNa]^+$ 527.2637, calculated 527.2630.

v). (1-mercaptoundec-11-yl)tetra(ethylene glycol) 2,2,2-trifluoroethyl ether (4)[9]

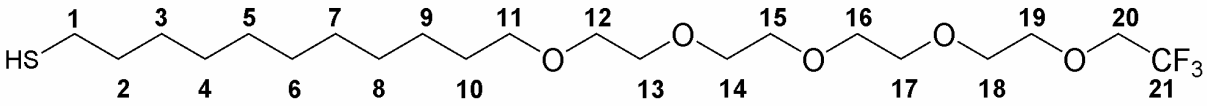

Figure III-29: (1-mercaptoundec-11-yl)tetra(ethylene glycol) 2,2,2-trifluoroethyl ether

δ_H 1.25–1.64 (19H, m, S-H, **2**-H, **3**-H, **4**-H, **5**-H, **6**-H, **7**-H, **8**-H, **9**-H, and **10**-H), 2.51 (2H, td, $^3J_{H,F}$: 7.19, $^3J_{H,H}$: 7.46, **1**-H), 3.45 (2H, t, $^3J_{H,H}$: 6.79, **11**-H), 3.56–3.70 (16H, m, **12**-H, **13**-H, **14**-H, **15**-H, **16**-H, **17**-H, **18**-H, and **19**-H), 3.92 (2H, q, $^3J_{H,F}$: 8.9, **20**-H); δ_C 24.6, 26.0, 28.3, 28.5, 29.0, 29.2, 29.5, 29.6, 34.0 (10C, **1**, **2**, **3**, **4**, **5**, **6**, **7**, **8**, **9**, and **10**), 70.0, 70.5, 70.6, 70.7, 71.5, 71.9 (9C, **11**, **12**, **13**, **14**, **15**, **16**, **17**, **18**, and **19**), 68.7 (1C, q, $^2J_{C,F}$: 35.9, **20**), 124.0 (1C, q, $^1J_{C,F}$: 279.8, **21**); δ_F -74.7 (3F, t, $^3J_{F,H}$: 8.8, **21**-F); ν_{MAX}*(film)/cm*$^{-1}$ 667.69 (S-C); 827.40, 965.80, 1154.13, 1279.49 (CF_3); 1350.50, 1457.68 (C-O-C); 2360.10, 2925.98 (C-H); ***HRMS m/z (****ES+)*: $[MNa]^+$ 485.2540, calculated 485.2525.

6) Synthesis of (1-mercaptoundec-11-yl)haxa(ethylene glycol) 2,2,2-trifluoropropyl ether (**5**)

i). Hexaethylene glycol monobenzyl ether (8c)[7]

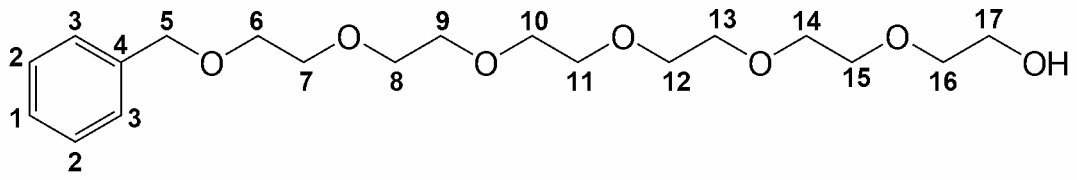

Figure III-30: Hexaethylene glycol monobenzyl ether

δ_H 2.59 (1H, s br, **17**-O*H*), 3.58–3.76 (24H, m, **6**-H, **7**-H, **8**-H, **9**-H, **10**-H, **11**-H, **12**-H, **13**-H, **14**-H, **15**-H, **16**-H, and **17**-H), 4.57 (2H, s, **5**-H), 7.27–7.38 (5H, m, **1**-H, **2**-H, and **3**-H); δ_C 61.6 (1C, **17**), 69.3, 70.2, 70.5, 72.4, 73.1 (12C, **5**, **6**, **7**, **8**, **9**, **10**, **11**, **12**, **13**, **14**, **15**, and **16**), 127.5, 127.6, 128.3 (5C, **1**, **2**, and **3**), 138.2 (1C, **4**); ν_{MAX}***(film)/cm***$^{-1}$ 699.46, 740.69 (Ar); 1104.59, 1350.41, 1453.92 (C-O-C); 2868.04 (C-H); 3030.26, 3062.60 (Ar); 3470.61 (O-H); ***HRMS m/z (****ES+)*: $[MNa]^+$ 395.2042, calculated 395.2046.

ii). 2-(2-(2-(2-(2-(2-benzyloxyethoxy)ethoxy)ethoxy)ethoxy)ethyl methanesulfonate (9c)[8]

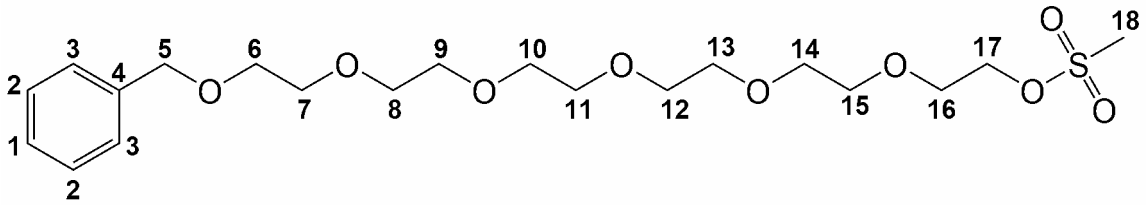

Figure III-31: 2-(2-(2-(2-(2-(2-benzyloxyethoxy)ethoxy)ethoxy)ethoxy)ethyl methanesulfonate

δ_H 3.08 (3H, s, **18**-H), 3.60–3.72 (20H, m, **6**-H, **7**-H, **8**-H, **9**-H, **10**-H, **11**-H, **12**-H, **13**-H, **14**-H, **15**-H, and **16**-H), 3.74–4.41 (4H, m, **16**-H, and **17**-H), 4.57 (2H, s, **5**-H), 7.28–7.37 (5H, m, **1**-H, **2**-H, and **3**-H); δ_C 37.6 (1C, **18**), 68.8, 69.2, 69.3, 70.4, 70.4, 70.5 (12C, **6**, **7**, **8**, **9**, **10**, **11**, **12**, **13**, **14**, **15**, **16**, and **17**), 73.1 (1C, **5**), 127.4, 127.6, 128.2 (5C, **1**, **2**, and **3**), 138.1 (1C, **4**); ν_{MAX}***(film)/cm***$^{-1}$ 700.89, 750.84 (Ar); 799.37, 921.35 (-SO_2-); 1101.86 (C-O-C); 1367.41,

1454.30 (C-O-C); 2873.99 (C-H); 3031.56 (Ar); ***HRMS m/z (ES+)***: $[MNa]^+$ 473.1829, calculated 473.1821.

iii). Hexaethylene glycol benzyl 3,3,3-trifluoropropyl ether (10e)[7]

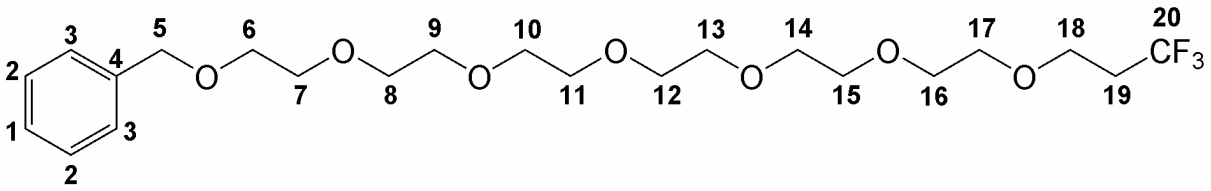

Figure III-32: Hexaethylene glycol benzyl 3,3,3-trifluoropropyl ether

δ_H 2.42 (2H, tq, $^3J_{H,F}$: 10.8, $^3J_{H,F}$: 6.8, **19**-H), 3.36–3.96 (28H, m, **5**-H, **6**-H, **7**-H, **8**-H, **9**-H, **10**-H, **11**-H, **12**-H, **13**-H, **14**-H, **15**-H, **16**-H, **17**-H, and **18**-H), 4.57 (2H, s, **4**-H), 7.28–7.38 (5H, m, **1**-H, **2**-H and **3**-H); δ_C 34.3 (1C, q, $^2J_{C,F}$: 28.0, **19**), 64.0 (1C, q, $^3J_{C,F}$: 3.6, **18**), 69.4, 70.5, 70.6, 73.2 (13C, **5**, **6**, **7**, **8**, **9**, **10**, **11**, **12**, **13**, **14**, **15**, **16**, and **17**), 127.5, 127.7, 128.3 (5C, **1**, **2**, and **3**), 138.2 (1C, **4**); δ_F -65.22 (t, $^3J_{H,F}$: 10.8, **20**-F); ν_{MAX}***(film)/cm^{-1}*** 699.27, 739.75 (Ar); 947.30, 1113.42, 1256.17 (CF_3); 1350.64, 1454.10 (C-O-C); 2870.08 (C-H); 3031.24, 3064.12 (Ar); ***HRMS m/z (ES+)***: $[MNa]^+$ 491.2226, calculated 491.2233.

iv). Hexaethylene glycol mono(3,3,3-trifluoropropyl) ether(11e)[9]

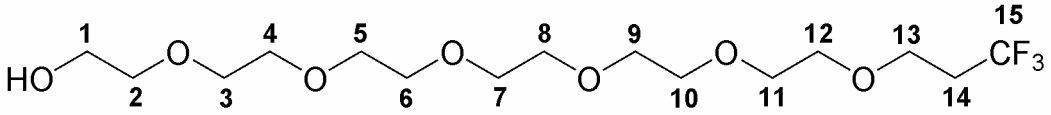

Figure III-33: Hexaethylene glycol mono(3,3,3-trifluoropropyl) ether

δ_H 2.42 (2H, tq, $^3J_{H,F}$: 10.8, $^3J_{H,H}$: 6.8, **14**-H), 2.55 (1H, s br, OH), 3.39–3.91 (26H, m, **1**-H, **2**-H, **3**-H, **4**-H, **5**-H, **6**-H, **7**-H, **8**-H, **9**-H, **10**-H, **11**-H, **12**-H, and **13**-H); δ_C 34.1 (1C, q, $^2J_{C,F}$: 28.3, **14**), 57.9, 61.4, 70.1, 70.3, 70.4, 72.4 (12C, **1**, **2**, **3**, **4**, **5**, **6**, **7**, **8**, **9**, **10**, **11** and **12**), 63.9 (1C, q, $^3J_{C,F}$: 3.6, **13**), 126.0 (1C, q, $^1J_{C,F}$: 276.0, **15**); δ_F -65.23 (3F, t, $^3J_{H,F}$: 10.8, **15**-F); ν_{MAX}***(film)/cm^{-1}*** 840.88, 946.78, 1139.04, 1256.73 (CF_3); 1350.66, 1443.59 (C-O-C); 2873.92 (C-H); 3471.16 (O-H); ***HRMS m/z (ES+)***: $[MNa]^+$ 379.1939, calculated 379.1944.

v). Hexaethylene glycol 3,3,3-trifluoropropyl undec-10-enyl ether (12e)[9]

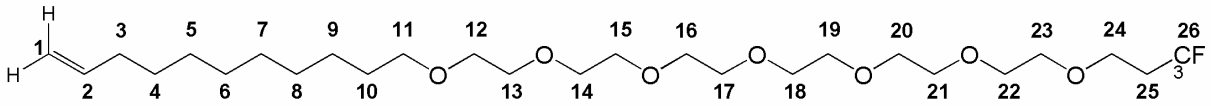

Figure III-34: Hexaethylene glycol 3,3,3-trifluoropropyl undec-10-enyl ether

δ_H 1.25–1.61 (14H, m, **4**-H, **5**-H, **6**-H, **7**-H, **8**-H, **9**-H, and **10**-H), 1.96–2.09 (2H, m, **3**-H), 2.41 (2H, tq, $^3J_{H,F}$: 10.8, $^3J_{H,H}$: 6.8, **25**-H), 3.44 (2H, t, $^3J_{H,H}$: 6.8, **24**-H), 3.55–3.66 (24H, m, **12**-H, **13**-H, **14**-H, **15**-H, **16**-H, **17**-H, **18**-H, **19**-H, **20**-H, **21**-H, **22**-H, and **23**-H), 3.69 (2H, t, $^3J_{H,H}$: 6.8, **11**-H), 4.79–5.08 (2H, m, **1**-H), 5.80 (1H, tdd, $^3J_{H,H}$: 17.1, $^3J_{H,Ha}$: 10.3, $^3J_{H,Hb}$: 6.7, **2**-H); δ_C 26.0, 28.8, 29.0, 29.4, 29.4, 29.5, 29.6, 33.7 (8C, **3**, **4**, **5**, **6**, **7**, **8**, **9**, and **10**), 34.3 (1C, q, $^2J_{C,F}$: 28.2, **25**), 64.0 (1C, q, $^2J_{C,F}$: 3.6, **24**), 70.0, 70.5, 70.6, 71.5 (13C, **11**, **12**, **13**, **14**, **15**, **16**, **17**, **18**, **19**, **20**, **21**, **22** and **23**), 114.0 (1C, **1**), 126.0 (1C, q, $^1J_{C,F}$: 277.6, **26**), 139.1 (1C, **2**); δ_F -65.23 (t, $^3J_{F,H}$: 10.8); ν_{MAX}*(film)/cm*$^{-1}$ 911.84, 1121.31, 1255.94 (CF_3); 1350.14, 1458.26 (C-O-C); 1640.93 ($CH=CH_2$); 2857.63, 2926.79 (C-H); 3076.89 ($=CH_2$); ***HRMS m/z*** *(ES+)*: $[MNa]^+$ 553.3312, calculated 553.3328.

vi). Hexaethylene glycol 10-acetylthiodecyl 3,3,3-trifluoropropyl ether (13e)[9]

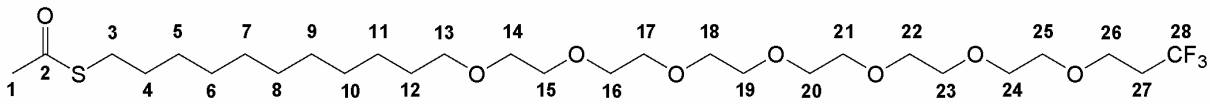

Figure III-35: Hexaethylene glycol 10-acetylthiodecyl 3,3,3-trifluoropropyl ether

δ_H 1.26–1.61 (18H, m, **4**-H, **5**-H, **6**-H, **7**-H, **8**-H, **9**-H, **10**-H, **11**-H, and **12**-H), 2.33 (3H, s, **1**-H), 2.43 (2H, qt, $^3J_{H,F}$: 10.8, $^3J_{H,H}$: 6.8, **27**-H), 2.87 (2H, t, $^3J_{H,H}$: 7.4, **26**-H), 3.45 (2H, t, $^3J_{H,H}$: 6.8, **13**-H), 3.55–3.68 (24H, m, **14**-H, **15**-H, **16**-H, **17**-H, **18**-H, **19**-H, **20**-H, **21**-H, **22**-H, **23**-H, **24**-H, **25**-H, **26**-H, **27**-H, and **28**-H), 3.71 (2H, t, $^3J_{H,H}$: 6.8, **3**-H); δ_C 26.0, 28.7, 29.0, 29.1, 29.4, 29.5, 29.5, 30.5 (11C, **1**, **3**, **4**, **5**, **6**, **7**, **8**, **9**, **10**, **11** and **12**), 33.9 (1C, q, $^2J_{C,F}$: 28.1, **27**), 64.0 (1C, q, $^3J_{C,F}$: 3.6, **26**), 70.0, 70.4, 70.5, 70.6, 71.5 (13C, **13**, **14**, **15**, **16**, **17**, **18**, **19**, **20**, **21**, **22**, **23**, **24**, and **25**), 126.5 (1C, q, $^1J_{C,F}$: 276.6, **28**), 196.3 (1C, **2**); δ_F -65.27 (3F, t, $^3J_{F,H}$:

10.4, **28**-F); $\boldsymbol{v_{MAX}}$***(film)/cm*$^{-1}$ 628.42 (-S-); 849.52, 952.76, 1135.09, 1256.02 (CF_3); 1354.00, 1457.18 (C-O-C); 1692.34 (C=O); 2857.10, 2927.44 (C-H); ***HRMS m/z (****ES+)*: $[MNa]^+$ 629.3311, calculated 629.3311.

vii). (1-mercaptoundec-11-yl)hexa(ethylene glycol) 3,3,3-trifluoropropyl ether (5)

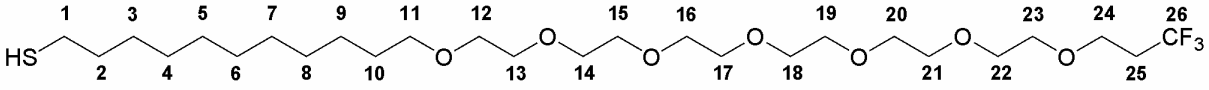

Figure III-36: (1-mercaptoundec-11-yl)hexa(ethylene glycol) 3,3,3-trifluoropropyl ether

$\boldsymbol{\delta_H}$ 1.26–1.66 (18H, m, **2**-H, **3**-H, **4**-H, **5**-H, **6**-H, **7**-H, **8**-H, **9**-H, and **10**-H), 2.42 (2H, tq, $^3J_{H,F}$: 10.8, $^3J_{H,H}$: 6.8, **25**-H), 2.49–2.56 (1H, m, S-H), 3.45 (2H, t, $^3J_{H,H}$: 6.8, **1**-H), 3.49–3.68 (24H, m, **11**-H, **12**-H, **13**-H, **14**-H, **15**-H, **16**-H, **17**-H, **18**-H, **19**-H, **20**-H, **21**-H, **22**-H, and **23**-H), 3.70 (2H, t, $^3J_{H,H}$: 6.8, **24**-H); $\boldsymbol{\delta_C}$ 23.8, 25.3, 27.5, 28.2, 28.7, 28.7, 33.2 (10C, **1**, **2**, **3**, **4**, **5**, **6**, **7**, **8**, **9**, and **10**), 33.6 (1C, q, $^2J_{C,F}$: 28.2, **25**), 57.5 (1C, **24**), 63.4, 69.2, 69.7, 70.7 (13C, **11**, **12**, **13**, **14**, **15**, **16**, **17**, **18**, **19**, **20**, **21**, **22**, and **23**), 125.4 (1C, q, $^1J_{C,F}$: 276.8, **26**); $\boldsymbol{\delta_F}$ -65.21 (3F, t, $^3J_{F,H}$: 10.6, **26**-F); $\boldsymbol{v_{MAX}}$***(film)/cm*$^{-1}$ 657.66 (S-C); 843.95, 950.09, 1144.60, 1256.25 (CF_3); 1350.34, 1456.74 (C-O-C); 2856.34, 2930.18 (C-H); ***HRMS m/z (****ES+)*: $[MNa]^+$ 587.3201, calculated 587.3205.

7) Synthesis of (1-mercaptoundec-11-yl)hexa(ethylene glycol) 2,2,2-trifluoroethyl ether (**6**)

i). Hexaethylene glycol benzyl ether 2,2,2-trifluoroethyl ether (10f)[7]

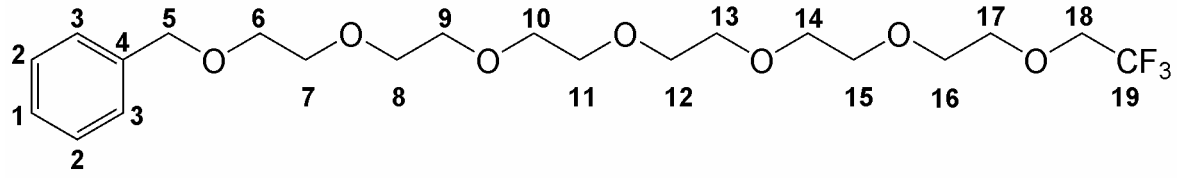

Figure III-37: Hexaethylene glycol benzyl ether 2,2,2-trifluoroethyl ether

δ_H 3.61–3.82 (24H, m, **6**-H, **7**-H, **8**-H, **9**-H, **10**-H, **11**-H, **12**-H, **13**-H, **14**-H, **15**-H, **16**-H, and **17**-H), 3.92 (2H, q, $^3J_{H,F}$: 8.8, **18**-H), 4.58 (2H, s, **5**-H), 7.28–7.39 (5H, m, **1**-H, **2**-H and **3**-H); δ_C 68.7 (1C, q, $^2J_{C,F}$: 33.8, **18**), 69.4, 70.5, 70.6, 70.6, 71.9, 73.1 (13C, **5**, **6**, **7**, **8**, **9**, **10**, **11**, **12**, **13**, **14**, **15**, **16**, and **17**), 124.0 (1C, q, $^1J_{C,F}$: 277.67, **19**), 127.5, 127.7, 128.3 (5C, **1**, **2**, and **3**), 138.3 (1C, **4**); δ_F -74.77 (t, $^1J_{C,F}$: 8.8, **19**-F); ν_{MAX}*(film)/cm*$^{-1}$ 699.27, 740.07 (Ar); 965.14, 1109.11, 1151.38, 1279.57 (CF_3); 1351.09, 1454.69 (C-O-C); 2869.75 (C-H); 3031.07, (Ar); ***HRMS m/z (****ES+)*: $[MNa]^+$ 477.2068, calculated 477.2076.

ii). Hexaethylene glycol mono(2,2,2-trifluoroethyl) ether (11f)[9]

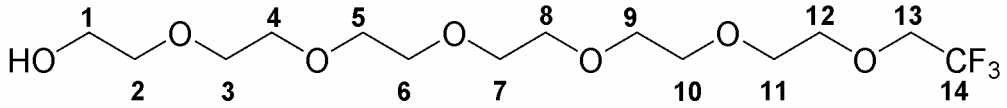

Figure III-38: Hexaethylene glycol 2,2,2-trifluoroethyl undec-10-enyl ether

δ_H 2.50 (2H, s br, **1**-H), 3.57–3.83 (23H, m, OH, **2**-H, **3**-H, **4**-H, **5**-H, **6**-H, **7**-H, **8**-H, **9**-H, **10**-H, **11**-H and **12**-H), 3.92 (2H, q, $^3J_{H,F}$: 8.7, **13**-H) ; δ_C 61.7 (1C, s, **1**), 68.7 (1C, q, $^2J_{C,F}$: 33.9, **13**),70.3, 70.5, 70.6, 71.9, 72.5 (11C, m, **2**, **3**, **4**, **5**, **6**, **7**, **8**, **9**, **10**, **11** and **12**), 124.0 (1C, q, J:

208.0, **14**); δ_F -74.72 (3F, t, $^3J_{H,F}$: 8.7, **14**-F); ν_{MAX}*(film)/cm*$^{-1}$ 846.03, 965.35, 1152.24, 1279.86 (CF_3); 1351.39, 1455.93 (C-O-C); 2873.22 (C-H); 3466.28 (O-H); ***HRMS m/z (ES+)***: $[MNa]^+$ 365.1789, calculated 365.1787.

iii). Hexaethylene glycol 2,2,2-trifluoroethyl undec-10-enyl ether (11f)[9]

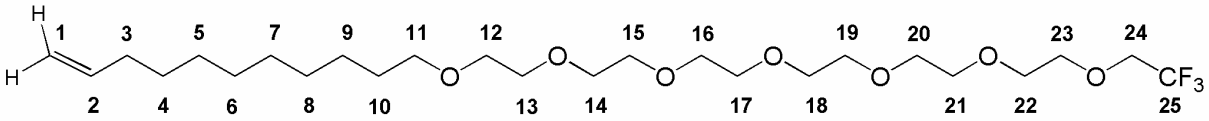

Figure III-39: Hexaethylene glycol 2,2,2-trifluoroethyl undec-10-enyl ether

δ_H 1.25–1.32 (14H, m, **4**-H, **5**-H, **6**-H, **7**-H, **8**-H, **9**-H, and **10**-H), 1.98–2.12 (2H, m, **3**-H), 3.45 (2H, t, $^3J_{H,H}$: 6.8, **18**-H), 3.63–3.70 (24H, m, **12**-H, **13**-H, **14**-H, **15**-H, **16**-H, **17**-H, **18**-H, **19**-H, **20**-H, **21**-H, **22**-H, and **23**-H), 3.92 (2H, q, $^3J_{H,F}$: 8.8, **24**-H), 4.85–5.05 (2H, m, **1**-H), 5.80 (1H, tdd, $^3J_{H,H}$: 17.1, $^3J_{H,Ha}$: 10.2, $^3J_{H,Hb}$: 6.7, **2**-H); δ_C 25.7, 26.0, 28.9, 29.1, 29.4, 29.4, 29.5, 29.6, 33.8, 35.7 (8C, **3**, **4**, **5**, **6**, **7**, **8**, **9**, and **10**), 68.7 (1C, q, $^2J_{C,F}$: 33.8, **24**), 70.0, 70.6, 70.7, 71.5, 71.9 (13C, **11**, **12**, **13**, **14**, **15**, **16**, **17**, **18**, **19**, **20**, **21**, **22** and **23**), 114.1 (1C, **1**), 139.2 (1C, s, **2**); δ_F -74.72 (t, $^3J_{F,H}$: 8.8); ν_{MAX}*(film)/cm*$^{-1}$ 965.77, 1153.10, 1251.57 (CF_3); 1350.30, 1461.72 (C-O-C); 1640.86 ($CH=CH_2$); 2857.37, 2926.44 (C-H); 3076.36 ($=CH_2$); ***HRMS m/z (ES+)***: $[MNa]^+$ 539.3176, calculated 539.3172.

iv). Hexaethylene glycol 10-acetylthiodecyl 2,2,2-trifluoroethyl ether (13f)[9]

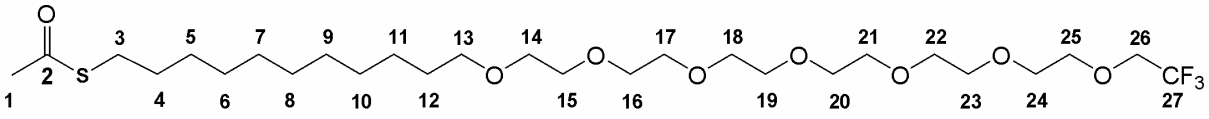

Figure III-40: Hexaethylene glycol 10-acetylthiodecyl 2,2,2-trifluoroethyl ether

δ_H 1.23–1.59 (18H, m, **4**-H, **5**-H, **6**-H, **7**-H, **8**-H, **9**-H, **10**-H, **11**-H, and **12**-H), 2.31 (3H, s, **1**-H), 2.85 (2H, t, $^3J_{H,H}$: 7.4, **3**-H), 3.43 (2H, t, $^3J_{H,H}$: 6.8, **13**-H), 3.53–3.82 (16H, m, **14**-H, **15**-H,

16-H, **17**-H, **18**-H, **19**-H, **20**-H and **21**-H), 3.90 (2H, q, $^{3}J_{H,F}$: 8.8, **22**-H); δ_C 26.0, 28.7, 29.0, 29.1, 29.4, 29.5, 29.6 (10C, **3**, **4**, **5**, **6**, **7**, **8**, **9**, **10**, **11**, and **12**), 30.6 (1C, **1**), 68.6 (1C, q, $^{2}J_{C,F}$: 33.9, **26**), 70.0, 70.5, 70.6, 71.5, 71.9 (12C, **14**, **15**, **16**, **17**, **18**, **19**, **20**, **21**, **22**, **23**, **24**, and **25**), 124.0 (1C, q, $^{1}J_{C,F}$: 279.6, **27**), 196.0 (1C, **2**); δ_F -74.71 (3F, t, $^{3}J_{F,H}$: 8.8, **27**-F); ν_{MAX}*(film)/cm*$^{-1}$ 627.37 (-S-); 847.17, 964.58, 1118.47, 1279.45 (CF_3); 1353.39, 1461.98 (C-O-C); 1692.97 (C=O); 2856.47, 2926.44 (C-H); ***HRMS m/z (****ES+)*: $[MNa]^+$ 615.3146, calculated 615.3154.

v). (1-mercaptoundec-11-yl)hexa(ethylene glycol) 2,2,2-trifluoroethyl ether (6)[9]

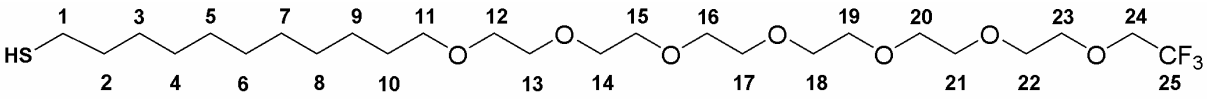

Figure III-41: (1-mercaptoundec-11-yl)hexa(ethylene glycol) 2,2,2-trifluoroethyl ether

δ_H 1.10–1.48 (18H, m, **2**-H, **3**-H, **4**-H, **5**-H, **6**-H, **7**-H, **8**-H, **9**-H, and **10**-H), 2.51 (2H, td, $^{3}J_{H,H}$: 7.47, $^{3}J_{H,(S)H}$: 7.25, **1**-H), 3.44 (2H, t, $^{3}J_{H,H}$: 6.8, **11**-H), 3.52–3.82 (24H, m, **12**-H, **13**-H, **14**-H, **15**-H, **16**-H, **17**-H, **18**-H, **19**-H, **20**-H, **21**-H, **22**-H, and **23**-H), 3.91 (2H, q, $^{3}J_{H,F}$: 8.8, **24**-H); δ_C 24.6, 26.0, 28.3, 28.5, 29.0, 29.2, 29.4, 29.5, 29.6, 34.0 (10C, **1**, **2**, **3**, **4**, **5**, **6**, **7**, **8**, **9**, and **10**), 68.7 (1C, q, $^{2}J_{C,F}$: 34.0, **24**), 70.0, 70.5, 70.7, 1.5, 71.9 (13C, **11**, **12**, **13**, **14**, **15**, **16**, **17**, **18**, **19**, **20**, **21**, **22**, and **23**), 124.0 (1C, q, $^{1}J_{C,F}$: 279.8, **25**); δ_F -74.8 (3F, t, $^{3}J_{F,H}$: 8.8, **23**-F); ν_{MAX}*(film)/cm*$^{-1}$ 667.56 (S-C); 827.39, 965.82, 1153.81, 1279.59 (CF_3); 1350.37, 1460.88 (C-O-C); 2355.79, 2925.62 (C-H); ***HRMS m/z (****ES+)*: $[MNa]^+$ 573.3043, calculated 573.3049.

V)Literature

1. Y. Liu, L. Mu, B. Liu, S. Zhang, P. Yang and J. Kong, *Chem.Comm.*, 2004, 1194-1195.
2. S. Balamurugan, L. K. Ista, J. Yan, G. P. Lopez, J. Fick, M. Himmelhaus and M. Grunze, *J. Am. Chem. Soc.*, 2005, **127**, 14548-14549.
3. C. Dicke and G. Hähner, *J. Phys. Chem. B*, 2002, **106**, 450.

4. C. Dicke and G. Hähner, *J. Am. Chem. Soc.*, 2002, **124**, 12619-12625.
5. S. V. Hiremath, D. R. Reddy and M. A. Kumar, *Indian Journal of Chemistry*, 1988, **27B**, 558.
6. Y. Hashimoto, Y. Sato, N. Takeshita, K. Kudo and K. Saigo, *Tetrahedron*, 1994, **50**, 8317.
7. D. A. Gustowski, M.Delgado, V. J. Gatto, L. Echengoyen and G. W. Gokel, *J. Am. Chem. Soc.*, 1986, **108**, 7553.
8. S. M. Rubenstein, V. Baichwal, H. Beckmann, D. L. Clark, W. Frankmoelle, D. Roche, E. Santha, S. Schwender, M. Thoolen, Q. Ye and J. C. Jaen, *J. Med. Chem.*, 2001, **44**, 3599.
9. C. Pale-Grosdemange, E. S. Simon, K. L. Prime and G. M. Whitesides, *J. Am. Chem. Soc.*, 1991, **113**, 12.

Chapter 4

Trifluoro Alkyl Oligo(Ethylene Glycol)-Terminated Alkanethiol Self-Assembeld Monolayer Characterization

No matter what the ultimate application, it is essential to have as complete characterisation of new surfaces as possible. After characterising each surfactant molecule with the common procedures used in organic chemistry: ^{1}H NMR, [1] ^{13}C NMR, [2] ^{19}F NMR, IR, [3] HRMS, [4] the novel trifluoroalkyl oligo(ethylene glycol)-terminated alkanethiol self-assembled monolayers which have been prepared were characterised according to some surface characterisation methods. Among the numerous characterisation techniques, [5] there is Infrared Spectroscopy (IR), [6] which allows certifying that the chemisorption have taken place on the substrate by detecting the chemical functions of the molecules on the surface. Quartz Crystal Microbalance [7] detects a mass per unit area giving the density of the monolayer as the self-assembling molecular weight is known. Raman Spectroscopy (RS) [8] is complementary to infrared spectroscopy as it also gives the vibrational motion of chemical bonds of the molecules on the substrate. Scanning Tunnelling Spectroscopy (STM), [9] or Atomic Force Microscopy (AFM) [10] are imaging techniques which allow the structure of the atoms on the substrate to be represented. Although, each procedure provides invaluable information about SAMs, only few techniques are commonly used, mainly contact angle measurement, X-ray Photoelectron Spectroscopy (XPS), and/or ellipsometry. [11-15]

Contact angle reflects the hydrophobicity of the termination, [16] it gives information concerning the hydrophobicity of the functional groups which are in direct contact with the liquid. [17]

XPS reveals the presence of atoms on the substrate, [18] it is possible to know if the assembly process has occurred, in other words if surfactant molecules have adsorbed on the noble metal substrate. In addition to the chemical composition, XPS also allows verification that the film is free of contamination. [19] The surface coverage of a monolayer can be inspected through its morphology with an atomic force microscope, [20] but XPS is more routinely used to determine the SAM density. [11]

Although the thickness of self-assembled monolayers can be determined by Plasmon surface polarization, [21] X-ray reflectivity, [22] X-ray standing waves, [23] or XPS with angular dependent measurements, [24] it is generally determined by ellipsometry measurements.

For ease of reference, the six self-assembling molecules and their compound numbers are reproduced here:

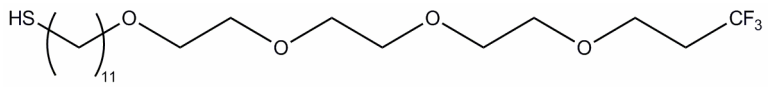

(1-mercaptoundec-11-yl)tri(ethylene glycol) 3,3,3-trifluoropropyl ether: **1**

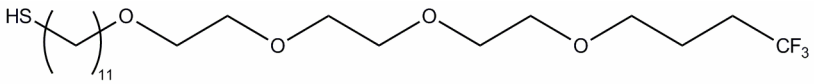

(1-mercaptoundec-11-yl)tri(ethylene glycol) 3,3,3-trifluorobutyl ether: **2**

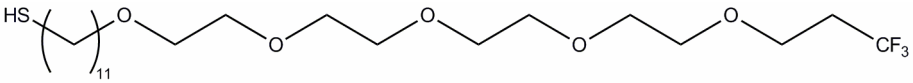

(1-mercaptoundec-11-yl)tetra(ethylene glycol) 3,3,3-trifluoropropyl ether: **3**

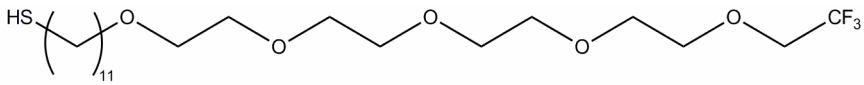

(1-mercaptoundec-11-yl)tetra(ethylene glycol) 2,2,2-trifluoroethyl ether: **4**

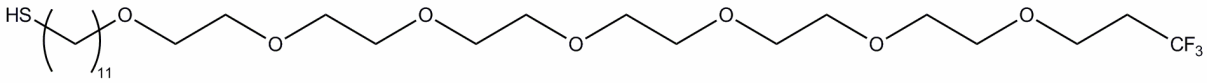

(1-mercaptoundec-11-yl)hexa(ethylene glycol) 3,3,3-trifluoropropyl ether: **5**

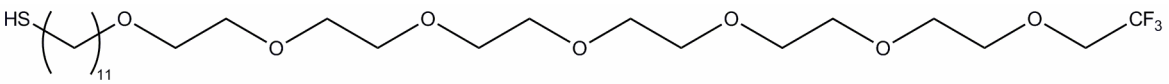

(1-mercaptoundec-11-yl)hexa(ethylene glycol) 2,2,2-trifluoroethyl ether: **6**

Figure IV-1: Six synthesized (1-mercaptoundec-11-yl)poly(ethylene glycol) 3,3,3-trifluoroalkyl ether molecules

I) Ellipsometry

1) Results

As described in chapter 2, the substrate was fully characterized. Next, the synthetic organic layer was added and fitted using a Cauchy model with two coefficients. The refractive index n is a function of the wave length according to the equation IV-1:

Equation IV-1: $n = A + \frac{B}{\lambda^2}$.

According to literature, [25] 1.45 was the value given to A which is the refractive index for high wavelengths. The thickness values measured for each SAM are presented in Table IV-1.

Ellipsometry provided a way to estimate the density of our SAMs referring to the packing density of alkanethiol films. In the alkanethiol monolayer, molecules are tilted by 30º from the surface normal. [11] These monolayers are densely packed and defect free. The density is such that the thickness of the layer equals the product of the length of the self assembling molecule by the cosine of the tilt angle. In films as dense as alkanethiol films, the thickness value measured by ellipsometry would equal this multiplication. Therefore the "height of single molecule" was calculated from the length of a self-assembling molecule (estimated with the software Gaussview) times the cosine of 30°.

The lower thickness value obtained from ellipsometry indicates a lower density compared to an alkanethiol film. The relative coverage was evaluated taking a densely packed alkanethiol film as 100% reference.

Self assembling molecule	SAM Thickness	Expected height of a single molecule	Relative coverage
1	1.79 ±0.02 nm	1.92 nm	81%
2	1.90 ±0.01 nm	2.10nm	82%
3	2.02 ±0.02 nm	1.97nm	82%
4	1.57 ±0.03 nm	2.96 nm	54%
5	2.51 ±0.04 nm	3.55 nm	70%
6	2.47 ±0.02 nm	3.26 nm	77%

Table IV-1: SAMs thicknesses, expected thicknesses, and relative coverage

2) Discussion

Herrwerth and co-workers [19] measured the density of similar methyl terminated films. They found a relative coverage of 77% for a methyl-tri(ethylene glycol)-terminated SAM. Apart from molecule **4**, our values were in agreement with their results.

Even increasing the solution concentration, the value was much lower for molecule **4**. The assumption of a lower density might be possible but not any suitable explanation was found up to now as NMR and IR spectroscopies showed that the synthesised surfactant molecule was pure and the solvent used for the solutions was the same for the six self-assembling molecules.

II) X-ray Electron Spectroscopy

The XPS survey spectra showed the presence of carbon, oxygen, fluorine, and gold as expected. The F1s gave one single peak around 688.7 eV. Another single peak was fitted for the O1s emission; this peak was around 532.9 eV. It was possible to distinguish the alkyl chain carbon atoms from those in the oligo(ethyleneglycol) groups. The first type of carbon atoms gave a peak which is used as reference and fixed at 284.6eV while the ether carbon peak was around 286.5 eV.

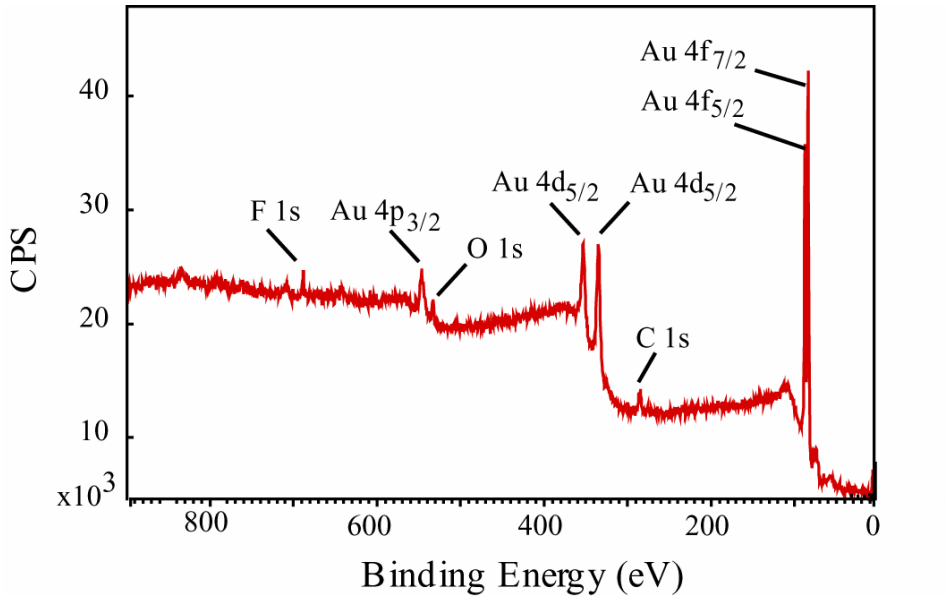

Figure IV-11: Typical XPS fullscan for a self assembled monolayer of (1-mercaptoundec-11-yl)oligo(ethylene glycol) 3,3,3-trifluoroalkyl ether

The XPS spectra were corrected for charging by referencing the aliphatic C(1s) peak of the hydrocarbons to 284.6 eV. Elemental compositions of the various surfaces were determined from the area under individual elemental peaks using sensitivity factors provided with the software as well as taking the transmission function of the analyser into account. The data base for the sensitivity factors is given in literature and is integrated in CasaXPS. [26] The spectra were fitted using a Gaussian peak shape. A Shirley background was subtracted for the quantitative analysis. Figure IV-12 is an example of the fit of a single region scan for the carbon in an $EG_3O(CH_2)_2CF_3$ SAM film.

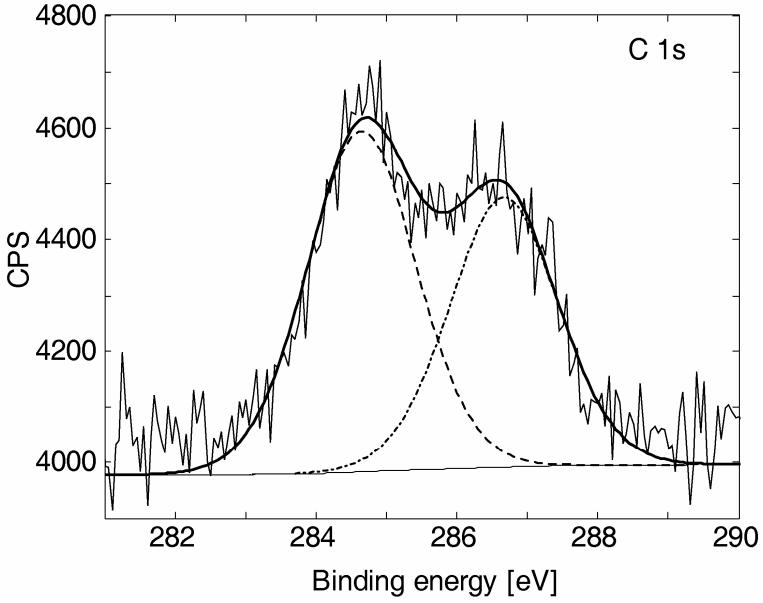

Figure IV-12: XPS carbon peaks for the $EG_3O(CH_2)_2CF_3$ film

The software generated the background and the peak as a Gaussian function form, a systematic error could be due to the estimation of the peak areas.

The measured area was multiplied by the relative sensitivities (RSF) and the transmission factors for each atom giving the atomic ratio for the molecules. Atomic ratios were measured and compared to theoretical values to ensure that there was no contamination.

The density of the films was determined following the method described by Herrwerth and co-workers. [19] The C/Au4f ratio was measured for a dodecanethiol (C_{12}) SAM and for an octadecanethiol (C_{18}) SAM. These two values were used to determine a straight line for alkanethiol films according to

Equation IV-2: $\ln(\frac{C}{Au4f}) = a*(effectivemolecularchainlength) + b$.

This equation was then used to determine the effective molecular length values for the molecules as described by Herrwerth and co-workers.

1) Results

Atomic ratios are shown in Table IV-4.

	1		2		3	
	Exp.	**Theor.**	**Exp.**	**Theor.**	**Exp.**	**Theor.**
C/O	4.2	5	3.9	5.25	3.7	4.4
C/F	4.9	6.6	4.9	7	5.2	7.3
O/F	1.2	1.3	1.3	1.3	1.4	1.6
C_{ether}/O	1.9	2	1.8	2	1.8	2
C_{ether}/F	2.2	2.67	2.3	2.67	2.6	3.33
C_{aliph}/C_{ether}	1.3	1.5	1.1	1.63	1.0	1.2
C/Au4f	0.57		0.61		0.58	

	4		5		6	
	Exp.	**Theor.**	**Exp.**	**Theor.**	**Exp.**	**Theor.**
C/O	4.6	4.2	2.6	3.57	3.2	3.71
C/F	6.3	7	6.7	8.33	5.8	8.66
O/F	1.4	1.67	2.3	2.33	1.8	2.33
C_{ether}/O	2.1	2	1.5	2	1.7	2
C_{ether}/F	2.8	3.33	3.8	4.66	3.1	4.66
C_{aliph}/C_{ether}	1.2	1.1	0.8	0.79	0.9	0.86
C/Au4f	0.43		0.76		0.68	

Table IV-4: XPS atomic ratios (experimental and theoretical) for the three synthesized molecules

The densities of molecules on the surface were extracted from the measured C/Au signal ratios. The C/Au4f ratio measured for the dodecanethiol and octadecanethiol SAMs was found to be 0.42 and 0.54 respectively. The equation of the straight line was established:

Equation IV-3: $\ln(\frac{C}{Au4f}) = 0.043 * (effectivemolecularchainlength) - 1.395$.

The effective molecular length for the molecule was deduced from this equation and Table IV-5 summarizes the results:

	1	2	3	4	5	6
Effective molecular length (nm)	1.9	2.1	2.0	1.3	2.6	2.3

Table IV-5: Experimentally determined molecular lengths of the synthesized molecules

Comparing the experimentally-determined molecular lengths with the theoretical lengths allowed the packing density of the films relative to an alkanethiol film to be quantified.

	1	2	3	4	5	6
Relative coverage	77%	81%	73%.	43%	73%	71%
Density (molecules/nm^2)	3.58	3.77	3.40	2.00	3.40	3.31

Table IV-6: Relative coverage compared to an alkanethiol SAM and density of the films

2) Discussion

All elemental ratios were close to the expected values with no indication of the presence of significant amount of contamination. The theoretical values are ideal values not taking into account the attenuation of the signal from atoms closer to the surface. Lower experimental values were therefore expected. The values were compared with those published for similar molecules in the literature. [19] As shown in Table IV-7, results compared well with the ones obtained by Herrwerth *et al.* They used XPS measurements to characterise SAMs made with similar molecules except for a CH_3 terminal group rather than a CF_3.

Surfactant	C1s ether/O1s ether	Surfactant	C1s ether/O1s ether
EG_3OPr	2.09/1	$EG_3O(CH_2)_2CF_3$ (1)	1.9/1
EG_3OBu	1.99/1	$EG_3O(CH_2)_3CF_3$ (2)	1.8/1
EG_6OPr	2.12/1	$EG_6O(CH_2)_2CF_3$ (5)	1.5/1
EG_6OEt	2.07/1	$EG_6OCH_2CF_3$ (6)	1.7/1

Table IV-7: C1s ether/O1s ether ratios for molecules 1,2, 5, and 6 and their counterparts

The values of the coverage were consistent with those obtained from ellipsometry. The density of the films was around 75% except for the monolayer composed of molecule 4. As the molecule was shown to be pure (according to NMR spectra and high-resolution mass spectroscopy) and the solvent used for the solution preparation was the same than for all the other surfaces, we did not find any explanation to date. This lower density made this film not comparable to the other five as this parameter has certainly a significant influence.

III) Contact Angle

The values were the average of three measurements taken at different locations on the surface. The water contact angle values obtained were 93, 96, 94, 67, 62, and 62° for molecules **1**, **2**, **3**, **4**, **5**, and **6** respectively.

In general, the lowest contact angles (62°) were found for the longest molecules, ie. the hexa(ethylene glycol) based SAMs. Decreasing the length of the hydrophilic oligoether end correlated with an increase in the contact angle for the tri(ethylene glycol) based molecules whose values were the highest. Individual pairs of molecules are compared in more detail below.

Self assembling molecules **1** and **2** differed by an additional CH_2 for molecule **2**. The close results indicated similarly densely packed films with a significant fraction of

hydrophobic groups exposed. The addition of one CH_2 group appeared to have a small effect on the hydrophobicity.

Self assembling molecules **1** and **3** differed by an additional oligoethylene glycol unit for molecule 3. The results were similar and indicated once more similarly densely packed films with a significant fraction of hydrophobic groups exposed. However, the hydrophobicity of the surface **3** was expected to be lower than for surface **1** as the number of ethylene glycol groups was higher. This can be explained by the fact that the group exposed to the surface and therefore in contact with water was the trifluoroalkyl moiety and that the oligo(ethylene glycol) groups were "hidden" and had no influence on the shape of the droplet.

The value obtained with the surface **4** was much lower than for the previous SAMs. As XPS and ellipsometry measurements suggested a lower density than for the five other films, the comparison with them was not relevant and this surface should be treated as a special case. We might however suppose that a lower density would lead to a higher hydrophilicity of the surface as self-assembling molecules would have more space and therefore could be fold and may more expose the OEG groups to the surface.

A noteworthy effect of the number of oligoethylene glycol groups was observed between **3** and **5**, giving a 22° lower contact angle for the hexa(ethylene glycol) based surfactant compared to the tetra(ethylene glycol) based one. Since surface **5** was composed of molecules with two additional oligo(ethylene glycol) units, these molecules could be seen as chains which become entangled and exposed more OEG groups to the surface. This idea was also highlighted by a similar contact angle for surfaces **5** and **6** where the influence of the length of the hydrophobic part was insignificant. A possible explanation may be due to the back-folding of some self-assembling molecules which leaded to the trifluoroalkyl group to be buried deeper into the monolayer.

Water contact angle measurements were previously performed for CH_3-counterparts [19] Herrwerth and co-workers measured the contact angles to estimate the surface hydrophobicity of oligoether SAMs. They wanted to observe the influence of this parameter on the protein resistance of surfaces. To study the influence of the hydrophobicity, among other parameters, they synthesised several monolayer constituents. The alkyl chain of their molecules was as long as ours: eleven methyl units separated the thiol group and the end of the surfactants. Their molecules comprised 1, 2, 3, or 6 oligo(ethylene glycol)units. This was why only molecules **1**, **2**, **5**, and **6** can be compared to their CH_3-terminated counterparts. Values for 1, 2, 5, and 6 and their homologous surfactants are presented in Table IV-8.

Surfactant[19]	Contact angle[19]	Surfactant	Contact angle
EG_3OPr	94°	$EG_3O(CH_2)_2CF_3$ (1)	93°
EG_3OBu	107°	$EG_3O(CH_2)_3CF_3$ (2)	96°
EG_6OPr	97°	$EG_6O(CH_2)_2CF_3$ (5)	62°
EG_6OEt	87°	$EG_6OCH_2CF_3$ (6)	62°

Table IV-8: Contact angle comparison between CH_3 and CF_3 terminated surfactants

Comparing with the corresponding CH_3-terminated surfactant films, the addition of one CH_2 group appeared to have a smaller effect on the hydrophobicity in the case of the CF_3-terminated surfactants, where only a moderate increase from 93 to 96° was found. On the other hand, the OEG unit addition effect was more pronounced between 2 and 5 than between EG_3OBu and EG_3OPr. Furthermore, the influence of the hydrophobic end length was not detectable for molecules **5** and **6** compared to EG_6OPr and EG_6OEt. The CF_3-terminated constituent monolayers showed generally slightly lower water contact angle values than their methyl terminated counterparts. As explained by Barriet *et al.*, stronger dipole moments with CF_3 groups interacted with the dipole moments of water molecules, decreasing the contact angle. [27] The imperceptible influence of the CH_2 addition for hexa(ethylene glycol) based molecules suggested a higher degree of disorder at the top of the molecules, such that the molecules exposed the OEG units to the surface more than the trifluoroalkyl end.

IV) Conclusions

The novel oligo(ethylene glycol), CF_3-terminated molecules were synthesised with the intention of preparing new self-assembled monolayers. XPS showed that self-assembling molecules chemisorbed well on the gold substrate and that there is no contamination of the surfaces. The aim was therefore achieved. The thickness measurements as well as the density determination demonstrated that these new SAMs were fully characterized.

V) Literature

1. J. Clayden, N. Greeves, S. Warren and P. Wothers, *Organic Chemistry*, Oxford University Press, Oxford New York, 2001.
2. R. T. Morrison and R. N. Boyd, *Organic Chemistry*, Sixth Edition edn., Prentic Hall International, Inc., EnglewoodCliffs.
3. T. W. G. Solomons, *Organic Chemistry*, Fifth Edition edn., John Wiley & Sons.
4. L. D. Field, S. Sternhell and J. R. Kalman, *Organic Structure from Spectra*, Second Edition edn., John Wiley & Sons, Chichester, 1995.
5. N. K. Chaki and K. Vijayamohanan, *Biosensors&Bioelectronics*, 2002, **17**, 1-12.
6. R. G. Nuzzo, L. H. Dubois and D. L. Allara, *J. Am. Chem. Soc.*, 1990, **112**, 558-569.
7. K. Bandyopadhyay and K. Vijayamohanan, *Langmuir*, 1998, **14**, 625-629.
8. K. Bandyopadhyay, M. Vijayamyhana, K. Venkataraman and T. Pradeep, *Langmuir*, 1999, **15**, 5314-5319.
9. G. E. Poirier, *Chem. Rev.*, 1997, **97**, 1117-1127.
10. L. C. Giancarlo and W. G. Flynn, *Annu. Rev. Phys. Chem.*, 1998, **49**, 297-319.
11. P. Harder, M. Grunze, R. Dahint, G. M. Whitesides and P. E. Laibinis, *J. Phys. Chem. B*, 1998, **102**, 426-435.
12. K. L. Prime and G. M. Whitesides, *J. Am. Chem. Soc.*, 1993, **115**, 10714-10721.
13. P. E. Laibinis, G. M. Whitesides, D. L. Allara, Y.-T. Tao, A. N. Parikh and R. G. Nuzzo, *J. Am. Chem. Soc.*, 1991, **113**, 7152-7167.
14. C. D. Bain, E. B. Troughton, Y.-T. Tao, J. Evall, G. M. Whitesides and R. G. Nuzzo, *J. Am. Chem. Soc.*, 1989, **111**, 321-335.
15. M. M. Walczak, C. Chung, S. M. Stole, C. A. Widrig and M. D. Porter, *J. Am. Chem. Soc.*, 1991, **113**, 2370-2378.
16. N. Tillman, A. Ulman and J. F. Elman, *Langmuir*, 1990, **6**, 1512-1518.
17. S. R. Holmes-Farley and G. M. Whitesides, *Langmuir*, 1987, **3**, 62-76.
18. P. E. Laibinis and G. M. Whitesides, *J. Am. Chem. Soc.*, 1992, **114**, 9022-9028.
19. S. Herrwerth, W. Eck, S. Reinhardt and M. Grunze, *J. Am. Chem. Soc.*, 2003, **125**, 9359-9366.
20. D. K. Aswal, S. Lenfant, D. Guerin, J. V. Yakhmi and D. Vuillaume, *Analytica Chimica Acta*, 2006, **568**, 84-108.
21. B. Rothenhausler, C. Duschl and W. Knoll, *Thin Solid Films*, 1988, **150**, 323-330.

22. M. Pomerantz and A. Segmuller, *Thin Solid Films*, 1980, **68**, 33-45.
23. T. Nakagiri, K. Sakai, A. Lida, T. Ishikawa and T. Matsushita, *Thin Solid Films*, 1985, **133**, 219-225.
24. Z. Yang, J. A. Galloway and H. Yu, *Langmuir*, 1999, **15**, 8405-8411.
25. C. Pale-Grosdemange, E. S. Simon, K. L. Prime and G. M. Whitesides, *J. Am. Chem. Soc*., 1991, **113**, 12-20.
26. D. Briggs, M. P. Seah, *Practical Surface Analysis, Auger and X-Ray Photoelectron Spectroscopy*, Wiley, 1995.
27. D. Barriet and T. R. Lee, *Curr. Opin. Colloid. Interface Sci.*, 2003, **8**, 236-242.

Chapter 5

Force-Distance Measurements on Trifluoroalkyl Oligo(Ethylene Glycol)-Terminated Alkanethiol Self-Assembled Monolayers

Like membranes, cells and viruses, SAMs are self-assembled systems [1] and are therefore good candidates as stable biointerfaces. [2, 3] The study of biointeraction, i.e. the adsorption of biomolecules on surfaces, is of great interest in the field of biomaterials as it is important for many medical [4] and biological applications. [5, 6] The investigation of protein adsorption is often complicated by surface heterogeneity and as a consequence SAMs, with their highly ordered structure, [7, 8] are often employed for studying biointeraction mechanisms. [9] This project aims to explore the interaction between biomolecules and surfactant films based on oligo(ethylene glycol) modified alkanethiols.

The objective is to control the protein-surface interaction by modulation of the surface environment. For potential biological applications, the surface of interest is often surrounded by a biological fluid, [10] which can be an aqueous salt solution whose ionic strength could potentially affect protein adsorption.

It is possible to observe a surface, following its exposure to a protein solution, and quantify biomolecule adsorption for the study of film-protein interactions. [11] We have used an alternate, simplified approach using AFM to measure force-distance curves of model systems. This chapter describes our investigations in this field.

Force-distance curve measurements are used in a number of applications. For instance, they allow the study of polymers, [12-14] for determination of the glass transition temperature of

polymer films, by measuring the adhesion between the AFM tip and the sample. [13, 15] The viscosity of a liquid in the vicinity of a surface can also be estimated by this technique. For example, Frangos and co-workers measured changes in the viscosity of a medium at the surface of titanium implants and were able to postulate that viscosity has a positive influence on biotolerance. [16] Another elegant application was described by Yang and co-workers, [17] who used force measurements to observe damage to the structure of bacterial cell walls after contact with an antibacterial surface. Humidity, through the presence of a thin water layer on a surface, is also detectable by measuring force-distance curves due to capillary force. [18] Applications of force-distance curves can be extended to the measurement of interactions between distinct entities by functionalisation of the AFM tip with one of the species of interest. Hierold and co-workers investigated the interactions between carbon nanotubes by attaching a nanotube to a conventional AFM tip and measuring the forces experienced when the surface of a second nanotube is approached. [19] For life-science applications, the tip can be modified to measure molecular recognition events. [20] One or more probe molecules are attached to the AFM tip in order to evaluate forces between single molecules. [14, 21] This methodology was pioneered by Pashley and co-workers. [22] For instance, specific biological recognition forces were estimated for receptor–ligand pairs [23, 24] Alternatively, the tip can be functionalized with proteins [25] in order to understand their interaction with a surface. With the advent of AFM probes, one can also directly measure the forces that govern interactions between proteins themselves. [26, 27] Thus, Gaub and co-workers functionalized an AFM tip with bovine serum albumin (BSA) [23, 28, 29] while Grunze and co-workers performed force-distance curve measurements with a fibrinogen functionalised tip. [30] As proteins are composed of hydrophobic and charged patches, Hähner and co-workers studied the protein/surface interaction by mimicking protein structure with a charged tip and tip made hydrophobic by covering it with gold and an alkanethiol self-assembled monolayer. [31]

I) Hydrophobic Tip Preparation

Hähner and co-workers [30, 32] observed a correlation between the force experienced by a hydrophobic probe and the protein adsorption properties of a film with tip attraction being representative of protein adsorption. A similar approach was therefore adopted for the study of biointeraction using the same tip functionalisation.

This study was performed with standard Si_3N_4 V-shaped AFM cantilevers (spring constant 0.06 and 0.12 N/m). Cantilevers were first placed under an optical microscope to check that no arm was broken or cracked and that the tip was at the extremity of the cantilever. It was also checked that the probes were not bent due to mechanical strain after their coverage on the tip side with 10 nm titanium and 50 nm gold layers via thermal evaporation. Hydrophobic probes were prepared by immersing the gold covered cantilevers in a millimolar ethanolic dodecanethiol (C_{12}) solution. Care was taken when putting the tips in the solution as surface tension could be high enough to break the cantilever if it was introduced parallel to the liquid surface. The cantilevers were smoothly laid down at the bottom of the beaker. Precaution was again required while rinsing the tips. The probes had to be taken out from the dodecanethiol solution, immersed in pure ethanol and dried with a gentle nitrogen flow.

To confirm that the tips were properly functionalized, force-distance curves were measured with a dodecanethiol film under liquid with different ionic strengths. A typical result is shown in Figure V-1 (ten curves are averaged each time).

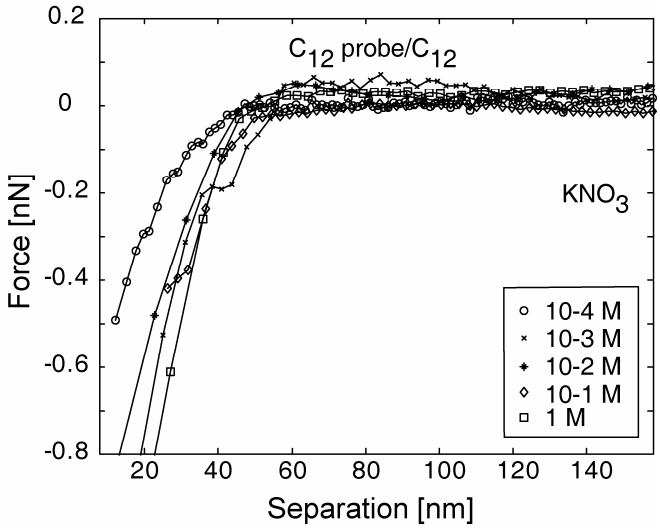

Figure V-1: Force-distance curves between a dodecanethiol SAM and a hydrophobic tip

The interaction was attractive and did not depend on the ionic strength of the environment, indicating a well functionalized tip (Figure V-2).

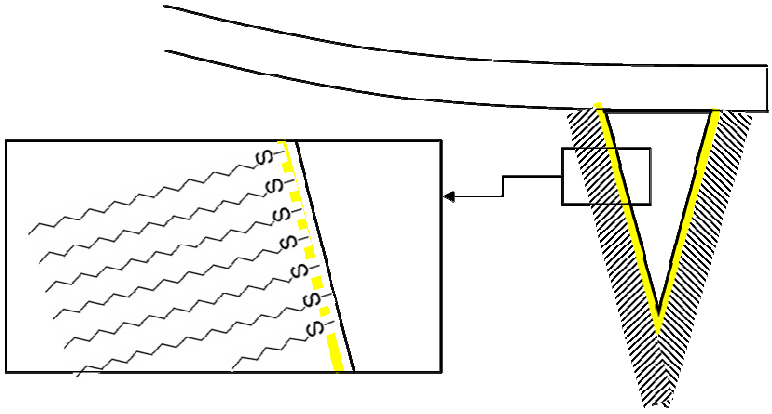

Figure V-2: Functionalised tip: Made hydrophobic by addition of a C_{12} SAM

II)Force Study

The samples were placed in the liquid cell of the AFM and covered with the aqueous media. Each force-distance curve was an average of ten approach and retraction cycles. During the acquisition, the scanner was immobilised in the x and y directions while cycles were produced

in the z direction at a frequency of 1 Hz. 2000 data points were recorded for each cycle. All curves were fitted according to the equation V-15.

1) Force-distance analysis of (1-mercaptoundec-11-yl)tri(ethylene glycol) 3,3,3-trifluoropropyl ether SAM

The study was initially performed with the basic self-assembling molecule, (1-mercaptoundec-11-yl)tri(ethylene glycol) 3,3,3-trifluoropropyl ether (**1**).

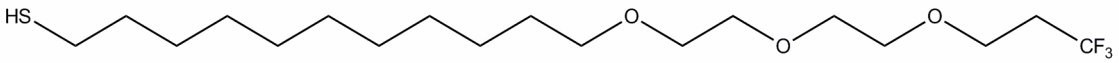

Figure V-3: (1-mercaptoundec-11-yl)tri(ethylene glycol) 3,3,3-trifluoropropyl ether (1)

A quantitative force analysis was not possible because the spring constant of the cantilever probably changed from the value given by the supplier following deposition of titanium, gold and the dodecanethiol SAM.

Figure V-4 displays force-distance curves for the surface obtained with this surfactant.

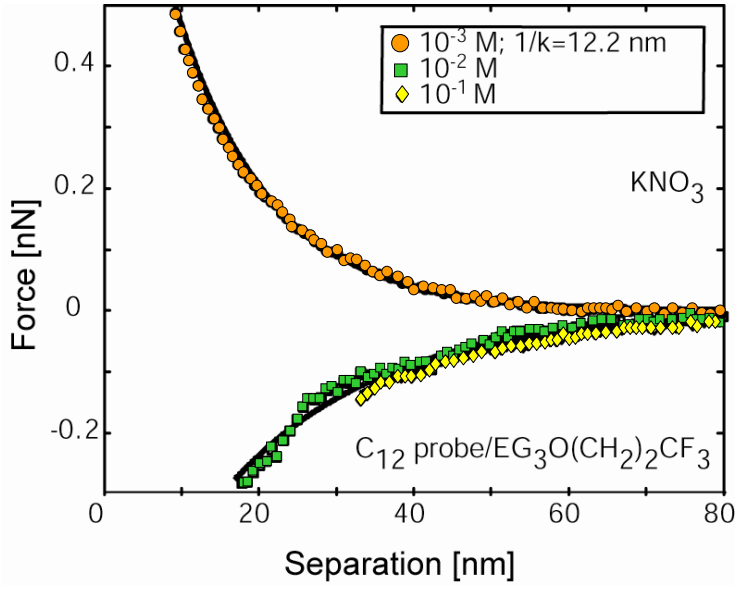

Figure V-4: Advancing force-versus-distance curves (averaged) measured with a hydrophobic C_{12}-probe on a (1-mercaptoundec-11-yl)tri(ethylene glycol) 3,3,3-trifluoropropyl ether SAM on gold in aqueous solution of different salt concentration

The force experienced by the hydrophobic tip approaching the synthetic organic film was a superposition of a hydrophobic attraction and an electrostatic repulsion described previously in chapter 2.

At low KNO_3 concentration, up 10^{-3} M, the force experienced by the hydrophobic tip was repulsive demonstrating that the dominant contribution was an electrostatic repulsion. From a single exponential fit according to

Equation V-1: $y = A\exp(-\kappa x)$

where A is a constant, a Debye length (κ^{-1}) of 12.2 nm was determined in a concentration of 10^{-3} M. [33] Theoretically the decay length is related to concentration by the expression:

Equation V-2: $\kappa^{-1} = 0.304/\sqrt{C}$,

which predicted a value of 9.6 nm.

When the ionic strength was increased from 10^{-3} to 10^{-2} M, a switch from repulsion to attraction was observed. Under ionic strength equal to and above 1 mM, the dominant force was the hydrophobic attraction.

The competing forces of hydrophobic attraction and electrostatic repulsion were responsible for the overall AFM force-distance curve shape. The intensity and the range of the two forces were the two parameters prevailing in the interpretation of the dominance of one interaction over the other during AFM force-distance curve measurements. This interpretation could be made by considering the force-distance curves measured by Hähner and co-workers while the tip experienced separately the electrostatic force (Figure V-5) or the hydrophobic attraction (Figure V-6).

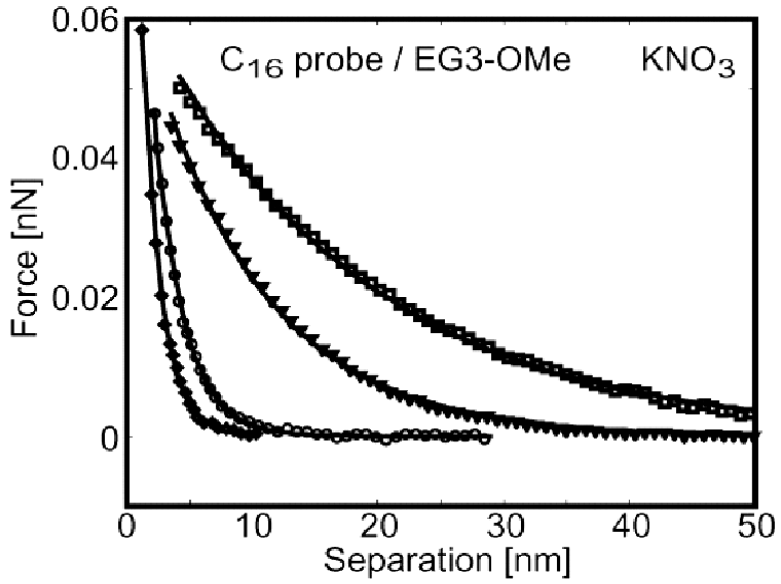

Figure V-5: Advancing force-versus-distance curves (averaged) measured with a hydrophobic C_{12}-probe on a (1-mercaptoundec-11-yl)tri(ethylene glycol) methyl ether SAM on gold in aqueous solution of different salt concentration (◊ 0.1 M, O 0.01 M, ▽ 1 mM, □ 0.1 mM). Reproduced from [32].

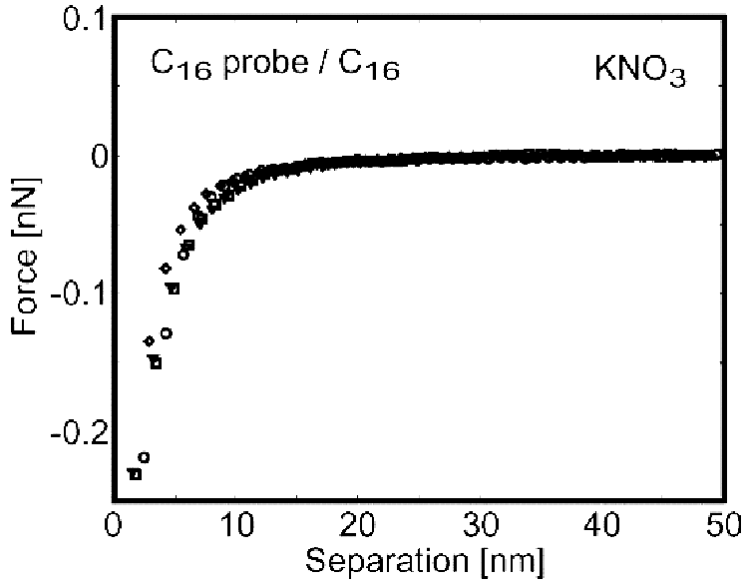

Figure V-6: Advancing force-versus-distance curves (averaged) measured with a hydrophobic C_{12}-probe on a hexadecanethiol SAM on gold in aqueous solution of different salt concentration (◊ 0.1 M, O 0.01 M, ▽ 1 mM, □ 0.1 mM). Reproduced from [32].

Despite the fact that a quantitative force analysis was not possible, comparison of the strengthof the interactions could be made because the curves were measured with the same tip. The hydrophobic attraction was revealed to be stronger than the electrostatic repulsion.

The range of the electrostatic repulsion was found to be dependent on the ionic strength whereas the range of hydrophobic attraction remained unaffected. The interaction felt by the approaching tip was governed by the longest range force except when the ranges were similar in which case the most intense force dictated probe displacement. The range of the repulsion generated by SAM **1** on gold was therefore higher than the attraction range at low ionic strength up to 10^{-3} M and lower in more concentrated salt solution.

Each force generated by the self-assembled monolayer could be attributed to a distinct part of the surfactant molecule. While the electrostatic repulsion originated from the oligo(ethylene glycol) groups, the attractive force was generated by the trifluoroalkyl moiety.

In addition to the study of SAM-tip interactions as a function of salt concentration, the influence of each part of the surfactant was also examined. Firstly, structure-force relationships of the hydrophobic moiety of the self-assembling molecule were explored, as this moiety was known to be solely responsible for the attractive contribution.

A survey of the literature allowed a first comparison of the results and the study of one parameter i.e. the composition of the hydrophobic end. Dicke *et al.* used a SAM composed of (1-mercaptoundec-11-yl)tri(ethylene glycol) methyl ether on polycrystalline gold to carry out identical force-distance curve measurements under different ionic strengths. [32] The interaction remained repulsive under all ionic strengths studied. It was known that the hydrophobic head group was solely responsible for the attractive contribution and as such any observed differences between the in-house system and that reported by Dicke *et al*. reflected structure-force relationships. The methyl group attraction was insignificant compared to the electrostatic repulsion under ionic strengths ranging from 0.1 mM to 0.1 M. For the (1-mercaptoundec-11-yl)tri(ethylene glycol) 3,3,3-trifluoropropyl ether, the trifluoro alkyl end exerted a noticeable attraction in at concentrations of 10^{-3} M and higher.

Thus, using a more hydrophobic end enhanced the attractive force and gave rise to a switchable system in highly concentrated ionic solutions where this force was dominant.

2) Force-distance analysis of (1-mercaptoundec-11-yl)tri(ethylene glycol) 4,4,4-trifluorobutyl ether SAM

In addition to the composition of the hydrophobic part of the surfactant, how chain length affected force-distance relationships was also examined. To this end the behaviour of a SAM identical in nature to that described previously was studied with the exception that an additional methylene unit was introduced at the hydrophobic top.

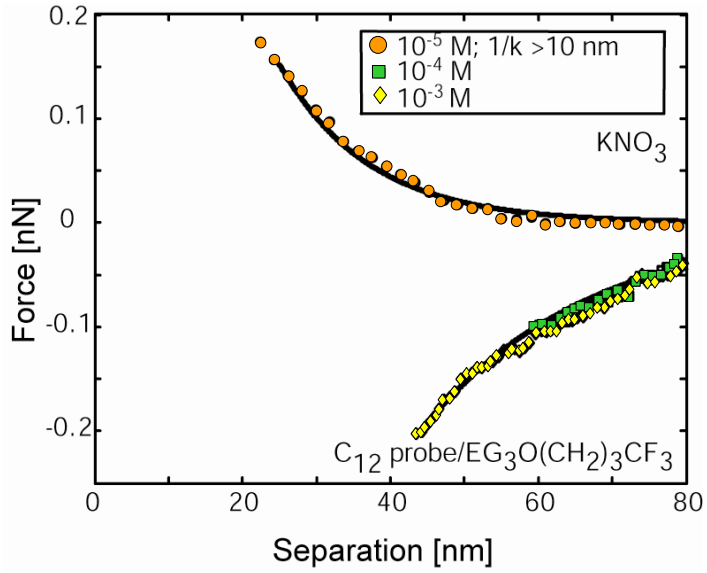

Figure V-7: Advancing force-versus-distance curves (averaged) measured with a hydrophobic C_{12}-probe on a (1-mercaptoundec-11-yl)tri(ethylene glycol) 4,4,4-trifluorobutyl ether SAM on gold in aqueous solution of different salt concentration

At low KNO_3 concentrations the force experienced by the hydrophobic tip was repulsive, behaviour identical to that observed previously for SAM **1**. However, the switch occurred at a significantly lower ionic concentration (below 10^{-5} M). At such low concentrations, the experimental determined Debye length has been reported to show some deviation from the theoretical Debye [33] and was attributed to dissolved CO_2. The cause of this dramatic shift in the switch concentration was related to relative changes to the intensity and range of the electrostatic and hydrophobic interactions. Increasing the strengthof the hydrophobic attraction enhanced its contribution to the net force over an extended range. This was manifested as an earlier onset for the switch from repulsion to attraction. To compare the

strengthof the two counteracting forces, force-distance curves had to be measured with the same tip.

Considering the force measured by Dicke *et al.* for (1-mercaptoundec-11-yl)tri(ethylene glycol) methyl ether SAM as being representative of the pure electrostatic repulsion and the force measured with alkanethiol monolayer as being representative of the pure hydrophobic attraction, a comparison of the intensity of the two forces could be made. The strengthof the attraction was found to be much higher than the repulsion.

The range of the electrostatic repulsion decreased when the salt concentration increased while the attraction range did not change. In low ionic concentrations, the repulsion is long range and the attraction is short range but the inequality changed direction at high ionic strength as the range of the electrostatic interaction is shorter than for low ionic strength while the hydrophobic range is constant. The part of the molecule creating the repulsion was identical in the two surfactants so that the range of the electrostatic repulsion could be considered similar for the two SAMs. As a consequence, the change in the switch concentration was linked to an increase in the attraction range for SAM **2**. The range of both the repulsion and the attraction were similar under lower ionic strength compared to molecule **1**. In other words, extending the hydrophobic head made the attraction range longer and decreased the switch concentration.

3) Force-distance analysis of (1-mercaptoundec-11-yl)tetra(ethylene glycol) 3,3,3-trifluoropropyl ether SAM

Finally, the affect of the number of the oligoethylene glycol groups on the nature of observed force-distance curves was also investigated. SAM **3** was prepared with an additional oligoetheylene glycol unit and results compared to SAM **1**.

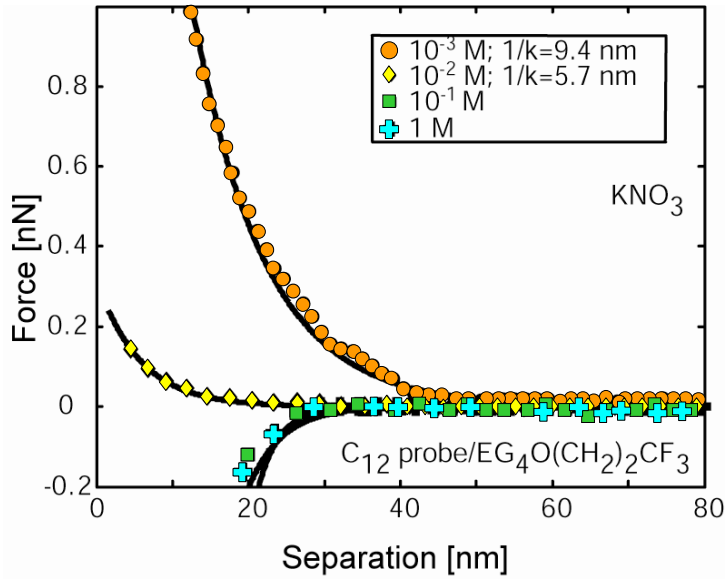

Figure V-8: Advancing force-versus-distance curves (averaged) measured with a hydrophobic C_{12}-probe on a (1-mercaptoundec-11-yl)tetra(ethylene glycol) 3,3,3-trifluoropropyl ether SAM on gold in aqueous solution of different salt concentration

At low KNO_3 concentrations the force experienced by the hydrophobic tip was still repulsive. An exponential fit to the force distance curve gave a Debye length of 9.4 nm and 5.7 nm in concentrations of 10^{-3} and 10^{-2} M, respectively. The Equation V-2 gave theoretical values of 3.1 and 9.6 nm for 10^{-2} M and 10^{-3} M KNO_3 solutions respectively. Thus, the measured decay lengths are in reasonable agreement with the theoretical values. The switch occurred at a higher concentration than with molecule **1**. Since the hydrophobic head groups were the same for surfactants **1** and **3**, the attraction they produce was also identical. Consequently, the higher switch concentration was linked to an increase in the repulsion range for molecule **3**. Repulsion remained the dominant force under more concentrated solutions than observed for the first surfactant.

4) Force-distance analysis of (1-mercaptoundec-11-yl)tetra(ethylene glycol) 2,2,2-trifluoroethyl ether SAM

Firstly, one methylene hydrophobic unit was removed from SAM **3**, giving rise to SAM, and as expected the switch concentration moved to higher values.

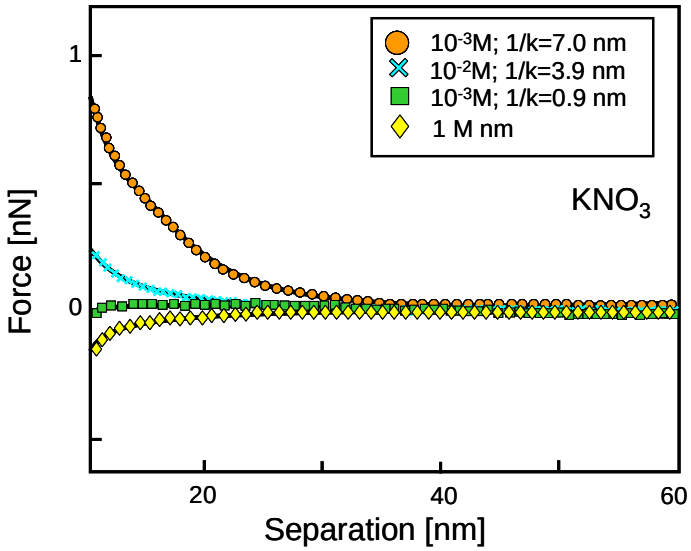

Figure V-9: Advancing force-versus-distance curves (averaged) measured with a hydrophobic C_{12}-probe on a (1-mercaptoundec-11-yl)tetra(ethylene glycol) 3,3,3-trifluoroethyl ether SAM on gold in aqueous solution of different salt concentration

Here, the crossover from repulsion to attraction occured between 10^{-1} and 1 M. This switch concentration seemed perfect as it encompassed the required 0.15 M needed for fibrinogen to survive. Thus, suppression of the extra methylene unit permited reversible immobilization at ionic strengths suitable for fibrinogen.

5) Force-distance analysis of (1-mercaptoundec-11-yl)hexa(ethylene glycol) 3,3,3-trifluoropropyl ether SAM

A second possibility to increase the switch concentration was also examined. The number of oligoethylene glycol groups was increased by two units using hexaethylene glycol as a starting material to give molecule **5**.

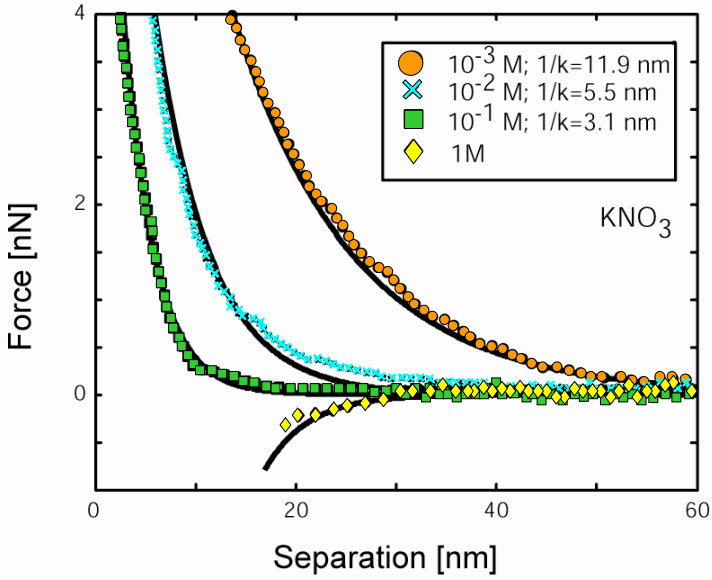

Figure V-10: Advancing force-versus-distance curves (averaged) measured with a hydrophobic C_{12}-probe on a (1-mercaptoundec-11-yl)hexa(ethylene glycol) 3,3,3-trifluoropropyl ether SAM on gold in aqueous solution of different salt concentration

The switch was again observed between 10^{-1} and 1 M, making the surface compatible with fibrinogen.

6) Force-distance analysis of (1-mercaptoundec-11-yl)hexa(ethylene glycol) 2,2,2-trifluoroethyl ether SAM

Both the length of the top trifluoro alkyl chain and the number of oligoethylene glycol groups were separately customized to increase the switch concentration. The two parameters were modified to give molecule **6** whose hydrophobic end was shorter and had more oligoethylene glycol units.

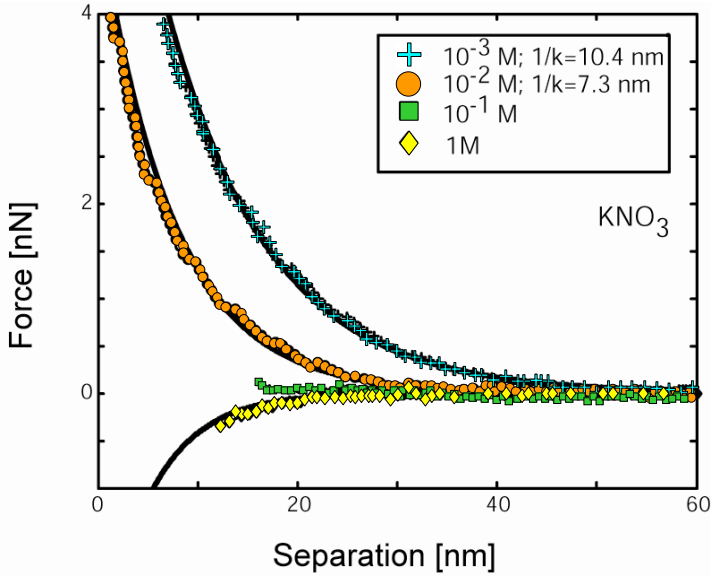

Figure V-11: Advancing force-versus-distance curves (averaged) measured with a hydrophobic C_{12}-probe on a (1-mercaptoundec-11-yl)hexa(ethylene glycol) 3,3,3-trifluoroethylether SAM on gold in aqueous solution of different salt concentration

With the two parameters modified simultaneously, the switch concentration was expected to be higher than for molecules **4** and **5**, but this double modification again brought the switch concentration to between 0.1 and 1 M.

The identical switch concentration for surfaces **5** and **6** showed that the influence of the length of the hydrophobic moiety was insignificant for these two hexa(ethylene glycol) based SAMs, probably because the trifluoroalkyl groups were not at the surface possibly as a consequence of the self-assembling molecules becoming tangled.

III) Conclusions

The combination of oligoethylene groups and a trifluoro alkyl part in the self-assembling molecule underlined the competition between the hydrophobic attraction and the electrostatic repulsion. The ionic strength dependence of the electrostatic repulsion resulted in the observation of a switch in the total force. Therefore, the self-assembled monolayers built from all the six synthesized surfactants presented a dynamic property. They could reversibly attract hydrophobic molecules by changing the ionic strength of the environment. The switch concentration depended on the length of the trifluoroalkyl top and the number of the oligoethylene glycol units. While adding one hydrophobic methylene group shifted the switch

to lower ionic strength, an additional oligoethylene glycol unit moved the switch to higher concentrations. The switch behaviour of these films offered potential for their application for reversible immobilisation of hydrophobic particles. These surfactant films could also be important in bio-related fields and as biosensors since they had the potential to adsorb/immobilise proteins reversibly if the switch could be tailored to occur at an ionic strength that was compatible with proteins. One of the common test proteins is fibrinogen [34, 35] whose natural environment has an ionic strength of approximately 0.15 M. [36] The switch concentration was therefore attempted to be tailored and materials designed with a switch at an ionic strength representative of fibrinogen's natural environment (i.e. 0.15 M). For SAMs **4**, **5**, and **6**, it was possible to bring this switch concentration in the range of the ionic strength of fibrinogen's natural environment. This made the three last surfaces eligible for the study of reversible adsorption of proteins.

IV) Literature

1. C. Vericat, M. E. Vela, G. A. Benitez, J. A. Martin Gago, X. Torrelles and R. C. Salvarezza, *J. Phys.: Condens. Matter.* , 2006, **18**, R867-R900.
2. R. G. Nuzzo and D. L. Allara, *J. Am. Chem. Soc.*, 1983, **105**, 4481-4483.
3. K. L. Prime and G. M. Whitesides, *Science*, 1991, **252**, 1164.
4. M. Kalltorp, S. Oblogina, S. Jacobsson, A. Karlsson, T. P. and P. Thomsen, *Biomaterials*, 1990, **20**, 2123-2137.
5. G. MacBeath, *Nature Biotechnology*, 2001, **19**, 828-829.
6. S. Fields, *Science*, 2001, **291**, 1221-1224.
7. A. Ulman, *An Introduction to Ultrathin Organic Fims* Academic Press, San Diego, 1991.
8. A. Ulman, *Chem. Rev.*, 1996, **96**, 1533-1554.
9. D. Bain and G. M. Whitesides, *Science*, 1988, **240**, 62.
10. E. Ostuni, L. Yan and G. M. Whitesides, *Colloid & Surfaces B: Biointerfaces* 1999, **15**, 3-30.
11. Z. Yang, J. A. Galloway and H. Yu, *Langmuir*, 1999, **15**, 8405-8411.
12. K. Kaliappan and B. Cappell, *Polyner*, 2005, **46**, 11416-11423.

13. B. Cappella and W. Stark, *Journal of Colloid & Interface Science*, 2006, **296**, 507-514.
14. T. Hugel and M. Seitz, *Macromol. Rapid. Commun.*, 2001, **22**, 989-1016.
15. O. K. C. Tsui, X. P. Wang, J. Y. L. Ho, T. K. Ng and X. Xiao, *Macromolecules*, 2000, **33**, 4198-4204.
16. J. J. Muyco, J. J. Gray, T. V. TRatto, C. A. Orme, J. McKittrick and J. Frangos, *Mater. Res. Soc. Symp. Provoc.*, 2005, **873E**.
17. L. Nan, Y. Liu, M. Lü and K. Yang, *J. Mater. Sci.: Mater. Med.*, 2008, **19**, 3057-3062.
18. N. A. Burmham, R. J. Cotton and H. M. Pollock, *Nanotechnology*, 1993, **4**, 64-80.
19. B. Bhushan, X. ling, A. Jungen and C. Hierold, *Phys. Rev. B*, 2008, **77**, 165428.
20. R. Barratin and N. Voyer, *Chem. Commun.*, 2008, 1513-1532.
21. J. Zlatanova, S. M. Lindsay and S. H. Leuba, *Progress in Biophysics & Molecular Biology*, 2000, **74**, 37-61.
22. W. A. Ducker, T. J. Senden and R. M. Pashley, *Nature*, 1991, **353**, 239.
23. E.-L. Florin, V. T. Moy and M. E. Gaub, *Science*, 1994, **264**, 415-417.
24. V. T. Moy, E.-L. Florin and M. E. Gaub, *Colloid Surf. A*, 1994, **93**, 343-348.
25. S. Kiduaki and T. Matsuda, *Colloids & Surfaces B: Biointerfaces*, 2002, **23**, 153-163.
26. D. J. Müller and A. Engel, *Biophys. J.*, 1997, **73**, 1633-1644.
27. D. Leckband, F.-J. Schmitt, J. Israelachvili and W. Knoll, *Biochemistry*, 1994, **33**, 4611-4624.
28. V. T. Moy, E.-L. Florin and M. E. Gaub, *Science*, 1994, **266**, 257-259.
29. V. T. Moy, E.-L. Florin and M. E. Gaub, *Colloids Surfaces A*, 1994, **93**, 343-348.
30. K. Feldman, G. Hähner, N. D. Spencer, P. Harder and M. Grunze, *J. Am. Chem. Soc.*, 1999, **121**, 10134-10141.
31. C. Dicke and G. Hähner, *J. Phys. Chem. B*, 2002, **106**, 4450-4456.
32. C. Dicke and G. Hähner, *J. Am. Chem. Soc.*, 2002, **124**, 12619-12625.
33. J. Israelachvili, *Intermolecular and Surface Forces*, Academic Press, San Diego, CA, 1992.
34. K. L. Prime and G. M. Whitesides, *J. Am. Chem. Soc. ,* 1993, **115**, 10714-10721.
35. S. Herrwerth, W. Eck, S. Reinhardt and M. Grunze, *J. Am. Chem. Soc.*, 2003, **125**, 9359-9366.
36. D. F. Waugh and M. J. Patch, *Journal of Physical Chemistry*, 1953, **57**, 377-382.

Chapter 6

Protein Adsoption on Trifluoro Alkyl Oligo(Ethylene Glycol)-Terminated Alkanethiol Self-Assembled Monolayers

The ability to control protein adsorption has attracted a high level of interest because it has diverse applications in chromatography, [1] drug delivery, [2, 3] cell study [4] (to maintain cells when they are growing and then to release them), and biofouling [5] (to understand biological adhesion mechanisms).

Mrksich *et al.* [6] studied the reversible immobilization of proteins on mixed SAMs containing a majority of alkanethiols with tetra(ethylene glycol) groups. By modulating an applied electric potential, the minor self-assembling component can either allow protein immobilization, [6] stop the binding after the release of a ligand of the self-assembling molecule, [7] or enable successive release and immobilization of a ligand giving rise to the release or migration and growth of cells. [8] Electric potential modulation was also employed by Langer *et al.* [9] to change the conformation of the self-assembling molecules leading to a quantitative control of the non specific adsorption of proteins as observed by Liu *et al.* [10] Nevertheless, more interest has been directed towards the design of thermally responsive surfaces. Schwendel and co-workers [11] and Valiokas co-workers [12] have shown the influence of temperature on the conformation of molecules constituting the layers of poly- and oligo(ethylene glycol) (PEG and OEG) terminated alkanethiolate self-assembled monolayers (SAMs) on Au and Ag. However, temperature switching typically does not represent an experimentally convenient method for studying the reversible adsorption of proteins because the conformation transition was observed around 60 °C by Valiokas *et al.* whereas this was

detected by lowering the temperature by Schwendel *et al.*; nonetheless, this came with an ice layer formation. However, using a different system Grunze and co-workers achieved variation of the amount of biomolecules adsorbed on a surface between room temperature and 37 °C. [13]

Several techniques can be employed to study protein adsorption at a solid-liquid interface. A qualitative detection of proteins is possible with atomic force microscope imaging, [14] by fluorescence spectroscopy [15] or with optical micrographs [8] each giving a picture of the surface covered with proteins. Nevertheless, a relative quantification of the amount of adsorbed proteins is often necessary to evaluate the surface's resistance. Quantitative interpretation can be achieved by radiolabeling, [14] (whereby the radioactivity of a surface covered by labeled proteins is measured) or with infrared spectroscopy by measuring the intensity of amide groups of the protein present at the surface. [16] Nonetheless, the two most frequently employed techniques are surface plasmon resonance (SPR) spectroscopy, [17-19] an optical technique that is sensitive to changes in the refractive index of an interface, and ellipsometry. [20] For example, Grunze and co-workers compared the thickness of the layer of adsorbed proteins on their SAM with the amount adsorbed on an alkanethiol monolayer using ellipsometry. [21]

The force-distance curves measured with an Atomic Force Microscope, discussed in the last chapter, suggested that our hydrophobized tip was repelled from surfactant films based on oligo(ethylene glycol) modified alkanethiols by an electrostatic force [22] that was attributed to the charging effect of the surface after adsorption of hydroxide ions from water. [23] This force is balanced by a hydrophobic interaction, [24] which originates at the trifluoro alkyl end. Our surfaces were revealed to be dynamic because they present a switch between attractive and repulsive forces on approach with the hydrophobic probe depending on the ionic conditions of the environment.

The etymological origin of the word « protein » conveys the importance of these molecules in biology as it is derived from the Greek word *proteios* which means "of the first rank". [25] Proteins represent more than 50% of the dry mass of cells and they intervene in almost all cellular functions. They store and transport substances, pass on messages from one part of the body to another, produce movement, defend against foreign substances and catalyse biochemical reactions, among many other functions. The human genome expresses tens of thousands of different proteins, each having a specific structure and function. The function of a protein is very specifically related to its structure, which is complex and varied. Every protein possesses a unique three-dimensional shape. Nevertheless, however diversified they are, proteins are all polymers made from the same set of amino acids. There are twenty

different amino acids that share fundamental structural characteristics. All of the amino acids posses an alpha carbon, which is the central point of attachment of several functional groups: an amino group, a carboxylic acid, and a side chain (group R). The various side chains determine the unique structure of the constituent amino acids. The structures of the R groups are diverse ranging from a simple hydrogen atom to complex arrangement of carbon chains and ring structures, also containing heteroatoms such as O, N and S.

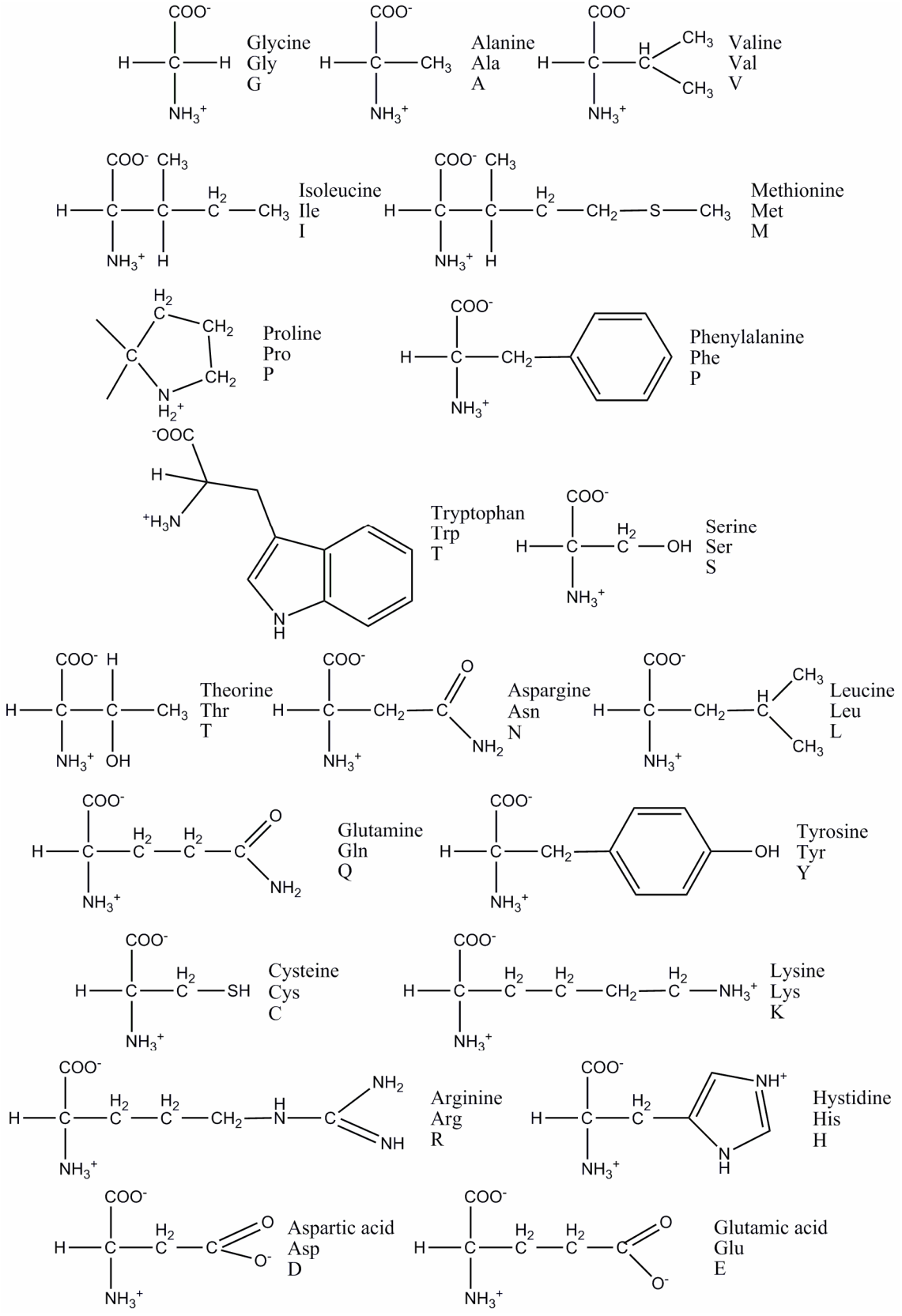

Figure VI-6: Covalent Structure and Abbreviations of amino acids. Reproduced from [25]

To form proteins, the linear chains of amino acids are linked together by amide bonds termed peptide bonds in this context, between the free amine and the carboxylic acid of the next amino acid. When amino acids are linked in such a chain, the chain folds in a way that accommodates hydrogen bonding interactions between the peptide bonds (a-helices and b-sheets) as well as interactions between the R. This combination of interactions defines the overall three-dimensional structure and chemical properties of the protein. [26] As a consequence, the function of a protein follows a precise molecular organization. Three levels of structural organization can be distinguished in the complex architecture of a protein: primary, secondary and tertiary. A fourth level appears when a protein consists of two or more polypeptide chains and these then associate with each other in a higher order structure. The primary structure of a protein is defined by the particular amino acid sequence. Any change in the primary structure (mutation) can have an enormous effect on the structure and conformation of the protein and therefore its capacity to function properly. In most proteins, segments of the polypeptide chain will coil (α-helices), due to hydrogen bonding interactions between the main chain peptide bonds, or they will be folded repeatedly (β-sheets). Such motifs contribute the secondary structure of the macromolecule. Only the hydrogen and oxygen atoms attached to the repetitive structure of the polypeptide are involved in these bonds.

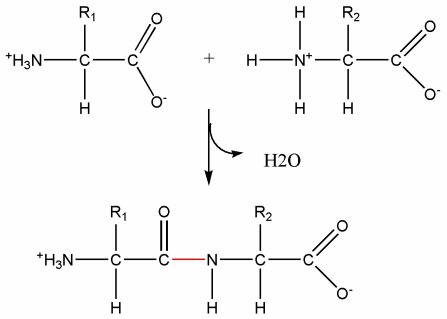

Figure VI-2: Condensation of two amino acids. Reproduced from [25]

The carbonyl oxygens of the peptide are ideally polarised to associate with the N-H hydrogen of another peptide bond. Such hydrogen bonds are weak when they are taken individually; however, when they are repeated and multiple in a relatively long section of the polypeptide chain, they give shape and stability to this section of the protein. The alpha helix is key example of secondary structure found in many proteins; it is a coil held in place by hydrogen bonds of all four amino acids. The beta pleated sheet is another type of secondary structure:

two or more regions of the polypeptide chain are parallel through hydrogen bonds. Beta pleated sheets form the dense part of numerous proteins. The tertiary structure of a protein is a higher level of folding beyond these motifs of secondary structure. It corresponds to all irregular contortions resulting from interactions between the different amino acid side chains. As mentioned above, some proteins are composed of two or more polypeptide chains assembled to form a functional macromolecule. Each polypeptide chain is a subunit. Quaternary structure is the overall structure of the protein resulting from the interaction between subunits [25] which can be illustrated with fibrinogen as example. Fibrinogen is a large protein produced by the liver which helps to stop bleeding by promoting blood clot formation. This protein strongly adsorbs onto hydrophobic surfaces [27] and therefore represents an ideal model for "sticky" proteins. [17, 28, 29] The different moieties which compose a fibrinogen molecule are represented in Figure VI-3.

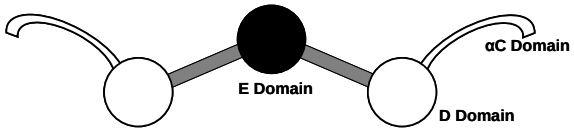

Figure VI-3: Schematic representation of fibrinogen molecule. Reproduced from [28]

Two identical moieties are bounded to the central E domain. Each moiety is made of a D domain, a α helix, and a αC domain. The adsorption mechanism was demonstrated to be different on hydrophobic and hydrophilic surfaces. [30]

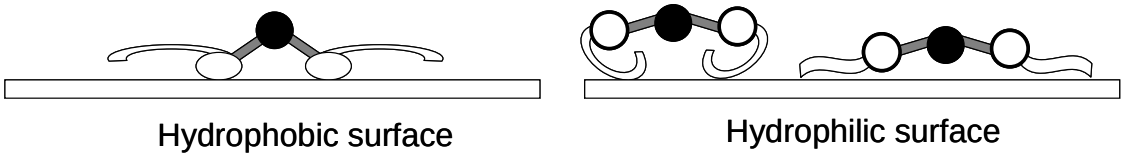

Figure VI-4: Schematic representation of the mechanism of fibrinogen adsorption to hydrophobic and hydrophilic surfaces. Represented from [30]

McDermott and co-workers have shown that fibrinogen molecules loosely bound to hydrophilic surfaces with their αC domains whereas their D domains allow a strong adsorption on hydrophobic surfaces.

While the previous chapter described how the salt concentration leads to a switch in the nature of the total force felt by a hydrophobic probe, this section is concerned with the

study of the influence of ionic strength of the liquid medium on the amount of protein adsorbed on a surface.

I) Description of the Method

Protein adsorption experiments were performed with fibrinogen following the same method described by Grunze *et al.* [21]

Each freshly prepared self-assembled monolayer was placed at the bottom of a 50 cm^3 beaker and covered with 5 cm^3 of deionised water. A 1 $mg.cm^{-3}$ fibrinogen solution was prepared by dissolving the protein in a diluted Phosphate Buffer Solution (PBS) whose ionic strength was controlled. 10 cm^3 of the biomolecule solution was added to each beaker containing a SAM, and allowed to stand for 15 minutes. 500 cm^3 of distilled water was poured into each beaker to remove the fibrinogen film which can form at the liquid surface. Surfaces were rinsed with distilled water and dried with nitrogen. The relative quantification of protein adsorption was evaluated with ellipsometry measurements, described in chapter 4, by comparing the thickness of the adsorbed fibrinogen layer on our synthetic organic films based on trifluoroalkyl oligo(ethylene glycol) modified alkanethiols and on dodecanethiol SAM. Therefore the 100% reference was attributed to the thickness of the protein layer adsorbed on the alkanethiol monolayer.

The values presented in this chapter are the averages of values obtained from several independent samples (between 4 and 7 samples for each SAM under each ionic strength). The length of the error bar indicates the standard error of the measurements.

II)Protein Adsorption Study

1) Protein Adsorption Study on (1-mercaptoundec-11-yl)tri(ethylene glycol) 3,3,3-trifluoropropyl ether SAM

The amount of protein adsorption in a solution with different ionic strength was initially studied with the SAM based on (1-mercaptoundec-11-yl)tri(ethylene glycol) 3,3,3-trifluoropropyl ether (**1**).

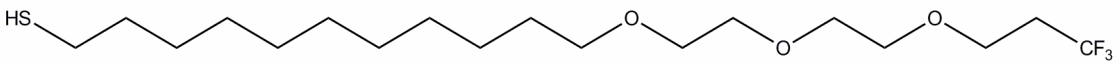

Figure VI-5: (1-mercaptoundec-11-yl)tri(ethylene glycol) 3,3,3-trifluoropropyl ether (1)

The fibrinogen adsorption was evaluated in PBS solution with the ionic concentration varied from 10^{-4} to 1 M.

Figure VI-6 displays relative fibrinogen adsorption on SAM **1** under different ionic strengths.

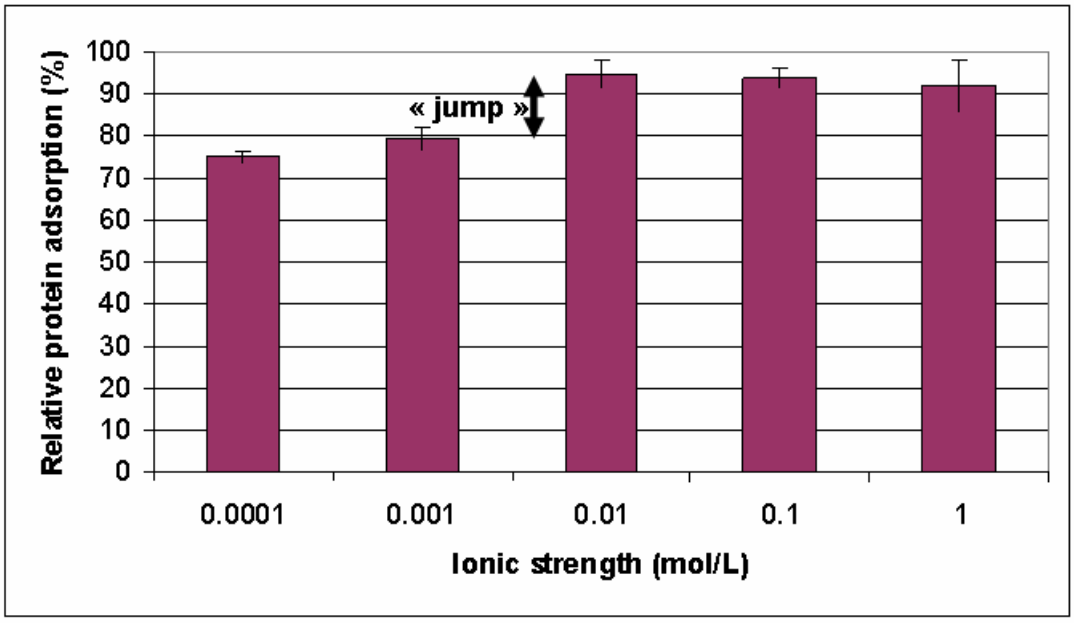

Figure VI-6: Dodecanethiol SAM relative fibrinogen adsorption on (1-mercaptoundec-11-yl)tri(ethylene glycol) 3,3,3-trifluoropropyl ether SAM on gold in aqueous solution of different salt concentration

After being immersed in a fibrinogen solution in PBS with a concentration of 10^{-4} M, the thickness of the adsorbed protein layer on SAM **1** was around 75% of the thickness of the same layer adsorbed on a dodecanethiol SAM. Immersing the substrate in a PBS solution ten times more concentrated (10^{-3} M) gave a slight increase of the protein layer thickness (75% to 79%). A larger change occured when the ionic strength was increased from 10^{-3} M to 10^{-2} M, where the percentage rised to 94%. The relative adsorption of fibrinogen reached a plateau at

a value of around 94% that was maintained when the substrate was exposed to more concentrated solutions. Consequently, there was a noticeable difference, which has been called “jump”, between the quantities of proteins adsorbed in solutions with ionic strengths ranging from 10^{-3} M to 10^{-2} M giving rise to variations in the relative amount of absorption from 75% to 94%.

These results were compared to the force-versus distance curves measured with a hydrophobic tip. According to these curves, the functionalised tip was repelled in aqueous solutions with a salt concentration up to 10^{-3} M while it was attracted at higher ionic strengths. A switch from repulsion to attraction was therefore observed between 10^{-3} and 10^{-2} M. Proteins could be mimicked by hydrophobic and charged tips leading to an expected correlation between the force experienced by the probe and the extent of fibrinogen adsorption.

The protein adsorption change occured at similar concentration values where the force experienced on approach with a hydrophobic probe changed from repulsive to attractive.

2) Protein Adsorption Study on (1-mercaptoundec-11-yl)tri(ethylene glycol) 4,4,4-trifluorobutyl ether SAM

The influence of the length of the hydrophobic moiety was studied by investigating (1-mercaptoundec-11-yl)tri(ethylene glycol) 4,4,4-trifluorobutyl ether (**2**).

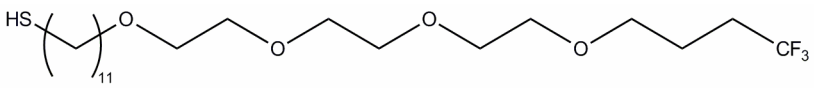

Figure VI-7: (1-mercaptoundec-11-yl)tri(ethylene glycol) 4,4,4-trifluorobutyl ether (2)

This surfactant molecule differed from **1** by one additional methylene (CH_2) group in the hydrophobic top end. As the length of the trifluoroalkyl group was greater compared to (**1**), the hydrophobic attraction was stronger while the repulsion was similar for SAMs composed of **1** and **2**. Since the density and contact angle of SAMs **1** and **2** were comparable this allowed it to study the influence of the hydrophobic part on fibrinogen adsorption.

Figure VI-8 displays the relative amount of fibrinogen adsorption as a function of the ionic strength of the solution.

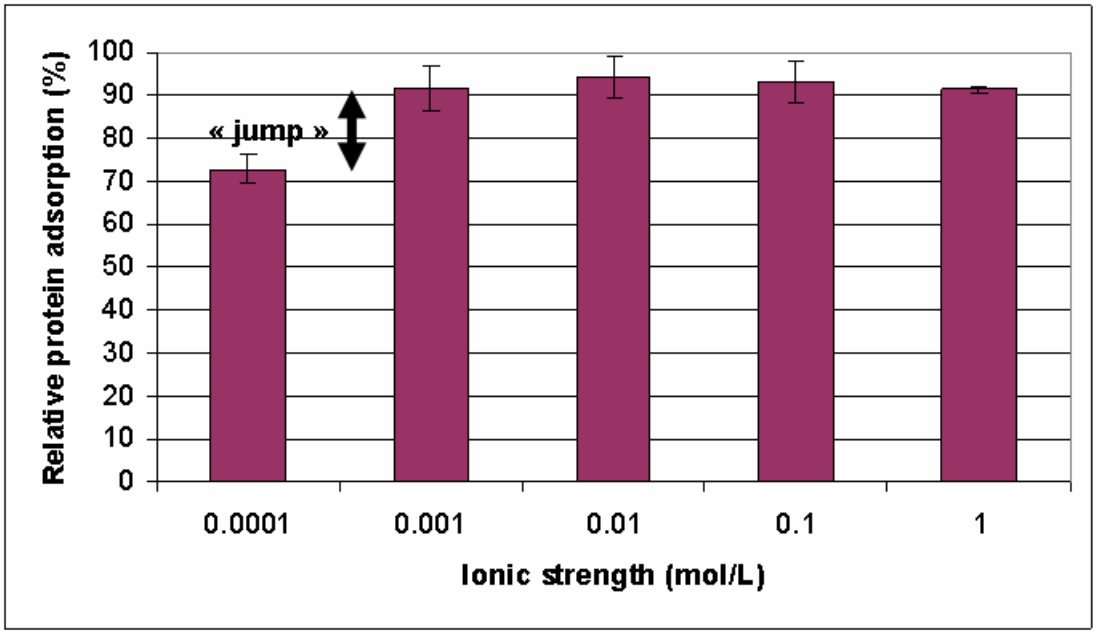

Figure VI-8: Dodecanethiol SAM relative fibrinogen adsorption on (1-mercaptoundec-11-yl)tri(ethylene glycol) 4,4,4-trifluorobutyl ether SAM on gold in aqueous solution of different salt concentration

The relative fibrinogen adsorption on a (1-mercaptoundec-11-yl)tri(ethylene glycol) 4,4,4-trifluorobutyl ether SAM observed following immersion in solution with a PBS concentration of 10^{-4} M was 72%. This percentage reached 92% when the ionic strength was 10^{-3} M or higher. The large change in protein adsorption with this synthetic, organic surface occured between salt concentrations of 10^{-4} and 10^{-3} M (*cf* 10^{-3} to 10^{-2} M for **1**).

These results were compared with the force-versus distance curves measured with a hydrophobic tip. Although the protein adsorption change occured at higher concentration values (between 10^{-4} and 10^{-3} M) than the switch concentration observed by AFM (between 10^{-4} and 10^{-5} M), the change in concentration moved in the same direction. When the length of the hydrophobic end of the self-assembling molecule was increased the AFM switch concentration and the "step" between the lowest and the highest amount of adsorbed fibrinogen was lower.

A comparison of the marked change in protein adsorption as a function of ionic strength obtained for **1** and **2** enabled an evaluation of the influence of the hydrophobic moiety; an additional methylene unit caused adsorption change to occur in solutions an order of magnitude weaker.

Another comparison was possible at fixed concentrations:

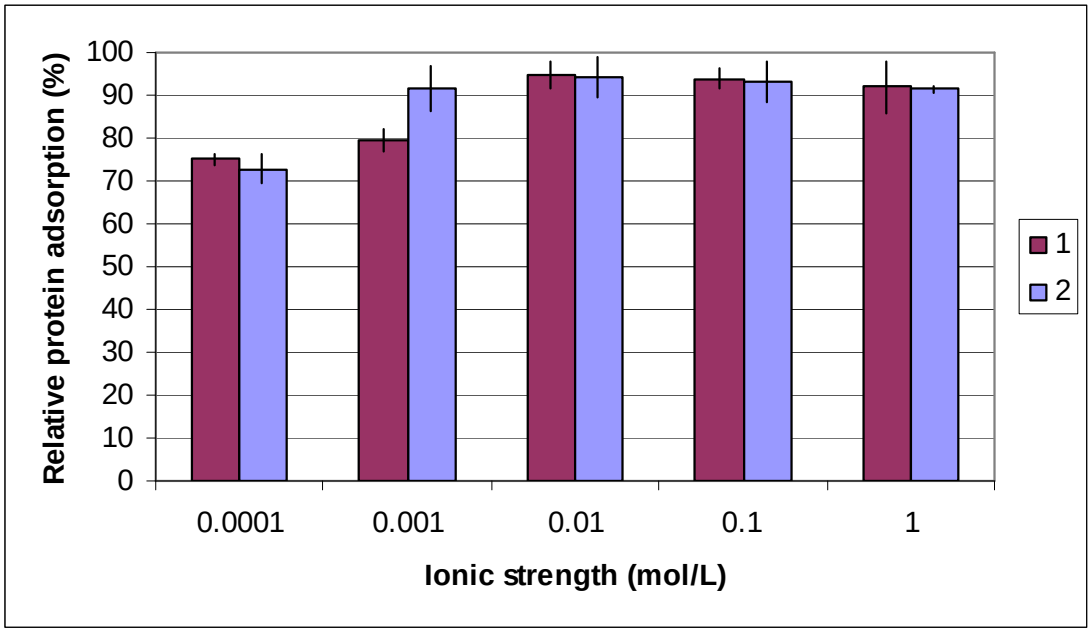

Figure VI-9: Comparison of the Dodecanethiol SAM relative fibrinogen adsorption on (1-mercaptoundec-11-yl)tri(ethylene glycol) 3,3,3-trifluoroproyl ether and (1-mercaptoundec-11-yl)tri(ethylene glycol) 4,4,4-trifluorobutyl ether SAM on gold in aqueous solution of different salt concentration

A comparison of the relative adsorption on this second SAM with the results from the organic film made of **1** revealed that the amount of adsorbed fibrinogen at low and high ionic strengths (regardless of the results obtained at ionic strength under which the "jumps" occurred) was rather similar within the error bar. Thus, an additional methylene unit shifted the "jump" to lower ionic strength.

3) Protein Adsorption Study on (1-mercaptoundec-11-yl)tetra(ethylene glycol) 3,3,3-trifluoropropyl ether SAM

The influence of the number of oligo(ethylene glycol) groups was also considered. The behaviour of (1-mercaptoundec-11-yl)tetra(ethylene glycol) 3,3,3-trifluoropropyl ether (**3**) was therefore studied.

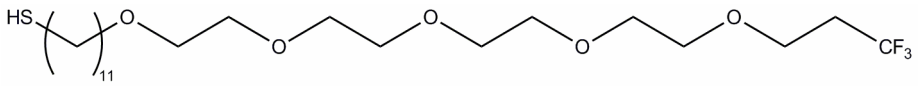

Figure VI-10: (1-mercaptoundec-11-yl)tetra(ethylene glycol) 3,3,3-trifluoropropyl ether (3)

The electrostatic repulsion was stronger while the hydrophobic attraction was similar for SAMs made of **1** and **3**. Since the density as well as the contact angle were similar for SAMs **1** and **3**, the study of the influence of the number of oligo(ethylene glycol) units on fibrinogen adsorption was possible.

Figure VI-11 displays the relative fibrinogen adsorption as a function of the ionic strength.

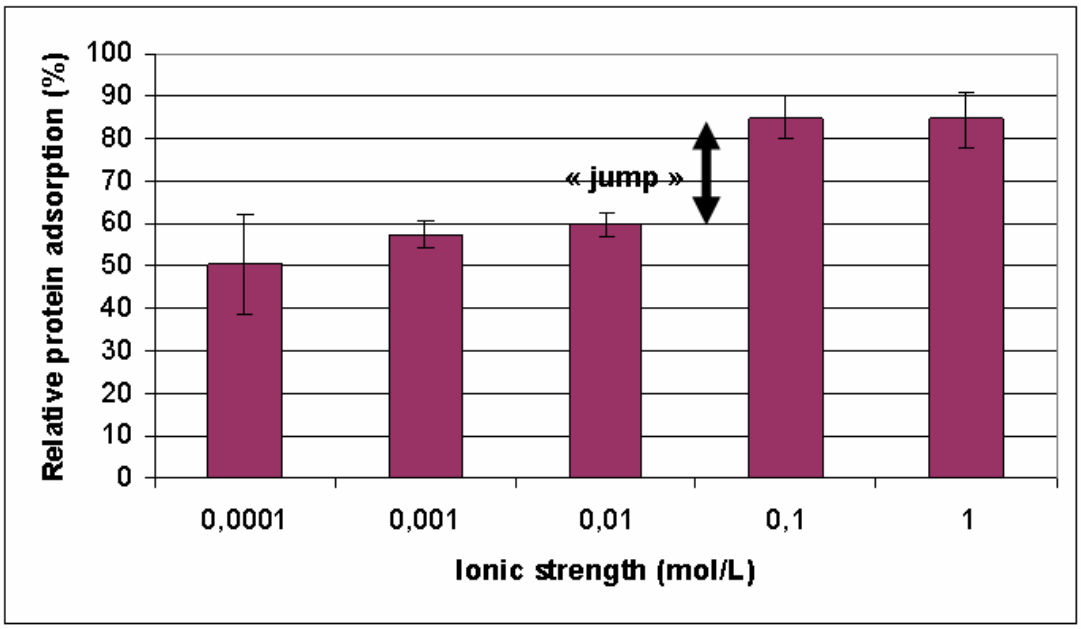

Figure VI-11: Dodecanethiol SAM relative fibrinogen adsorption on (1-mercaptoundec-11-yl)tetra(ethylene glycol) 3,3,3-trifluoropropyl ether SAM on gold in aqueous solution of different salt concentration

The relative fibrinogen adsorption on SAM **3** observed following immersion in 10^{-4} M PBS solution is 50%. The relative adsorption increased stepwise to 57 % and 60% at ionic strengths of 10^{-3} and 10^{-2} M, respectively. The relative adsorption reached 85% at ionic strengths of 10^{-1} M and higher. Appreciable changes in protein adsorption for this synthetic surface occured between salt concentrations of 10^{-2} and 10^{-1} M.

A comparison with the force-distance curves measured with a hydrophobic tip showed an obvious correlation between the protein adsorption and the number of oligo(ethylene

glycol) groups. The protein adsorption change occured at the same concentration values under which the force on approach with a hydrophobic probe changes from repulsive to attractive, between 10^{-2} and 10^{-1} M. An additional oligo(ethylene glycol) unit increased the concentration at which the force experienced by the hydrophobic tip changed from repulsive to attractive and the rate of adsorption amount by a factor of 10 (between 10^{-2} and 10^{-1} M for **3** and between 10^{-3} and 10^{-2} M for **1**).

The results in fibrinogen adsorption at fixed concentrations were also compared:

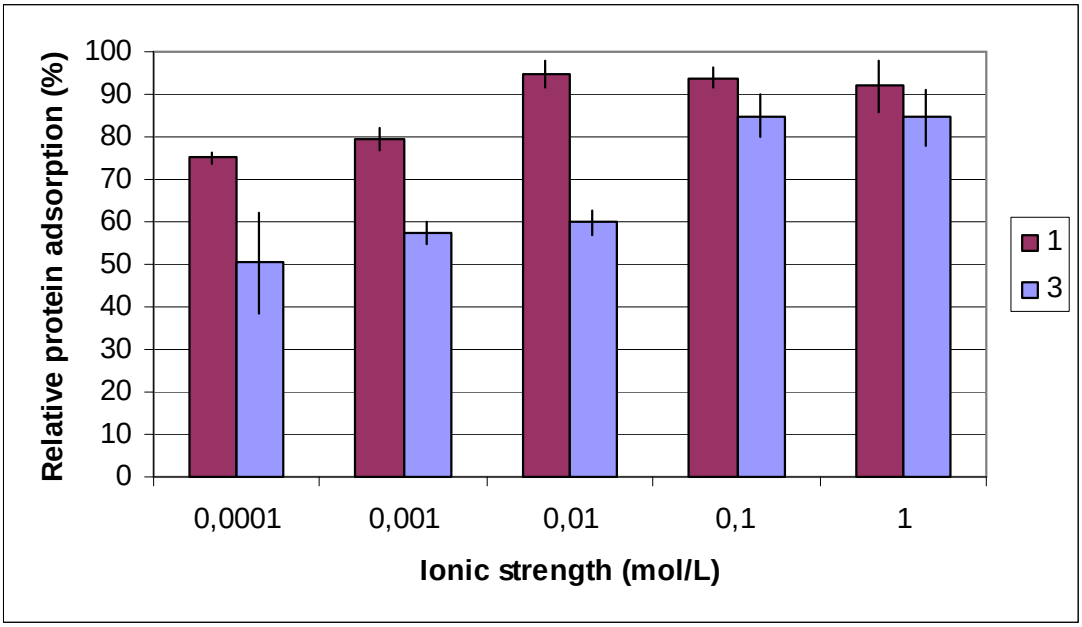

Figure VI-12: Comparison of the Dodecanethiol SAM relative fibrinogen adsorption on (1-mercaptoundec-11-yl)tri(ethylene glycol) 3,3,3-trifluoroproyl ether and (1-mercaptoundec-11-yl)tetra(ethylene glycol) 3,3,3-trifluoropropyl ether SAM on gold in aqueous solution of different salt concentration

It was shown that the addition of an OEG group reduced the amount of fibrinogen adsorbed on the surface, *i.e.* SAM **3** was more resistant to the protein adsorption than the first organic film. This reduction was moreover higher where a repulsive force was observed which indicated that this repulsive interaction was stronger from a SAM with an additional OEG unit.

4) Protein Adsorption Study on (1-mercaptoundec-11-yl)hexa(ethylene glycol) 3,3,3-trifluoropropyl ether and (1-mercaptoundec-11-yl)hexa(ethylene glycol) 2,2,2-trifluoroethyl ether SAMs

In the previous sections the effect of an additional methylene or oligo(ethylene glycol) unit was discussed. This study has been extended to the addition of two extra OEG groups and the omission of a methylene unit. The behaviour of (1-mercaptoundec-11-yl)hexa(ethylene glycol) 3,3,3-trifluoropropyl ether (**5**) and (1-mercaptoundec-11-yl)hexa(ethylene glycol) 2,2,2-trifluoroethyl ether (**6**) was therefore studied.

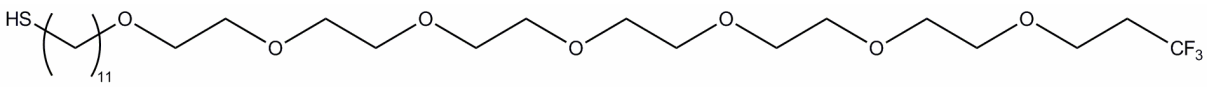

(**5**)

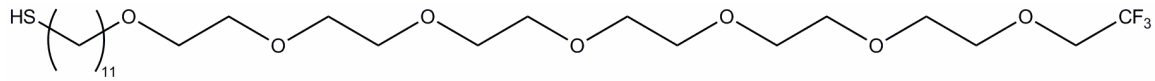

(**6**)

Figure VI-11: (1-mercaptoundec-11-yl)hexa(ethylene glycol) 3,3,3-trifluoropropyl ether (5) and (1-mercaptoundec-11-yl)hexa(ethylene glycol) 2,2,2-trifluoroethyl ether (6)

These self-assembling molecules exhibited two additional OEG groups and a hydrophobic end identical to **3 (5)** and with one less CH_2 unit (**6)**. The contact angle measured on these two SAMs was around 30° lower than that of the SAMs **1-3**.

Figure VI-14 displays the relative fibrinogen adsorptions for **5** and **6** as a function of the ionic strength of the protein solution.

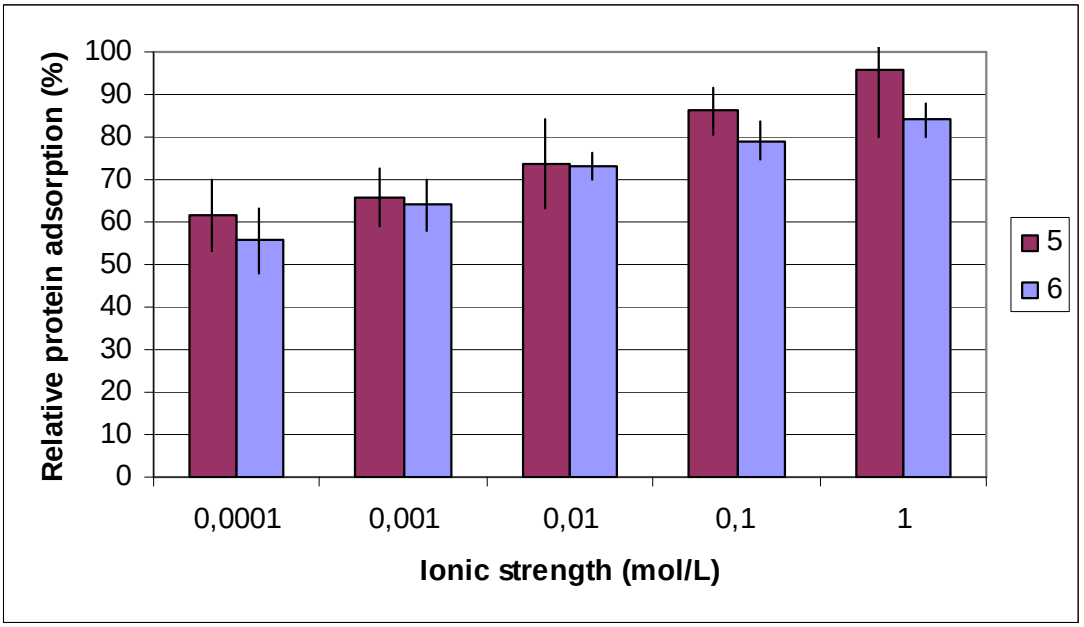

Figure VI-14: Dodecanethiol SAM relative fibrinogen adsorption on (1-mercaptoundec-11-yl)hexa(ethylene glycol) 3,3,3-trifluoropropyl ether and a (1-mercaptoundec-11-yl)hexa(ethylene glycol) 2,2,2-trifluoroethyl ether SAMs on gold in aqueous solution of different salt concentration

The relative fibrinogen adsorption on **5** and **6** after immersion in solution with a PBS concentration of 10^{-4} M was 62% and 56% of the fibrinogen adsorption on a dodecanethiol SAM under the same aqueous media. The relative adsorption on both films increased stepwise with increasing PBS concentration and reached 96 % and 84% in 1 M solution for **5** and **6**, respectively. The amount of adsorbed fibrinogen was always slightly lower on **6** compared to **5**.

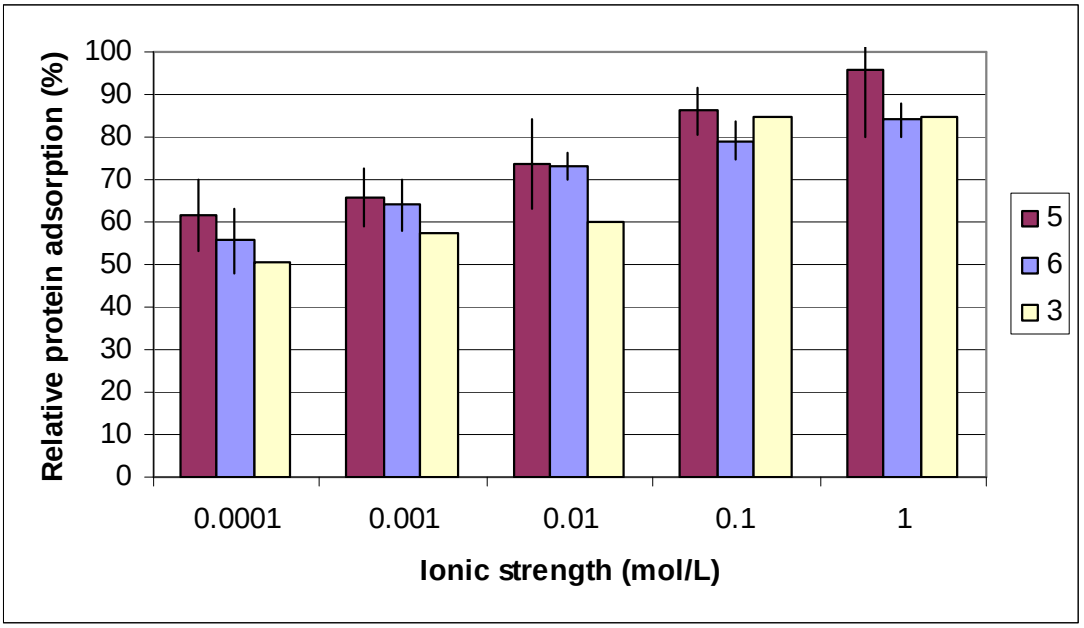

Figure VI-15: Dodecanethiol SAM relative fibrinogen adsorption on (1-mercaptoundec-11-yl)hexa(ethylene glycol) 3,3,3-trifluoropropyl ether, on (1-mercaptoundec-11-yl)hexa(ethylene glycol) 2,2,2-trifluoroethyl ether, and on (1-mercaptoundec-11-yl)tetra(ethylene glycol) 3,3,3-trifluoropropyl ether SAMs on gold in aqueous solution of different salt concentration

The influence of the force originating from the surface seemed weaker as a switch from repulsion to attraction of a hydrophobic tip, observed between 10^{-1} and 1 M, did not correspond to such a continuous change of the amount of fibrinogen at the surface. However, the amount of proteins adsorbed was relatively high even at low concentrations. This could be a reason why there was no clear "jump" visible here.

The slight increase with increasing ionic strength was similar to compounds **1**, **2**, and **3**. A final explanation for this was not found.

These results can be discussed in view of the work of Grunze and co-workers. [21] They studied SAMs with different structures in order to understand the parameters involved in the protein resistance of oligoether SAMs. Four of their surfactant molecules were similar to **1**, **2**, **5** and **6** except that they had a final CH_2 rather than a CF_3 group; they were called EG_3OPr, EG_3OBu, EG_6OPr, and EG_6OEt, respectively. Grunze and co-workers studied the impact of the surface wettability on the protein adsorption property by plotting the amount of protein adsorption as a function of the contact angle. This graph is reproduced below with additional symbols representing the results obtained with the synthetised surfaces under the same PBS concentration, under 10^{-1} M.

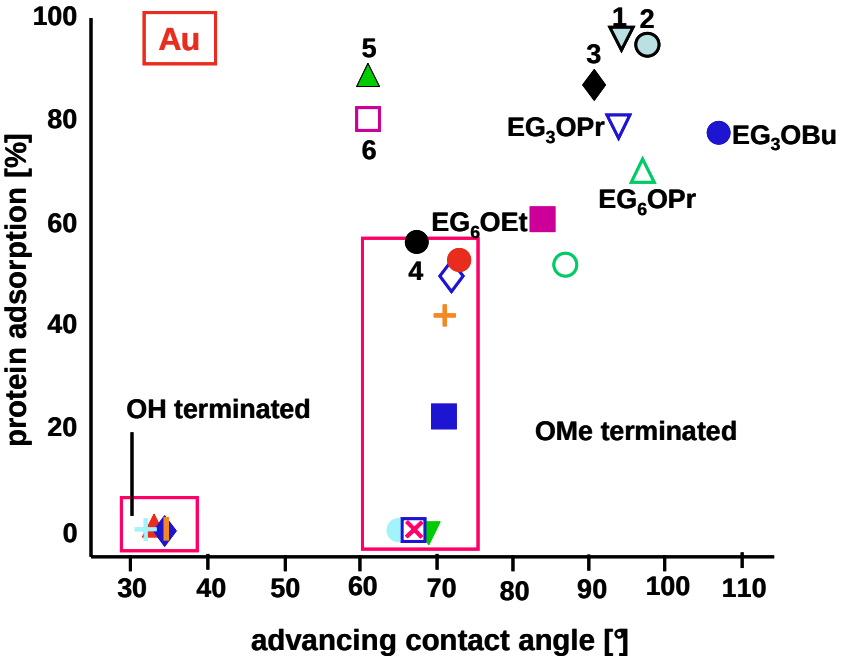

Figure VI-16: Amount of protein adsorption on a given oligoether SAM on gold normalized to the amount of protein adsorbed on a monolayer of hexadecanethiol on gold (100%) versus advancing aqueous contact angle of the SAM in 10^{-1} M PBS solution. Symbols: red ▲, EG_2OH; orange │, EG_3OH; green +, EG_6OH; blue ♦, TRI_3OH; blue ■, EG_1OMe; green ▼, EG_2OMe; light blue ●, EG_3OMe; red ×, EG_6OMe; blue □, TRI_3OMe; red ●, PRO_2OMe; blue ◊, PRO_3OMe; orange +, PRO_4OMe; purple ■, EG_3OEt; green ○, EG_6OEt; blue ▽, EG_3OPr; green △, EG_6OPr; blue ●, EG_3OBu; Light blue ▼, 1; light blue ●, 2; black ♦, 3; black ●, 4; green ▲, 5; purple □, 6. Reproduced from [21].

Grunze and co-workers defined two regions and deduced from their results that water contact angles higher than 70° reduced full protein resistance. Contact angle and amount of protein adsorption values obtained for **1** and **2** were close to those for EG_3OPr and EG_3OBu and their symbols were in the same area of the graph. The symbols for **5** and **6** compared to EG_6OPr, and EG_6OEt were on both sides of the "70° limit" because the contact angle on **5** and **6** was much lower (around 30° lower). This could show that the influence of the wettability on the amount of protein adsorption was different with the synthesised fluorinated surfactant molecules. Although the amount of adsorption on **3** and **6** follew the same trend as seen by Grunze: a lower adsorption on surfaces with a lower contact angle, the adsorption amount was similar on **3** and **5**. A dramatic decrease was not noticed in the adsorption amount when the contact angle was lower than 70°.

5) Protein Adsorption Study on (1-mercaptoundec-11-yl)tetra(ethylene glycol) 2,2,2-trifluoropropyl ether SAM

In order to extend the study of the influence of the length of the hydrophobic and hydrophilic moieties, the behaviour of (1-mercaptoundec-11-yl)tetra(ethylene glycol) 2,2,2-trifluoroethyl ether (**4**) was also investigated.

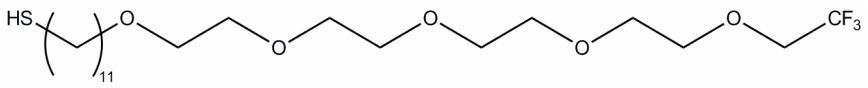

Figure VI-17: (1-mercaptoundec-11-yl)tetra(ethylene glycol) 2,2,2-trifluoroethyl ether (4)

This surfactant differed from **3** by one methylene group less in the hydrophobic top end. Similar to **5** and **6**, the contact angle was around 30° lower than those observed for SAMs **1**-**3**. Ellipsometry and XPS analyses revealed that the coverage of the monolayer was (inexplicably) 30 % lower than all the other synthesised monolayers.

Figure VI-18 displays the relative fibrinogen adsorption as a function of the ionic strength.

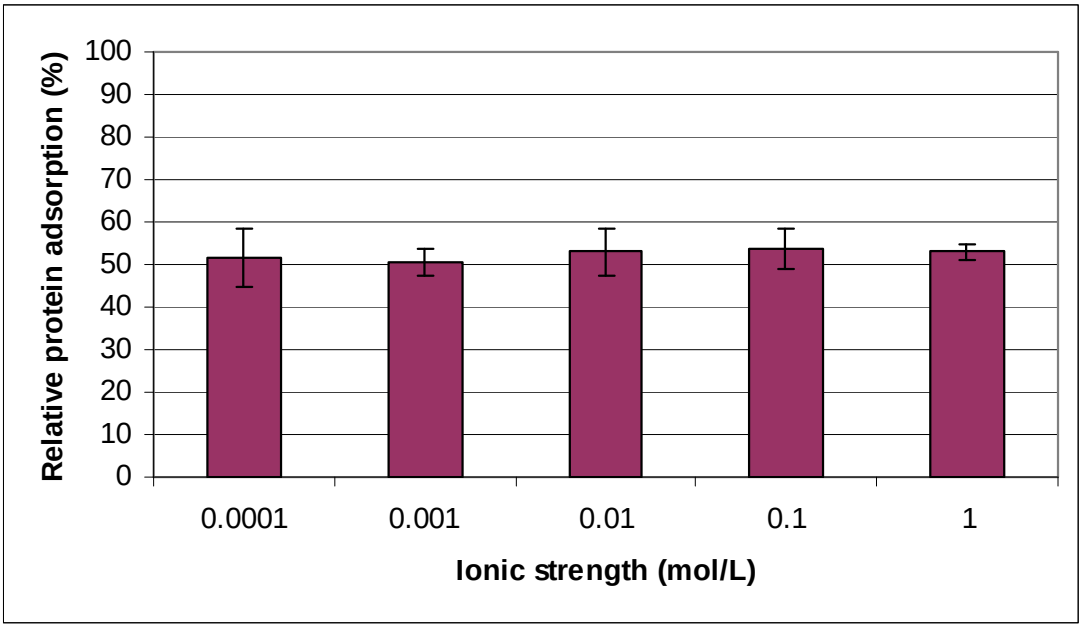

Figure VI-18: Dodecanethiol SAM relative fibrinogen adsorption on (1-mercaptoundec-11-yl)tetra(ethylene glycol) 2,2,2-trifluoroethyl ether SAM on gold in aqueous solution of different salt concentration

The relative fibrinogen adsorption on SAM **4** observed by immersion in solutions with a PBS concentration ranging from 10^{-4} M to 1 M was almost constant at 52%. This value was the lowest observed so far and suggested that the reduced density made the SAM more resistant to protein adsorption. The influence of the density was not studied systematically. A layer which was surprisingly discovered to be less tightly packed than the others was the reason why it was possible to observe the influence of this parameter. A relaxed lateral packing density might yield a system of lower order and higher exposure of the repulsive oligo(ethylene glycol) groups to the surface.

It could be noticed that the force did not affect the adsorption of proteins on a low dense film because the amount of adsorption was constant under an increasing ionic strength of the liquid environment while a switch from repulsion to attraction was observed between 10-1 and 1M.

III) Conclusions

With the experiments carried out with the three first mollecules, it has been shown that the combination of three or four oligo(ethylene glycol) groups and a trifluoro propyl or butyl part in the self-assembling molecule highlighted a possible modulation of the relative amount of adsorbed protein by changing the ionic strength of the liquid medium. The three SAMs exhibited similar densities and wettabilities and as such it was possible to link this modulation to the influence of the forces originating from the surface.

The impact of the composition of the surfactant molecule was illustrated by the dependence of the marked change in adsorption as a function of ionic strength on the length of the trifluoroalkyl top and the number of the oligoethylene glycol units. Adding one hydrophobic methylene group shifted the “jump” to 10 times weaker ionic strengths whilst the addition of one oligo(ethylene glycol) unit moved the “step” in the opposite direction by an order of magnitude. It was also observed that an increase in the length of the hydrophobic moiety leaded to a slight increase in the amount of adsorbed fibrinogen under any liquid medium condition whereas an additional OEG unit generally decreased the adsorption.

For all films studied a slight increase in the amount of proteins was observable with increasing ionic strength and below the “jump” concentration. No further investigation was performed to study this phenomenon. Nevertheless, one possible explanation was that the ionic strength affected the conformation of the fibrinogen or the self-assembling molecules on the surface.

It could be notice that the amount of fibrinogen adsorbed on the synthesised SAMs was never zero. Even under the ionic strength where the force which originated from the organic layer was repulsive, the surface was not totally inert to fibrinogen adsorption. This suggested that it was not the only parameter governing this phenomenon.

With the experiments carried out with all the mollecules, it has been shown that for dense films, the amount of adsorbed fibrinogen on an alkanethiol SAM based on oligo(ethylene glycol) groups and a trifluoroalkyl head could be influenced by changing the concentration of the salt of the liquid environment. When the number of oligo(ethylene glycol) units was six giving rise to a higher wettability of the surface, the amount of proteins adsorbed on the surface was observed to be progressively adjustable with the salt concentration.

A stronger influence of the adsorption amount was observed for SAMs with lower wettability, based on three or four oligo(ethylene glycol) units, because the impact of the force which originated from the surface was more relevant. The stronger impact of this parameter was reflected by a considerable jump in the amount of fibrinogen on the surface,

which was visible when immersing the substrates in two solutions whose concentrations differed by a factor 10. The amount of fibrinogen adsorbed at the solid-liquid interface could be increased or reduced by extending the length of the hydrophobic head or by adding one oligo(ethylene glycol) groups, respectively. Moreover, these two modifications shifted the "jump" of the amount of adsorbed fibrinogen to lower and higher salt concentration respectively.

IV) Literature

1. H. Kanazawa, K. Yamamoto, Y. Matsushima, N. Takai, A. Kikuchi, Y. Sakurai and T. Okano, *Anal. Chem.*, 1996, **68**, 100-105.
2. C. C. Barrias, M. C. L. Martins, M. C. S. Miranda and M. A. Barbosa, *Biomaterials*, 2005, **26**, 2695-2704.
3. D. L. Huber, R. P. Manginell, M. A. Samara, B. I. Kim and B. C. Bunker, *Science*, 2003, **301**, 352-354.
4. Y. Akiyama, A. Kikuchi, M. Yamato and T. Okano, *Langmuir*, 2004, **20**, 5506-5511.
5. D. Cunliffe, C. D. Alarcon, V. Peters, J. R. Smith and C. Alexander, *Langmuir*, 2003, **19**, 2888-2899.
6. M. N. Yousaf and M. Mrksich, *J. Am. Chem. Soc.*, 1999, **121**, 4286-4287.
7. C. D. Hodneland and M. Mrksich, *J. Am. Chem. Soc.*, 2000, **122**, 4235-4236.
8. W.-S. Yeo, M. N. Yousaf and M. Mrksich, *J. Am. Chem. Soc.*, 2003, **125**, 14994-14995.
9. J. Lahann, S. Mitragotri, T.-N. Tran, H. Kaido, J. Sundaram, I. S. Choi, S. Hoffer, G. A. Somorjai and R. Langer, *Science*, 2003, **299**, 371-374.
10. Y. Liu, L. Mu, B. Liu, S. Zhang, P. Yang and J. Kong, *Chem. Commun.*, 2004, 1194-1195.
11. D. Schwendel, R. Dahint, S. Herrwerth, M. Schoerhloz, W. ZEck and M. Grunze, *Langmuir*, 2001, **17**, 5717-5720.
12. R. Valiokas, M. Ostblom, S. Svedhem, S. C. T. Svensson and B. Liedberg, *J. Phys. Chem. B*, 2000, **104**, 7565-7569.

13. S. Balamurugan, L. K. Isrta, J. Yan, G. P. Lopez, J. Fick, M. Himmelhaus and M. Grunze, *J. Am. Chem. Soc.*, 2005, **127**, 14548-14549.
14. E. Delamarche, G. Sundarababu, H. Biebuyck, B. Michel, C. Gerber, H. Sigrist, H. Wolf, H. Ringsdorf, N. Xanthopoulos and H. J. Mathieu, *Langmuir*, 1996, **12**, 1997-2006.
15. M. Veiseh, M. H. Zareie and M. Zhang, *Langmuir*, 2002, **18**, 6671-6678.
16. P. Harder, M. Grunze, R. Dahint, G. M. Whitesides and P. E. Laibinis, *J. Phys. Chem. B*, 1998, **102**, 426-436.
17. R. G. Chapman, E. Ostuni, M. N. Liang, G. Meluleni, E. Kin, L. Yan, G. Pier, H. S. Warren and G. M. Whitesides, *Langmuir*, 2001, **17**, 1225-1233.
18. E. Ostuni, B. A. Grzybowski, M. Mrksich, C. S. Roberts and G. M. Whitesides, *Langmuir*, 2003, **19**, 1861-1872.
19. S. Chen, L. Liu and S. Jiang, *Langmuir*, 2006, **22**, 2418-2421.
20. Y.-Y. Luk, M. Kato and M. Mrksich, *Langmuir*, 2000, **16**, 9604-9608.
21. S. Herrwerth, W. Eck, S. Reinhardt and M. Grunze, *J. Am. Chem. Soc.*, 2003, **125**, 9359-9366.
22. C. Dicke and G. Hähner, *J. Am. Chem. Soc.*, 2002, **124**, 12619-12625.
23. Y.-H. M. Chan, R. Schweiss, C. Werner and M. Grunze, *Langmuir*, 2003, **19**, 7380-7385.
24. J. Israelachvili, *Intermolecular and Surface Forces*, Second Edition edn., Academic Press, San Diego, 1992.
25. L. Stryer, *Biochimie*, 5eme Edition, Flammarion medicine-sciences, Paris, 2003.
26. D. Voet, *Biochimie*, 2eme Edition, De Boeck, Bruxelles, 2005.
27. E. Ostuni, R. G. Chapman, R. E. Holmlin, S. Takayama and G. M. Whitesides, *Langmuir*, 2001, **17**, 5605-5620.
28. M. Mrksich, G. B. Sigal and G. M. Whitesides, *J. Am. Chem. Soc.*, 1995, **11**, 4383-4385.
29. K. L. Prime and G. M. Whitesides, *J. Am. Chem. Soc.*, 1993, **115**, 10714-10721.
30. T. C. Ta, M. T. Sykes and M. T. McDermott, *Langmuir*, 1998, **14**, 2435-2443.

Chapter 7

Conclusions and Outlook

This thesis involves ultrathin films of self-assembled monolayers. SAMs are easily prepared and have a great flexibility with respect to functionalisation leading to their use for various applications such as biointerfaces. According to their order, stability, and membrane appearance, SAMs are good candidates for the study of protein/surface interactions.

In this project, extensive effort has led to the synthesis of six novel trifluoro alkyl polyethylene glycol alkanethiols. The seven step synthetic pathway has been followed similarly for the six molecules. One starting molecule was either trifluoroethanol, trifluoropropanol or trifluorobutanol and molecules were composed of three, four, or six oligo(ethylene) groups. Each intermediate was characterised by nuclear magnetic resonance, infrared, and high-resolution mass spectroscopies. The six pure liquid compounds were dissolved in dimethylformamide and gold substrates were immersed in these solutions to give self-assembled monolayers. The properties and the quality of these organic layers were characterised by X-ray photoelectron spectroscopy, contact angle goniometry, and ellipsometry measurements. The surface coverage relative to an alkanethiol SAM was around 75 % except for one monolayer which has a much lower density for an unexplained reason. The contact angle was 94° on tri and tetra(ethylene glycol) based SAMs and droped to 62° when this number reached six and for the less dense film.

The forces acting on proteins which originated from the surface were studied *via* AFM force-distance curve measurements with a hydrophobic probe in aqueous solution. Varying the ionic strength of the liquid environment revealed that an electrostatic repulsion and a hydrophobic attraction acted on the probe with a swing of dominant force. The concentration of the switch from repulsion to attraction was shown to be adjustable by changing the number of oligo(ethylene glycol) or methylene units in the surfactant molecule. This concentration

increased with a higher number of oligo(ethylene glycol) groups and decreased with a longer hydrophobic end. Therefore, it was possible to tailor self-assembling molecules to observe a switch between 10^{-1} and 1 M which surrounded the concentration of the natural environment of fibrinogen.

The study of the influence of this total force acting on proteins, as well as the wettability and the density of the films, was performed by measuring the relative amount of fibrinogen adsorbed on our films by ellpisometry. These measurements revealed an impact of these three factors on the adsorption rate. When films were not tightly packed, the amount of fibrinogen adsorbed on the solid-liquid interface did not depend on the ionic strength. Therefore, it was suggested that a low density might have a stronger influence than the total force making impossible a variation of the amount of adsorbed fibrinogen with the chosen external parameter. For tightly packed films, both the wettability and the force had an impact on the protein adsorption. When the contact angle was 60°, the effect of the force was not dominant since an increasing ionic strength gave rise to a progressively higher adsorption. It was prevailing when the contact angle was 92° which enabled a 15 % or 20 % change of the relative adsorption by increasing or decreasing the salt concentration by a factor of ten.

Thus, the amount of adsorbed proteins on the surface could be altered by changing the salt concentration of the liquid medium with a highest influence for tightly packed films having a 92° contact angle.

I hope that someone will be sincerely interested in the few ideas described throughout this thesis and use it for future projects. Below, I try to point some research directions.

Higher wettability and lower and constant fibrinogen adsorption seemed linked to a lower density. It was suggested that the self-assembling molecules, having more space, could get tangled and present more oligo(ethylene glycol) groups than the trifluoro alkyl/OEG combination at the surface. Therefore, it would be interesting to check the conformation of the molecules of the least dense film.

An additional assumption was made concerning the influence of the ionic strength on the conformation of the molecules of the films. Consequently, observing their conformation in solution with different salt concentration would be particularly appealing.

Another extension would be the study of positively charged surfaces with surfactant molecules containing nitrogen atoms rather than oxygen on the adsorption of positively charged proteins.